UNIVERSITY OF NOVA GORICA
GRADUATE SCHOOL

PHOTOACTIVE NANOCOMPOSITE THIN FILMS ON GLASS AND THERMOSENSITIVE SUBSTRATES

DISSERTATION

Nives Vodišek

Mentor: prof. dr. Urška Lavrenčič Štangar

Nova Gorica, 2019

UNIVERZA V NOVI GORICI
FAKULTETA ZA PODIPLOMSKI ŠTUDIJ

FOTOAKTIVNE NANOKOMPOZITNE TANKE PLASTI NA STEKLU IN TERMIČNO NEOBSTOJNIH PODLAGAH

DISERTACIJA

Nives Vodišek

Mentorica: prof. dr. Urška Lavrenčič Štangar

Nova Gorica, 2019

UNIVERSITY OF NOVA GORICA
GRADUATE SCHOOL

Nives Vodišek, *Photoactive nanocomposite thin films on glass and thermosensitive substrates,* Dissertation, (2019)

If you want the rainbow,
you have to put up with the rain.

Hvala vsem, ki ste mi pomagali, da sem prišla »do mavrice«.

POVZETEK

Fotokataliza je postala v zadnjih nekaj desetletjih zelo razširjena; uporablja se predvsem za čiščenje vode in zraka, za samočistilne ter protibakterijske površine. Fotokatalitski proces spada med napredne oksidacijske procese in kot fotokatalizatorji so največkrat uporabljeni polprevodniki. Najbolj znan in najpogosteje uporabljen polprevodnik je (nano) titanov dioksid, ki lahko neselektivno razgradi organske snovi ob UV sevanju. Pri obsevanju TiO_2 z UV svetlobo se pojavi tudi fotovzbujena hidrofilnost, ki še dodatno izboljša samočistilni učinek. Ena od glavnih pomanjkljivosti TiO_2 je, da se za njegovo fotoaktivacijo uporablja UV svetloba, ki predstavlja le pet odstotkov sončnega spektra. Za boljši odziv TiO_2 na vidno svetlobo se razvijajo novi postopki, na primer dopiranje, kombiniranje z drugimi polprevodniki, modifikacija morfologije površine itd.

Doktorsko delo ima pet glavnih poglavij. Prvo poglavje je osredotočeno na krajši pregled obstoječe literature in razlago nekaterih osnovnih pojmov.

V drugem poglavju je predstavljen namen doktorskega dela. Pripravila sem transparentne fotoaktivne tanke plasti na steklu in temperaturno občutljivih podlagah. Izbrala sem štiri različne občutljive podlage: polivinil kloridna (PVC) folija, polimetil metakrilat (PMMA) plošča in poliesterska (PES) tkanina, prevlečena s slojem polivinila in akrila z (D1) ali brez (D2) dodatne poliviniliden fluoridne (PVDF) prevleke. Postopek priprave filmov smo obogatili z vpeljavo cirkonija, tako naj bi izboljšali aktivnost samih TiO_2 filmov, končni raztopini je bil dodan tudi SiO_2, ki je izboljšal mehanske lastnosti filmov.

Tretje poglavje je posvečeno eksperimentalnemu delu. V poglavju je opisan podroben proces sinteze tankih plasti. Sol-gel postopek sem uporabila za pripravo začetnih Ti-Zr solov izhajajoč iz titanovega in cirkonijevega alkoksida. Pripravila sem štiri različne Ti-Zr sole z 0, 5, 10 in 20 množinskimi % cirkonija glede na titan. Raztopine za nanašanje so vsebovale Ti-Zr sol, SiO_2 vezivo, 1-propanol in 2-propoksietanol; tanke plasti pa so bile nanešene s tehniko potapljanja. Tanke filme po nanosu ni bilo potrebno termično obdelati na visoki temperaturi, ker je fotoaktivna anatazna faza že prisotna po sušenju vzorcev. Tako so bili vzorci na steklu toplotno obdelani v peči pri 150 ° C, vzorce na termično neobstojnih podlagah pa sem utrdila zgolj s toplotno pištolo.

Praškaste vzorce in tanke plasti smo karakterizirali z naslednjimi metodami: UV-Vis, FTIR-ATR spektroskopijo in spektroskopijo z odklonom laserskega žarka, rentgensko

praškovno difrakcijo, presevno elektronsko mikroskopijo in termično analizo. Najpomembnejša lastnost fotokatalizatorja je fotoaktivnost, ta je bila določena na tankih plasteh z dvema različnima metodama; kvantitativno z merjenjem koncentracije hidroksiteraftalne kisline po razgradnji teraftalne kisline; in kvalitativno, z opazovanjem razgradnje barvila resazurin. Z dvema dodatnima metodama smo izmerili fotoaktivnost tankih plasti na stekleni podlagi, z elektronsko paramagnetno resonanco in z merjenjem kontaktnega kota po razgradnji metil stearata pri UV obsevanju.

Zelo pomembna lastnost tankih plati je mehanska odpornost in z merjenjem le te lahko ocenimo, če je bila imobilizacija na podlago uspešna. Mehansko stabilnost filmov smo določili z Wolff-Wilborn-ovo metodo.

V četrtem poglavju je opisana karakterizacija materialov s spremljajočo razpravo o rezultatih, ki je razdeljena na tri glavne dele: **i)** karakterizacija praškastih vzorcev; **ii)** karakterizacija tankih plasti na stekleni podlagi in **iii)** karakterizacija tankih plasti na termično neobstojnih podlagah.

V zaključku so povzete glavne ugotovitve. Ena od naših začetnih hipotez ni bila potrjena, saj tanke plasti z višjo vsebnostjo cirkonija niso bile aktivnejše, izkazovali pa so večjo mehansko odpornost. Vsi vzorci so bili, kljub nizki temperaturi pripravi, transparentni in fotoaktivni. Imobilizacija fotokatalizatorjev je bila uspešna na steklu kot tudi na termično neobstojnih podlagah.

Ključne besede: steklo, imobilizacija, nanokompoziti, nanomateriali, PES, fotokataliza, PMMA, PVC, samočistilne površine, SiO_2, plastične podlage, tanke plasti, TiO_2, ZrO_2.

SUMMARY

Photocatalysis is a well-known process for the last few decades; it is predominantly used for water and air purification, but also for self-cleaning and antibacterial surfaces. The photocatalytic process is one of the advanced oxidation processes, where semiconductors are mainly used as photocatalysts. The most known and used semiconductor is nanosized titania, which can non-selectively decompose organic matters. One of the side effects of nano TiO_2 under UV irradiation is photoinduced hydrophilicity, which furthermore improves the self-cleaning effect. The main drawback of TiO_2 is that for its activation UV light is needed, which represents only 5 percent of the solar spectrum. Consequently, actinic irradiance power is low and the response of photocatalyst is limited. Novel approaches are being introduced to improve TiO_2 response to visible light such as doping, coupling, modification of surface morphology and others.

The thesis consists of five principal chapters. The first chapter is focused on a short literature review and explanation of some basic terms and principles that are related to this thesis.

The aim of the research was to prepare transparent photocatalytically active thin films on glass and thermosensitive substrates. Four thermosensitive substrates were used: polyvinyl chloride (PVC) foil, polymethyl methacrylate (PMMA) sheet and polyester (PES) fabric coated with a polyvinyl and acrylic coating, with (D1) or without (D2) an additional polyvinylidene fluoride topcoat. The synthesis of films was modified with the introduction of zirconium aiming at improving the photocatalytic activity of the TiO_2 films, and the final films had a SiO_2 phase present for increased mechanical robustness.

The third chapter is dedicated to the experimental part of the thesis. The detailed process of synthesis is described. The sol-gel process was used to prepare initial Ti-Zr sols, colloidal aqueous solutions with TiO_2 and ZrO_2 nanoparticles derived from titanium and zirconium alkoxides. The four different Ti-Zr sols were prepared with 0, 5, 10 and 20 molar % of Zr according to Ti. The depositing solution was prepared by mixing Ti-Zr sol, SiO_2 sol binder, 1-propanol and 2-propoxyethanol, and then thin films were deposited by dip-coating technique. After the deposition, samples did not require high-temperature calcination since the photocatalytic anatase phase was present already after drying the deposited layers. Coated glass slides were put into a

furnace at 150 °C, while samples on thermosensitive substrates were just treated by a heat gun. Samples in powder and thin film form were characterized by UV-Vis, FTIR-ATR and laser beam deflection spectroscopy, X-ray diffraction, scanning electron microscopy and thermal analysis. One of the main aspects of the photocatalyst is its activity. Photocatalytic activity of the thin films was determined, either quantitatively by the formation of fluorescent hydroxyterephthalic acid, one of the first degradation products of terephthalic acid deposit, or qualitatively by a visual-based method where degradation of resazurin ink was observed. Two additional methods were used on glass samples, electron paramagnetic resonance, and degradation of methyl stearate by observing the change in water contact angle under UVA irradiation. Mechanical stability of films on various substrates is an essential factor, describing how successful was immobilization of the photocatalytic materials on the substrate. It was determined by the pencil hardness test, *i.e.,* Wolff-Wilborn method.

In the fourth chapter, titled "Results and Discussion," the most important part of the thesis is placed. Materials characterization and associated discussion of the results are divided into three major parts: **i)** powder samples characterization; **ii)** characterization of thin films on a glass substrate, and **iii)** characterization of films on thermosensitive substrates.

In the conclusions, the main findings of the Ph.D. research work are summarized. One of our initial hypotheses was disapproved, thin films were not more active with a higher content of zirconium. However, they were more durable. All the obtained films were transparent and photoactive, despite the low-temperature synthesis procedure. Besides commonly used glass substrate, immobilization on thermosensitive substrates was also successful.

Keywords: *glass substrate, immobilization, nanocomposite, nanomaterials, PES, photocatalysis, PMMA, PVC, self-cleaning surfaces, silica, plastic substrates, thin films, titania, zirconia.*

Table of contents

List of figures

List of tables

List of acronyms and abbreviations

1-PrOH -   1-propanol

AOP   -   advanced oxidation process

ATR   -   attenuated total reflection

BET   -   Brunauer-Emmett-Teller

CA   -   contact angle

CB   -   conduction band

CL   -   cathodoluminescence

CVD   -   chemical vapor deposition

DMPO   -   5,5-dimethyl-1-pyrroline-N-oxide

DRS   -   diffuse reflectance spectroscopy

DSC   -   differential scanning calorimetry

DSMZ   -   Deutsche Sammlung von Mikroorganismen und Zellkulturen

EPR   -   electron paramagnetic resonance

EtOH   -   ethanol

FEG   -   field emission gun

FTIR   -   Fourier-transform infrared spectroscopy

HEC   -   hydroxyethyl cellulose

HTPA   -   hydroxyterephthalic acid

IARC   -   International Agency for Research on Cancer

LBDS   -   laser beam deflection spectroscopy

NP   -   nanoparticles

PB   -   probe beam

PCA   -   photocatalytic activity

PES   -   polyester

PMMA-   polymethyl methacrylate

PVC   -   polyvinyl chloride

PVDF -   polyvinylidene fluoride

ROS   -   reactive oxygen species

Rz   -   resazurin

SEM   -   scanning electron microscopy

TEM   -   transmission electron microscopy

TEOS -   tetraethyl orthosilicate

TGA   -   thermogravimetric analysis

TOs   -   temperature oscillations

TPA   -   terephthalic acid

TTIP -   titanium tetraisopropoxide

UV   -   ultraviolet light

UVA   -   ultraviolet A light ($\lambda = 315$–400 nm)

UV-Vis -   ultraviolet-visible spectroscopy

VB   -   valence band

WCA   -   water contact angle

XRD   -   X-ray diffraction

ZTB   -   zirconium tetrabutoxide

1 INTRODUCTION WITH THEORETICAL BACKGROUND

So far, more than 190 semiconductors have been attempted for application as a photocatalyst [1]. Photocatalysts are used in various shapes and environments, for example, powders of nanoparticles in the water purification process. Photocatalytic coatings are considered to be sustainable materials as they only need sunlight for their activation and regeneration [2]. In photocatalytic applications, nanosized TiO_2 is mainly used, it absorbs UV light (< 400 nm) and can photo-stimulate redox reactions on its surface producing reactive oxygen species (ROS) such as hydroxyl radical ($^\bullet OH$), superoxide radical ($^\bullet O_2^-$) and singlet oxygen ($^1O_2$), and the production of them contributes to destroying organic compounds and the biocidal activity with strong oxidative power [3,4]. The origin of the photocatalytic activity of TiO_2 is in the separation of electron-hole pairs that are formed in the particle bulk upon UV irradiation and reach the surface to perform redox reactions [5].

Doping TiO_2 or coupling TiO_2 with another metal oxide are commonly employed in order to retard the fast charge recombination and, in some cases, enable visible light absorption by creating defect states in the bandgap. In the former case, the conduction band electrons or valence band holes are trapped in the defect sites or transferred to a coupled semiconductor, inhibiting the recombination and enhancing the interfacial charge transfer [6].

Most surfaces, especially those of organic origin, provide a suitable place for microorganisms growth at proper humidity and temperature [7]. Outdoor surfaces are exposed to various weather conditions and generally cannot be kept as clean as indoor surfaces. That is why applying photocatalytic self-cleaning material to these surfaces would be of high interest, such surfaces with the help of sun and water are maintained clean for a longer time and resistant against microbes' overgrowth. There are some additional environmental aspects of such coatings **i)** thermosensitive surfaces require low-temperature synthesis (and curing) of a thin film, and aggressive solvents should be omitted, *i.e.*, the synthesis should follow green chemistry principles; **ii)** the resulting coating is photoactive when exposed to natural weather conditions, *i.e.*, there is less or no need for additional chemicals or processes to maintain such surfaces clean and functional. However, nanoparticles that necessarily constitute the photoactive coating

structure should be well immobilized on the support in order to prevent their release in the environment and possible harmful effects herewith.

1.1 Photocatalysis

In general, the photocatalysis term is used for describing reactions that occur under the action of light. Photocatalysis connects photochemistry and catalysis research field. So, photocatalysis is a process in which the catalyst and light are simultaneously used to generate or speed up a chemical reaction; the catalyst or the substrate can absorb light. Generally, in photocatalysis, light is not a catalyst in a reaction, but it is involved in the generation of active catalytic species [8]. Hence, the term can be defined as "catalysis driven acceleration of a light-induced reaction" [9]. Photocatalysis is a process that can be used for several purposes, such as degradation of organic pollutants in water or air, production of hydrogen, self-cleaning surfaces and antimicrobial activities. A wide range of application is rooted in the possibility to employ the sunlight and to promote reactions under very mild conditions; photocatalysis operates under ambient conditions provided that an adequate radiation source is available [1,10]. Photodecomposition of organic substances by photocatalysis depends on various parameters: the ones regarding the photocatalyst are size, crystallinity, morphology, surface area, bandgap, electron-hole pair's lifetime; the environmental parameters include temperature, pH, irradiation intensity, and amounts of catalyst, pollutants, and their mixture.

The overall heterogeneous photocatalysis can be summarized in five steps [11]:
    (1) Reactant diffusion to catalyst surface,
    (2) Adsorption of reactant onto the surface,
    (3) Chemical reaction on the catalyst surface,
    (4) Desorption of final products from the catalyst surface,
    (5) Diffusion of final products from the catalyst surface.

Semiconducting materials are the most suitable candidates for a photocatalyst, because of their electronic structure which is characterized by filled valence band and an empty conduction band. They differ in bandgap energy, light absorption properties, characteristics of charge transport and lifetime of excited states [9]. Semiconductor should have following features to be suitable as photocatalyst: **i)** photoactivity properties; **ii)** bandgap energy corresponding to visible or/and near UV light; **iii)**

photostability; **iv)** chemical and biological inertness; **v)** non-toxicity; **vi)** simple production.

Semiconductor photocatalysis consists of three fundamental steps (Figure 1.1) [9,12]:

- ♦ When light irradiates the surface, and if the energy of that light is equivalent or larger than the semiconductor's bandgap energy, valence band electrons get excited and move to the conduction band, forming electron-hole pairs.
- ♦ Holes are formed in the valence band. They can oxidize donor molecules and react with adsorbed H_2O molecules (or preferably the surface OH species) to generate hydroxyl radicals ($^•OH$).
- ♦ Electrons from the conduction band react with oxygen to form superoxide ions ($^•O_2^-$) or adsorbed organic species and consequently reduce them.
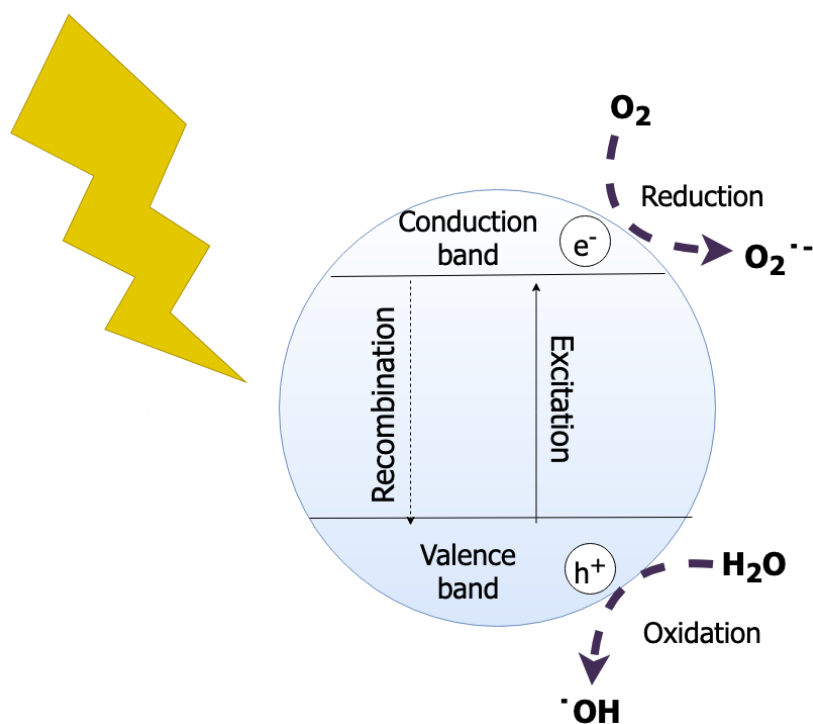
Figure 1.1 General scheme of photocatalyst excitation.

It is important to emphasize that the generated charge carriers, conduction band electrons (e^-) and valence band holes (h^+), need to migrate to the semiconductor's surface, where they can reduce or oxidize adsorbed electron donors and acceptors by interfacial charge transfer and should not recombine extensively in bulk and transform energy to heat. Hence, we need to slow down recombination of electron-hole pairs and extend excitation wavelength to a lower energy range to have better photocatalytic activity [13,14]. The process of photocatalytic oxidation of organic substances might

3

happen directly by a valence band hole before it is trapped within various species or by indirect oxidation [15].

1.2 TiO_2

TiO_2 is widely used in various applications. Firstly, it was used as a pigment; then after the discovery of its photocatalytic character in a nanocrystalline form, it became the most used photocatalyst. Due to its properties such as brightness, high chemical stability in acidic and basic environments, low cost, high refractive index, high dielectric constant, high insulation resistance and nontoxicity, it is used in paints, coatings, plastics, fibers, paper, food, medicine, cosmetics, toothpastes, sunscreens and in many thin-film optical devices [16,17].

In 1913, the first use of TiO_2 as a pigment was reported when it was noticed that coloring of various metal oxides was improved with the addition of TiO_2 [16]. Later on, production of the pigments started in Norway and the United States. In France in 1923 production of pure anatase started. From then on, the production of TiO_2 increased dramatically over the years.

Fujishima and Honda in 1972 discovered the phenomenon of splitting water on TiO_2 electrode under UV light. That was one of the breakthroughs for a new era in heterogeneous photocatalysis [9].

Another significant characteristic of nanosized TiO_2 under UV light, which was discovered by accident in 1995 by TOTO laboratory, is superhydrophilicity, termed "photoinduced amphiphilic surface" [15,18]. The initial water contact angle of several ten degrees drastically decreased upon illumination; the same occurred with some organic liquids [19].

The TiO_2 powder is industrially produced by two procedures: sulfate and chloride process. Most commonly used ores for TiO_2 production are ilmenite ($FeTiO_3$), rutile and anatase ore. Ilmenite ore is mainly used in the sulfate process, while rutile ore or titanium slugs in the chloride process [16].

Depending on the application or required shape of the photocatalyst, sol-gel processing or sputtering can also be applied.

Crystalline structures

Three main crystal structures of TiO_2 are anatase, rutile, and brookite. It is essential that TiO_2 is not amorphous because only crystalline and semicrystalline forms exhibit activity. Stability of TiO_2 can be size dependent; anatase is most stable for particles below 11 nm, rutile above 35 nm, brookite in the middle from 11 to 35 nm [19,20]. For photocatalytic applications rutile and anatase are mostly used, brookite is – because of its difficult fabrication – less investigated. The most popular commercially available photocatalytic TiO_2 powder is P25 (Evonik Degussa), and it is a mixture of rutile and anatase polymorphs, enabling higher activity compared to most other commercial powders. In the case of a single phase, anatase is proven to be more photocatalytically effective polymorph than rutile for the majority of pollutants tested. Anatase has an indirect, whereas rutile has a direct bandgap. Indirect bandgap semiconductors generally exhibit longer charge carrier lifetimes (Figure 1.2) [21].
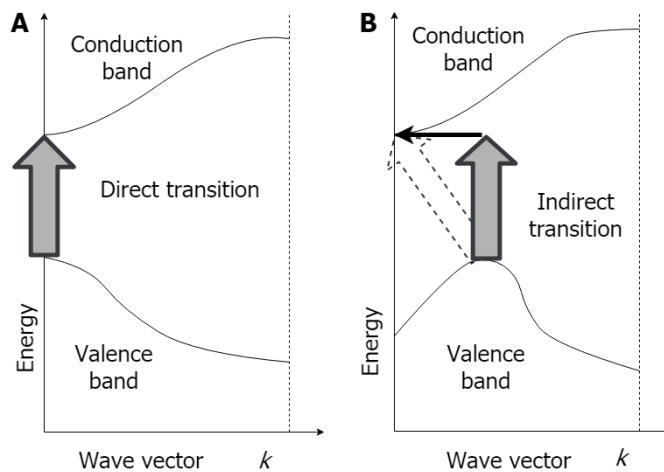
Figure 1.2 Absorption process of light by direct (A) and indirect (B) bandgap semiconductors [16].

It was also confirmed that charge carriers in anatase are excited deeper in bulk, 5 nm for anatase and 2.5 nm for rutile, that is why surface reactions are more pronounced in anatase, and consequently it exhibits better photocatalytic activity [22]. Anatase and rutile have both tetragonal structures, where distortion of the octahedra is slightly larger for anatase. Rutile is the most thermodynamically stable form; anatase phase transforms into rutile under high-temperature heat treatment.

Nanosized TiO_2 is more prone to absorb UV light in comparison to the larger size and is therefore used as a photocatalyst in powder or thin film form [23]. Nanoparticles of

TiO$_2$ are relatively easy to prepare, they are inexpensive, have strong catalytic activity, and these are the main reasons that TiO$_2$ is still the most used photocatalyst worldwide.

Moreover, some studies even prove that micro- or nanosized TiO$_2$ are not photomutagenic or photogenotoxic to humans [24]. As it was already mentioned before, distinct phenomena occur under UV irradiation on nanosized TiO$_2$: photocatalytic activity and photoinduced surface wettability. Main drawbacks of TiO$_2$ that affect photocatalytic efficiency are high electron-hole pairs' recombination and limited activation to UV spectral range.

Photoinduced hydrophilicity of TiO$_2$ layers is ascribed to photoreduction of Ti^{4+} to Ti^{3+} state under UV light (Figure 1.3), which is followed by preferential adsorption of molecular water at some specific oxygen vacant sites on TiO$_2$ surface, new OH groups on the surface area are formed and surface energy increases [15,25]. Afterward, when UV source is removed, the water contact angle on TiO$_2$ surface slowly returns to its initial value, since hydroxyl groups gradually desorb from the surface in the form of H$_2$O$_2$ or H$_2$O + O$_2$ [26] and initial state appears again. It was also observed that thin films with rougher surface exhibit faster transformation from hydrophobic to the hydrophilic character under UV irradiation [26]. TiO$_2$ even has amphiphilic property, which means that it also shows an oleophilicity in combination with hydrophilicity induced by sunlight irradiation [15].
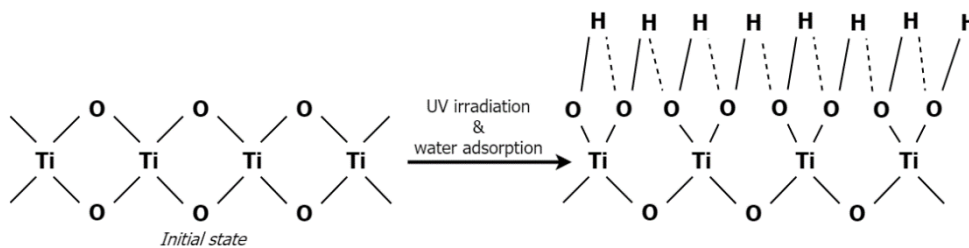
Figure 1.3 Photoinduced superhydrophilic conversion on the TiO$_2$ surface. [15]

1.3 Nanocomposites with TiO$_2$

Modifications of TiO$_2$ are done in order to reach specific goals, whether it be improved absorption of VIS-irradiation, decreased charge carriers' recombination, increased crystallinity or others. In general, we can divide these modifications into two main approaches: **i)** modifying catalyst itself regarding morphology, crystallinity, and

electronic properties; **ii)** combining catalyst with other compounds like grafting, the addition of co-catalyst or dye, doping.

The photocatalytic efficiency of the catalyst can be improved by decreasing the particle size of the photocatalyst, which may bring following consequences: **i)** accelerated redox reactions on a surface; **ii)** distance between photoabsorption site and the surface becomes shorter; **iii)** accelerated recombination of electron-hole pairs [16]. Surface area increases and consequently, the amount of adsorption sites increases. However, downsizing also may have negative effects, such as faster recombination reactions, sensitivity to longer wavelengths decreases due to the quantum size effect. Grinding or ultrasonication are often used as mechanical downsizing methods.

By mixing various crystal phases, one can obtain higher activity than with single phases due to synergism; of course, the proper ratio between phases needs to be achieved. Another crystal structure feature that affects activity is the selection of exposed crystal facets [27], so by manipulating the surface, we can improve the photocatalytic efficiency of the material.

Doping is the process in which the substances (dopants) are introduced inside the crystal; the electronic structure is altered by creating an intermediate state in bandgap and/or narrowing the bandgap. Doping received much attention because, with the help of a dopant, photocatalyst may become responsive to visible light. Most of the present studies are dealing with developing visible responsive photocatalyst. Non-metal dopants such as nitrogen, fluorine, sulfur, carbon, boron are used; their response can be even better if species such as $V^{5+/4+}$, $Fe^{3+/2+}$, $Cu^{2+/+}$ and $Pt^{4+/3+}$ are added. The second group that is also used as dopants are metal ions Cr^{3+}, Fe^{3+}, some rare earth, and noble metals [16]. However, when metal ions are not inside the crystal but bound on the surface, the term used is deposition or grafting. Metal ions become clusters of hydroxides or oxides coupled with the host photocatalyst, depending on the employed method of deposition.

Our goal was to enhance the activity with the addition of another semiconductor, ZrO_2. A coupled photocatalyst's design of nanocomposite relies on its component band structure, which is in general determined by surface area, defect density, crystallinity and quantum size effect [14]. Figure 1.4 shows one of the possible charge-transfer processes involved in coupled semiconductor systems. Electrons photoexcited in the

conduction band of a higher-level semiconductor get injected into the lower semiconductor's conduction band [14].
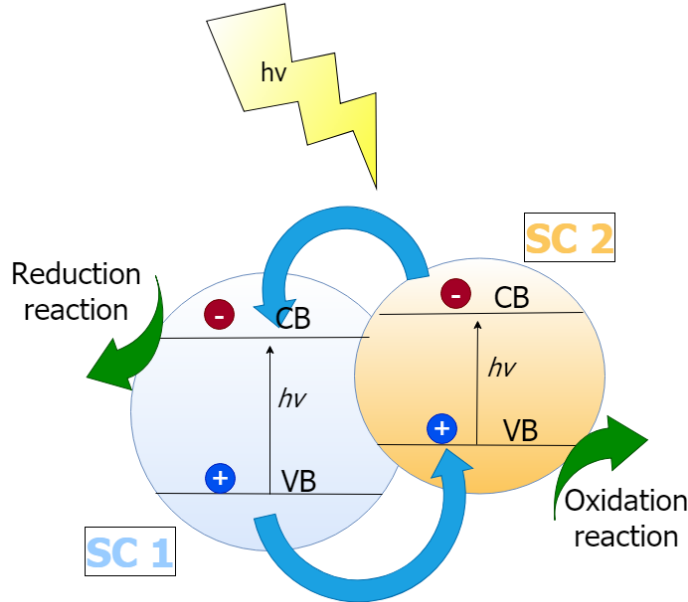
Figure 1.4 Design of charge transfer in a coupled semiconductor system.

Composite with ZrO₂

Among semiconductors that have been used to couple with TiO_2 in order to improve its photocatalytic activity, ZrO_2 is considered to be a good candidate. The Zr-doping of TiO_2 possibly suppresses the recombination of electrons and positive holes by their trapping [28]. ZrO_2 increases the surface area, stabilizes the anatase phase and enables the existence of stable electron-hole pairs [29–36]. ZrO_2 has relatively high permittivity, large bandgap, a high negative value of conduction band potential and excellent thermal and chemical stability [37,38]. The reported bandgap energy range of ZrO_2 is between 3.25 and 5.1 eV, depending on the preparation technique [39]. It has been reported that the addition of small amounts of ZrO_2 into TiO_2 can decrease the particle size of TiO_2 due to the different nuclei, coordination geometry and an increase in the surface area [33,34,40]. Elder et al. [35] found that TiO_2 nanoparticles with added ZrO_2 are stable in size even in the case of calcined samples as confirmed by transmission electron microscopy (TEM). They also found that the included ZrO_2 is amorphous directly after preparation and remains in the amorphous phase after annealing (T = 450 °C). As verified in [41], TiO_2 nanoparticles tend to undergo aging effects when they are stored at room temperature in ambient air. The samples prepared in the study by Elder

et al. [35], especially the annealed samples, were re-investigated six months after their preparation and annealing. While aging phenomena took place in the case of a non-annealed pure TiO_2 sample, room storage did not affect the crystallite size of the TiO_2-ZrO_2 nanocomposites. Even the particle size of the old sample of pure TiO_2 after annealing at 500°C seems to become some nanometers larger than that of the freshly prepared and annealed sample [41]. The ZrO_2-TiO_2 photocatalyst showed a high specific area and small crystal size. The XRD pattern for the Zr/Ti = 0.1 sample indicated that the addition of ZrO_2 stabilized the anatase phase of TiO_2 up to 800°C [42].

Addition of SiO$_2$

Silica (SiO_2) can be found in nature in various polymorph forms, because of various impurities; in the laboratory, it is usually prepared by the sol-gel method [43]. SiO_2 is used as a protective layer between the glass substrate and TiO_2 layer to prevent migration of harmful sodium ions from the soda-lime glass during high-temperature heat treatment [44]. Silica may enhance activity and may also suppress phase transformation from anatase to rutile, improve wear resistance, reduce frictions, improve adhesion to glass [45–47]. SiO_2 has also been reported to pronounce the hydrophilicity of films, which can be maintained even in the dark due to a high number of Si-OH surface groups [48–51]. SiO_2 may act as a binding component, improving adherence to the substrate and commonly as a dispersing agent for TiO_2 nanoparticles [52].

1.4 Synthesis and deposition of thin films

Most of the studies of TiO_2 photocatalysis were made on powder samples in water purification applications, where one of the major limitations is the separation of (nano)powder photocatalyst after treatment. Nanofiltration or some other collecting techniques need to be used so that the photocatalyst is recovered and not released after treatment in the environment.

On the other hand, with immobilization of photocatalyst, the separation technique is avoided. One of the main limitations of an immobilized photocatalyst compared to suspended photocatalyst is a lower surface-to-volume ratio, which can be improved

with porous structures of the photocatalyst or surface modification, among others. The other drawback of immobilized TiO₂ is that the substrate (support) may negatively affect photocatalyst activity.

In comparison to solid-state processes, "soft chemistry" enables to control reaction pathways on a molecular level, allowing synthesis of well-defined and uniform particles, with high purity and homogeneity [53]. However, many reaction parameters need to be taken into account, such as pH, temperature, mixing conditions, oxidation rate, hydrolysis, and condensation rate. In general, resulting precipitates in aqueous sol-gel chemistry are amorphous and need high-temperature annealing, which is the main drawback why it is not used for some thermosensitive materials. Nonetheless, in the case of TiO₂, sol-gel method involving an alkoxide precursor can be modified and the semi-crystalline structure is obtained under low temperature [54].

Sol-gel

Sol-gel (Figure 1.5) is one of the most popular techniques for the preparation of thin films [55]. Sol-gel processes are frequently used because of low process temperature, relatively low costs, the possibility to shape the material in monoliths, films, fibers, and powders that are transformed into ceramic materials, the flexibility of application to the broad range of substrates (sizes and shapes), homogeneity of film. We can roughly divide the sol-gel method into an aqueous and non-aqueous process.

Sol-gel can be simply defined as a formation of solid from solution [53,55]. Inorganic (metal salts – chlorides, nitrates, sulfates) or organic (alkoxide) reactants are used as a precursor. A sol is defined as a colloidal dispersion of particles in a liquid; a gel is defined as a substance that contains a three-dimensional solid skeleton, whose pores entrap liquid phase [55].

Sol-gel process includes five key steps: **i)** dissolution of metal organic precursors in organic solvents that are miscible with water or dissolution of inorganic salts in water to prepare a homogeneous solution; **ii)** transformation of solution into sol by adding a suitable reagent (usually water or its acid/alkaline solution); **iii)** aging, which induces the sol to change into gel by polycondensation; **iv)** shaping gel into the desired form, for example, thin films, spheres, fibers, grains; **v)** thermal treatment [53,55,56].
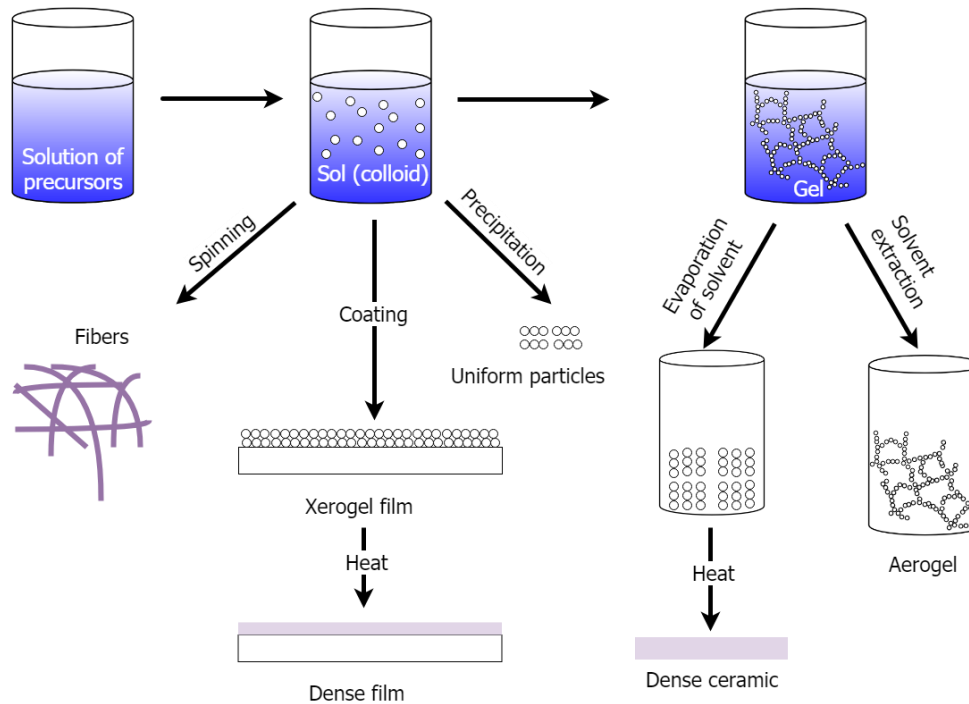
Figure 1.5 Sol-gel process [57,58].

Hydrolysis and condensation run simultaneously during the sol-gel process in most cases. During hydrolysis (Equation 6), metal alkoxide reacts with water and forms metal hydroxide (M-OH). Later on, condensation reactions between two hydroxylated metal species lead to M-O-M bonds under release of water (oxolation, Equation 7), the reaction between hydroxide and alkoxide leads to metal oxide species (M-O-M) bonds under release of alcohol (alkoxolation, Equation 8) [26,55].

The reaction of hydrolysis:

$$Ti(OR)_4 + H_2O \rightarrow HO\text{-}Ti(OR)_3 + ROH \qquad\qquad 6$$
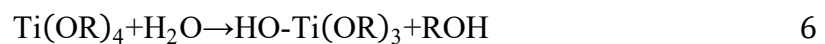
The condensation reaction between metal hydroxide liberates small molecules, such as water or alcohol:

$$(OR)_3Ti\text{-}OH + HO\text{-}Ti(OR)_3 \rightarrow (OR)_3Ti\text{-}O\text{-}Ti(OR)_3 + H_2O \qquad 7$$

$$(OR)_3Ti\text{-}OH + HO\text{-}Ti(OR)_3 \rightarrow (OR)_3Ti\text{-}O\text{-}Ti(OR)_3 + ROH \qquad 8$$
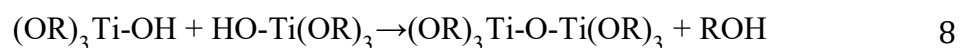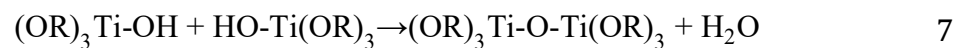
An important role in the sol-gel process is that of water and the molar ratio between water and precursor, which affects the structural progression of the final product. Nature or shape of the product also depends on the type of chosen catalyst. Acidic one is used for thin films – low linkage between branches in gel is obtained, alkaline is used for particles, powders – resulting gel is highly branched [26]. Acids also help to protonate alkoxide groups and boost the hydrolysis reaction kinetics [59] and help with

11

increasing the electrostatic stability of the sol. Of course, there are also other parameters that affect the sol-gel process such as chosen alkoxide and solvent, additives that can be optionally added to reach the desired final product, a timeline of the process, temperature [55]. Sol-gel processing has various applications in the fields of optics, electronics, catalysis, space technology, bio- & chemical sensors, medicine (controlled drug release), fibers, photochromic applications and many others.

Thin films

TiO_2 thin films can be prepared by various methods, like sol-gel, chemical vapor deposition (CVD), flame hydrolysis, sputtering, spray pyrolysis, hydrothermal synthesis, pulsed laser deposition, atomic layer deposition. Producing thin films with sol-gel consists of following steps: preparation of sol from precursor via hydrolysis and condensation, deposition of sol on the substrate, drying and thermal treatment. As it was already mentioned, water to precursor ratio is important. An increased ratio typically results in a thicker film. Lower pH can cause hydrolysis to be faster than condensation, and may also produce thicker films [53]. Advantages of the sol-gel process are low temperature, easiness of coating large areas, optical quality, purity [55]. Most common coating techniques that are used are dip-coating, spin-coating, spray coating, brushing, and these techniques can be applied to various shapes and sorts of substrates. The same as it holds for powder photocatalyst, crystal structure and size of crystals also play an important role in insufficient absorption of light of thin films photocatalyst. Figure 1.6 presents some factors that may influence the film structure. One of the essential requirements for self-cleaning films is that in most cases they should be transparent or should not drastically change the appearance of the substrate, and the film should not deteriorate the lightfastness of the substrate. Lightfastness is a property of a dye or pigment that describes their resistance toward fading under (UV) light.
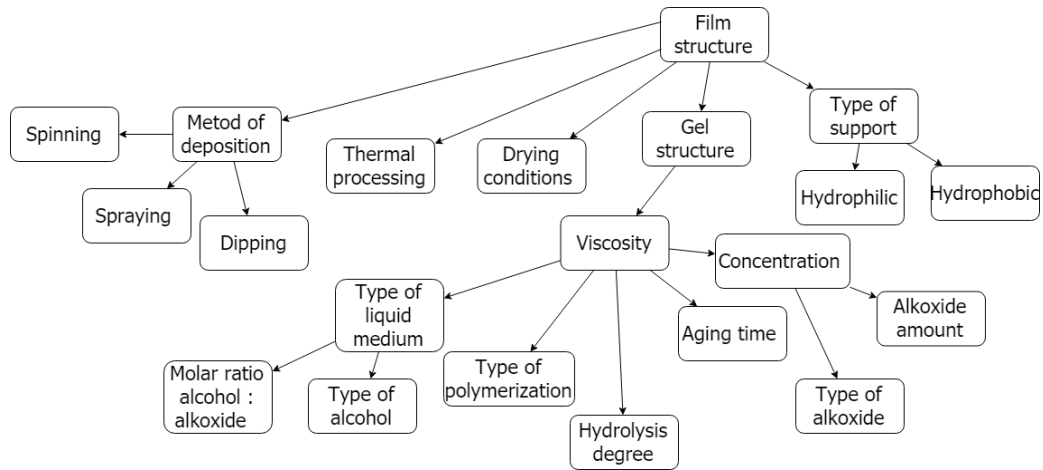
Figure 1.6 Factors that influence film structure [26].

Dip-coating

Dip-coating is a coating technique, during which the substrate is dipped into a sol solution and withdrawn under controlled conditions. Atmosphere conditions control evaporation of the solvent; evaporation leads to gelation process and formation of transparent films due to small particles in the sol. The deposited film needs to be densified by a thermal process; temperature requirements depend on the film's composition [55].

Five steps of a dip-coating process are [16]: (1) dipping substrate, (2) pulling up a substrate, (3) deposition and withdrawing of the substrate, gelation of film, (4) drainage, an excessive solution is flowing down, and (5) evaporation of the solvent (Figure 1.7).
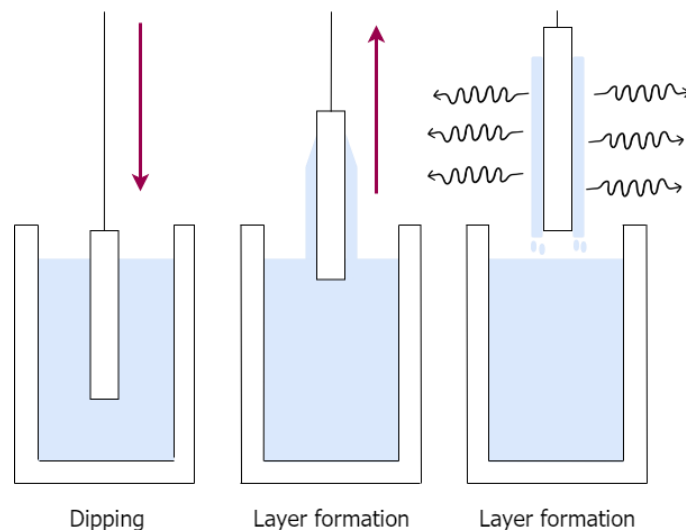
Figure 1.7 Scheme of dip-coating technique. Dipping (step 1), layer formation (step 2,3), solvent evaporation (step 4,5).

13

The thickness of resulting films mainly depends on withdrawal speed, amount of solid phase and viscosity of the deposition solution. Throughout the withdrawing process six forces are acting on a coating [55]: **i)** viscous drag upward on the liquid by moving substrate, **ii)** force of gravity, **iii)** resultant forces of surface tension in the concavely shaped meniscus, **iv)** inertial force of surface tension on the boundary layer liquid arriving at deposition region, **v)** surface tension gradient, **vi)** disjoining and conjoining pressure (significant for films with the thickness under 1 µm).

An interesting characteristic of the dip-coating technique is also that with selecting a sol with suitable viscosity, the resulting film can be thicker, but it can still maintain high optical quality. With dip-coating, films of uniform thickness can be obtained in large quantities.

Spin-coating

Spin-coating is a technique that is used for deposition of films to a flat substrate. A small amount of coating solution is put on a sample's center. The sample is then rotated at high speed, so that coating solution is spread onto a sample by centrifugal force. The spin-coating process is composed of four stages: (1) deposition, (2) spin up, (3) spin-off, (4) solvent evaporation with subsequent gelation [16,26]. Spin-coating is effective for coating smaller scale materials.

Spray-coating

The coating solution is pushed through a nozzle, and very fine droplets are formed and applied onto a substrate. Spray-coating is a fast process in which less sol is needed than in dip-coating. It can be used on intricate shapes and various substrates; that is why it is widely used in the industry. However, it is harder to maintain the thickness and uniformity of the film. The substrate can have room temperature, or it is heated up to a specific temperature, to assure better adhesion.

1.5 Self-cleaning surfaces

In general, the self-cleaning surface is defined as a surface that is capable of keeping itself clean, avoiding the deposition of dirt [26]. Self-cleaning surface got much attention over the years because it may improve lifestyle, reduce pollution with

cleaning supplies, reduce cleaning time, lower maintenance costs, improve cleaning of hard accessible places. That is why self-cleaning technology seems to be promising for various applications such as building glass, vehicle parts, tunnel lighting, household, eyeglass, greenhouses, solar panels, traffic signs, mirrors, public screens, in the textile industry, electronic devices, drug delivery systems, and many others. Therefore, many studies have been made recently for fabricating surfaces and understanding mechanism of self-cleaning property. First self-cleaning window panes were produced in 2001 by Pilkington Glass company, the product was called Pilkington Activ™, and was made by a chemical vapor deposited nanocrystalline TiO_2 [26].

Natural self-cleaning surfaces work by interfacial wettability or interfacial force action [26]. Interfacial wettability can be determined by contact angle and hysteresis. Some models have been used for interpretation of wettability (Figure 1.8).
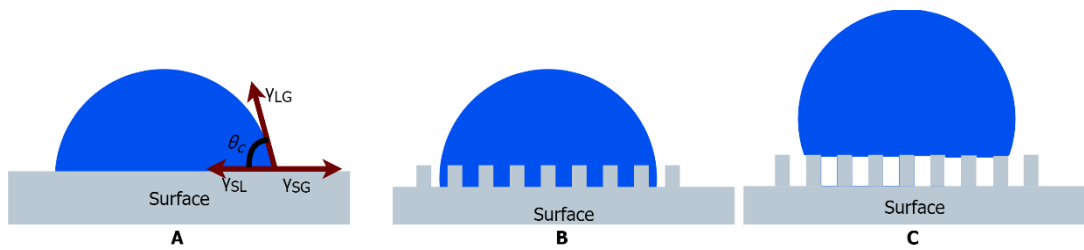
Figure 1.8 Liquid droplet in the Young (A), Wenzel (B) and Cassie model (C).

Young's model (A, Figure 1.8) is one of the most known and is describing the state on an ideal rigid surface with Young's equation (Equation 9):

$$\gamma_{SG} = \gamma_{SL} + \gamma_{LG} \cos \theta_C \qquad\qquad 9$$

θ – contact angle, γ_{SG} – interfacial surface tension between solid and gas; γ_{SL} – interfacial surface tension between solid and liquid; γ_{LG} – interfacial surface tension between liquid and gas

Contrary to Young model, Wenzel model (B, Figure 1.8) defines wetting on a rough surface by the following equation:

$$\cos \theta_W = r \cos \theta_Y , (r \geq 1) \qquad\qquad 10$$

θ_W – apparent contact angle, θ_Y – Young's contact angle, r – surface roughness factor (ratio of an actual surface area and an apparent area)

Wenzel model shows a relation between surface tension and structure of a homogeneous surface. As we can see in Figure 1.8, an actual surface area is greater

than apparent; that is why r factor is greater than 1. This model can be only applied to the thermodynamically stable surface and this is one of the model's limitations.

For a heterogeneous surface Cassie-Baxter model is proposed (C, Figure 1.8) by the following equation:

$$\cos\theta_c = f_1\cos\theta_1 + f_2\cos\theta_2, (f_1 + f_2 = 1) \qquad 11$$

θ_c – apparent contact angle in C-B model, θ_1 and θ_2 – intrinsic contact angles of components, f_1 and f_2 apparent area fraction

Hydrophilic and hydrophobic principle

There are two main principles of self-cleaning phenomenon, hydrophobic and hydrophilic. Photocatalysis is usually associated with hydrophilic surfaces, like in the case of titania. On (super)hydrophilic surfaces water spreads over the surface, whereas on (super)hydrophobic one water forms round droplets. The contact angle between surface and water can hence describe the character of the surface. When contact angle (CA) is below 90 degrees it means that surface is hydrophilic, when it is below 5 ° it is named superhydrophilic; when CA is higher than 90 degrees surface is hydrophobic, and it is superhydrophobic when the contact angle is over 150 degrees [26]. On hydrophobic self-cleaning surfaces water forms droplets, while rolling down, they also take the dust and dirt particles; on hydrophilic self-cleaning surfaces, water is homogeneously spread over the surface and also carries away the dirt [26,60]. Inspiration for making self-cleaning surfaces was acquired from nature, where few plant and animal species exist that have a surface with a self-cleaning mechanism. One of the most known are lotus leaves; water droplets roll off the leaf surface taking with it the dust and dirt particles. Inspired by it, numerous surface modifications imitating its structure to achieve superhydrophobic property were acquired.

Various methods are used to produce self-cleaning surface using bottom-up or top-down approach: chemical etching, laser etching, plasma etching, wet chemical reaction, hydrothermal reactions, electrochemical deposition, lithography, self-assembly and layer-by-layer (LBL) methods, electrospinning, chemical vapor deposition, physical vapor deposition, a sol-gel method, polymerization reaction, *etc.* Surface geometrical micro/nanostructure and low surface energy are two main features of self-cleaning surfaces. On isotropic superhydrophobic surfaces, droplets can roll off a surface in any direction, in contrast to anisotropic superhydrophobic surfaces in

which surface structures are arranged along one direction, and consequently, droplets roll off in this specific direction. In nature, isotropic hydrophobic surfaces are lotus leaves and cicada wings; anisotropic surfaces are rice leaves, duck feathers, goose feathers, and butterfly wings.

Superhydrophilic self-cleaning surfaces can also be found in nature. Many underwater creatures have superhydrophilic and oleophobic properties, fish scales, shark skins, snail shells, and pilot whale skins, and this inspires researchers to fabricate underwater self-cleaning and antifouling surfaces [26].

The third principle of self-cleaning action is either sole photocatalysis or combined superhydrophilicity and photocatalysis, where the latter additionally decomposes dirt components.

TiO_2 self-cleaning mechanism

Self-cleaning action of TiO_2 is a combination of photocatalysis and photoinduced superhydrophilicity; dirt is removed by a uniform spreading of water over the whole surface and by photocatalytic decomposition of organic contaminants [61]. When nanosized TiO_2 is irradiated with light of the appropriate wavelength, the wettability of a surface is increased in such a way that the water no longer forms droplets but a continuous film instead. In other words, under irradiation, the contact angle of water on these surfaces drops to virtually 0 ° [17]. This effect, known as photoinduced superhydrophilicity, is closely related to the photocatalytic activity in the sense that it originates from electron-hole pair formation; although not all the photocatalytically active materials present photoinduced superhydrophilicity behavior and vice versa [1,25]. TiO_2 also has an oleophilic surface under irradiation (it lasts a few hours after stopping irradiation); this amphiphilic effect is a particular feature of TiO_2 [15]. The superhydrophilicity is also reversible, so after irradiation stops, contact angle recovers to its initial value [62]. Addition of silica can prolong the hydrophilicity of the TiO_2 surface in the dark [63]. The rough surface of TiO_2 coating enables a faster transformation from hydrophobic to a hydrophilic surface under UV irradiation [26].

The combination of photocatalytic and photoinduced superhydrophilic properties opens up a massive range of applications for nanosized TiO_2, for example, antifogging glass and mirrors, antibacterial sanitary surfaces, self-cleaning construction materials

(self-cleaning ceramic tiles, pollutant-abating paints, asphalt, and cement) and even odor eliminating textile [1]. The photoinduced superhydrophilicity effect has also been proposed as a way to cool down the surface of buildings and therefore, reduce the energy consumption for air conditioning [64].

Outdoor conditions limit self-cleaning applications; TiO_2 requires a significant level of UV irradiation and weather conditions (rain). Therefore, it is beneficial to develop self-cleaning films that have extended response into a visible part of the solar spectrum.

1.6 Antimicrobial properties

Antimicrobial agents are substances that inhibit the growth of or kill microorganisms [65]. Almost all surfaces can be a suitable basis to grow microorganism at the proper humidity and temperature. For example, patches of mold or mildew on indoor walls can affect the respiratory health of the occupants. This problems and other factors accelerate the development of antimicrobial agents that are effective and not harmful to humans. However, many antimicrobial agents have been avoided because of their possible harmful or toxic effect [7].

Photooxidative processes that occur under the illumination of photocatalytic thin films produce reactive oxygen species (ROS). Hydroxyl radicals not only degrade organic molecules but can also damage cells of bacteria, viruses, algae, fungi, protozoa, and bacteriophage [65,66]. The exact process of antibacterial action is not fully known, but oxidative species probably attack outer and inner cell membranes – DNA can be damaged by hydroxyl radicals [67,68]. Sunlight itself also has a bactericidal effect [69], but total disinfection by solar, UVC or UVA irradiation is not always possible, and microorganisms can recover if inactivation is incomplete [70]. It was reported that 99,99 % reduction of *Escherichia coli* could be reached on TiO_2 samples under visible light irradiation [71].

Thin films for antimicrobial application should have similar properties as self-cleaning thin films: **i)** long-term photocatalytic activity, **ii)** good adhesion to a substrate, **iii)** mechanical stability and **iv)** capability to inhibit or reduce microorganisms under sunlight or indoor light [2].

Colony count method is the most common method used for assessment of antimicrobial photocatalytic activity. However, the antimicrobial effect can also be tested by fluorescence and colorimetric methods, which enable observing viability, membrane integrity, metabolic activity, specific components of cells. The critical parameters of methods are the sensitivity, the reproducibility, and the dynamic range. An important parameter is also a timeline of an experiment to collect data and reliable results. Highly desirable are methods that can assure reliable results in a short period [72] and are accomplishable within a given laboratory that has available instrumentation and knowledge [2].

Application of a particular method also depends on the shape of photocatalyst; testing methods need to be designed and adjusted to assess different photocatalytic materials in relevant testing conditions optimally. Most standardized methods are still based on counting the number of the colonies (CFUs – colony forming units) growing before and after the treatment since bacterial cell proliferation is directly correlated to their physiological condition. It is a straightforward and direct method, but also gives a little information about sub-lethal injuries that can suspend or prevent cell recovery and it cannot be used for the evaluation of bacterial growth kinetics [72]. The results can be expressed by the log reduction or by reduction percent. When reduction is less than 20 % it means that there is no significant efficiency, from 50 to 70 % it means that material has a significant bactericidal effect, for reduction value greater than 70 % it means that material has a powerful antibacterial effect [73]. Main disadvantages of colony count method are **i**) method is less suitable when compared photocatalysts do not differ much in terms of activity, **ii**) low sensitivity and accuracy of method because it gives data about cells that can form colonies and does not give information about cell impairments where growth is delayed. To meet requirements and keep standards, we consider only plates that have from 30 to 300 colonies and great care must be taken during dilution and planting to ensure the accuracy of results [72]. Hence, if possible, a combination of standard colony count plate method and fluorescence or colorimetric methods are desirable in order to gain accurate results of the assay [2].

The potential use of photocatalytic thin films for antimicrobial applications is self-disinfecting surfaces for sanitary, food packaging, food preparation surfaces, indoor walls, textiles, water disinfection, health and medical care products, medical devices, air-conditioning filters.

1.7 Environmental point of view

Here, I briefly describe two sides of titania effect on the environment, firstly how nanosized titania can help to clean wastewater, air or surfaces; and secondly how titania can have a negative effect on the environment, human and/or animal health.

TiO_2 photocatalysis is categorized as an advanced oxidation process (AOP). In general, AOPs are chemical treatment methods in which organic materials are removed by oxidation with highly reactive hydroxyl radicals. One of the main advantages of AOPs is that they are highly effective at ambient temperatures and normal pressures.

One of the concerns of pollutants photodegradation is that after or during the decomposition process, we cannot assure that the final products are not toxic. They can be even more dangerous than the parent compounds. We do not know how pollutants affect each other, especially when going from lab scale to real applications, the exact composition of pollutants is not known, they can vary because of weather, location and other conditions.

Nanoparticles (NPs) are not something new, they have been present in the environment throughout the earth's history, but in the last years the production of synthetic nanoparticles grew, and many more applications are implemented which are leading to a release of NPs [74,75]. Moreover, the same properties that make them superior may, on the other hand, pose a considerable risk to our health and environment. Detection of NPs is not easy, advanced instrumentation is needed, or the detection of NPs is delayed because equipment cannot be brought to the source of exposure [76]. That is why some alternative methods, sensors are being invented to measure the actual negative effect of NPs on the ecosystem (*e.g.,* plate-based sensor). Risk assessment requires understanding mobility, reactivity, toxicity and persistence of nanoparticles [75].

TiO_2 NPs are widely used in paints, lacquers, sunscreens, plastics, inks, papers, creams, lip balms. TiO_2 is also a food colorant, and it is commonly used as a food additive marked as E 171, although here TiO_2 is not primarily used in nano size, but could contain NPs [77,78]. So, "free" nanosized particles of TiO_2, like NPs of any other material, represent a threat to our health. TiO_2 was also classified as a possible carcinogen to humans (IARC: Group 2B) after it was found carcinogenic for testing animals [79,80].

One of the ways to prevent leaking of TiO_2 photocatalyst into the environment during application is immobilization, which usually means a slight decrease in activity, surface area and reactivity. However, with the proper design of the photocatalysts and reactors, high activities could still be achieved.

2 RESEARCH GOALS

Hypotheses of the thesis were the following:

o Despite low-temperature synthesis and the low-temperature heat-treatment, photocatalytically active transparent films will be obtained.

o Coupling TiO_2 with ZrO_2 will improve the photocatalytic activity of thin films.

o Successful immobilization of the same kind of films deposited on glass substrates can be done on thermosensitive substrates as well.

The main goal of Ph.D. work was to prepare TiO_2-ZrO_2 photoactive and transparent nanocomposites that would result in self-cleaning and anti-fogging properties of the surfaces. The plan was to prepare TiO_2 film and TiO_2 with various ZrO_2 content. Firstly, we decided to add ZrO_2 for enhancement of TiO_2 activity; results did not confirm this hypothesis, but we discovered other benefits. SiO_2 was added later on because TiO_2-ZrO_2 did not form uniform films. Thin films were prepared on a glass substrate, polymethyl methacrylate sheet, polyvinyl chloride sheet and two different membranes for air-supported buildings. We deposited the films by the dip-coating technique.

The main objectives of the Ph.D. work were:

a) Preparation of the following novel nanocomposites based on sol-gel synthesis: **i)** TiO_2-ZrO_2, with a 5, 10 and 20 molar percent of Zr with respect to Ti; **ii)** TiO_2-ZrO_2-SiO_2, with a 5, 10 and 20 molar percent of Zr with respect to Ti, silica concentration was kept the same in all solutions; **iii)** TiO_2, TiO_2-SiO_2 sols were prepared as a reference.

b) Optimization of layers on different substrates: glass, textile, plastic – thermosensitive materials.

c) Characterization of the as-developed materials using various techniques (SEM, UV-VIS, FTIR-ATR, XRD, TGA-DSC, DRS, LBDS, pencil hardness test).

d) Investigation of photocatalytic activity with different methods and its correlation with materials characteristics determined by the techniques mentioned above.

e) Determination of antimicrobial properties of films by counting colony method, with *Escherichia coli* and *Staphylococcus aureus*.

f) Toxicity test with *Daphnia magna*.

3 EXPERIMENTAL

3.1 Chemicals and substrate description

Listed below are the chemicals that were used for sample preparation and characterization:

1-propanol (Sigma-Aldrich), 2-propanol (Carlo Erba), 2-propoxyethanol (Sigma-Aldrich), 4-hydroxy-2,2,6,6-tetramethylpiperidine (Tempol, Sigma-Aldrich), Agar (Sigma-Aldrich), Calcium chloride-2-hydrate (Fluka), Ethanol 96 % (Itrij), Ethanol absolute (Carlo Erba), Free radical 4-oxo-2,2,6,6-tetramethylpiperidine N-oxyl (Tempone, Sigma-Aldrich), Hydrochloric acid 37 % (Carlo Erba), Hydroxyethyl-cellulose (Fluka), Levasil 200/30 % (Obermeier), Magnesium sulfate-7-hydrate (Fluka), Methyl stearate 97 % (Aldrich), NaOH (VWR), n-hexane (VWR), Peptone from soybean (Biolife), Perchloric acid 70 % (Sigma-Aldrich), Potassium chloride (Fluka), Resazurin (Sigma-Aldrich), Silicone grease (Merck), Sodium chloride (AppliChem), Sodium hydrogen carbonate (Fluka), 5,5-dimethyl-1-pyrroline N-oxide (DMPO, Sigma-Aldrich), Terephthalic acid (Alfa Aesar), Tetraethylorthosilicate 98 % (Acros Organics), Titanium tetraisopropoxide 98 % (Aldrich), Toluene SeccoSolv® (Merck), Yeast extract (Fluka), Zirconium tetrabutoxide 80 wt.% (Aldrich).

Glass substrate

Microscopic glass slides from two different manufacturers were used, Lab Logistics Group GmbH (Germany) and Menzel-Gläser (Germany). Both have low iron content. Slides had cut edges and no frosted end. Dimensions of the glass slides were 26 mm $\times$ 76 mm $\times$ 1.0 mm.

PMMA (Polycasa® CAST)

We used cast polymethyl methacrylate sheets from Polycasa®. PMMA substrate is composed of 90 - 95 % PMMA and 10 - 5 % of additives, as stated in the technical data sheet [81]. Additives are stabilizers, plasticizers, dyes & pigments, release agents. A shortened list of characteristics is collected in Table 3.1. PMMA sheets are used for various applications, such as signs, displays, furniture, sanitary fittings, gift articles, shop fittings, solariums. Dimensions of samples that were used in this work were 80 mm $\times$ 40 mm $\times$ 3.0 mm.

Table 3.1 Characteristics of PMMA substrate from the technical data sheet.

	Property	**PMMA**
General	Density	1.19 g/cm^3
	Water absorption	0.2 %
Mechanical	Tensile strength	75 MPa
	Elongation	6 %
	Tensile modul	3400 MPa
	Flexure strength	120 MPa
	Flexure modul	3200 MPa
Thermal	Vicat temperature	110 °C
	Specific heat capacity	2.16 J/g K
	Linear thermal expansion	0.07 mm/m °C
	Thermal conductivity	0,19 W/m K
	Max. service temperature continuous	80 °C
	Max. service temperature short term	90 °C
	Degradation temperature	>280 °C
Optical	Light transmission	92 %
	Refractive index	1.492

PVC

PVC sheet Polikristal (Tekniglass) from Polimark was used. Polyvinyl chloride is a thermoplastic polymer, and it is one of the most used plastics in the world after polyethylene. It is used for clothing, pipes, insulating materials in electrical wire, bottles, packaging, medical tubing, blood bags, PVC window frames, garden hoses, traffic cones. Some of the properties are listed in Table 3.2.

Table 3.2 PVC characteristics.

Property	**PVC**
Tensile strength	2.60 N/mm^2
Notched impact strength	2.0 – 45 KJ/m^2
Thermal coefficient of expansion	80×10^{-6}
Maximal constant use temperature	60 °C
Density	1.38 g/cm^3

D1 (T2103) and D2 (B6105)

Substrates D1 and D2 are both from the same manufacturer, Sioen Industries NV, Belgium. They have the same base, polyester fabric coated with PVC and acrylic coating. However, D1 has an additional top lacquering SIOFLUO. This polyvinylidene

fluoride (PVDF) top coat is hydrophobic and improves dirt repellency and enables simpler cleaning. Some characteristics of D1 and D2 are listed in Table 3.3.

Table 3.3 Characteristics of D1 and D2 substrate summarized from a technical data sheet.

Property		D1 (T2013)	D2 (B6105)
Fabric		100 % polyester	100 % polyester
Weaving style		P2/2	P2/2
Weight		900 g/m^2	900 g/m^2
Fabric coat		PVC/acrylic	PVC/acrylic
Lacquering		SIOFLUO	/
Embossing		Glossy	Glossy
Breaking strength	Warp	4000 N/5 cm	4000 N/5 cm
	Weft	4000 N/5 cm	3500 N/5 cm
Tear strength	Warp	600 N	600 N
	Weft	500 N	500 N
Adhesion		120 N/5 cm	100 N/5 cm
Temperature resistance		from - 30 to 70 °C	from - 30 to 70 °C
Fire behavior		M2/B1	M2
Application		Tent and Tensile architecture	Buildings and industrial doors

Bacteria

Two kinds of bacteria were used for antimicrobial activity tests, *Escherichia coli* (*E. coli* K12 (DSMZ 498)) and *Staphylococcus aureus (*DSMZ 1104*)*. The cultures were acquired from the German Collection of Microorganisms and Cell Cultures – DSMZ (Germany).

3.2 Synthesis and thin film preparation

The primary sol was prepared by following the idea of low-temperature preparation of anatase films [40,82]. 15 mL of titanium tetraisopropoxide (TTIP) and 2.5 mL of absolute ethanol (EtOH) were mixed in a flask (Figure 3.1). Depending on the pre-determined Zr/Ti ratio, zirconium tetrabutoxide (ZTB) was added (0, 5, 10 and 20 mol. %) to TTIP and EtOH. The mixture was then stirred for at least 90 minutes. Separately in a beaker, 45 mL of deionized water and 1 mL of perchloric acid were mixed. This HClO$_4$ solution was then dropwise added to the alkoxide solution. When the solution was thoroughly mixed, hydrolysis and condensation exothermic reactions of metal

27

alkoxides took place, resulting in a white precipitate of hydrated amorphous TiO_2 and ZrO_2.
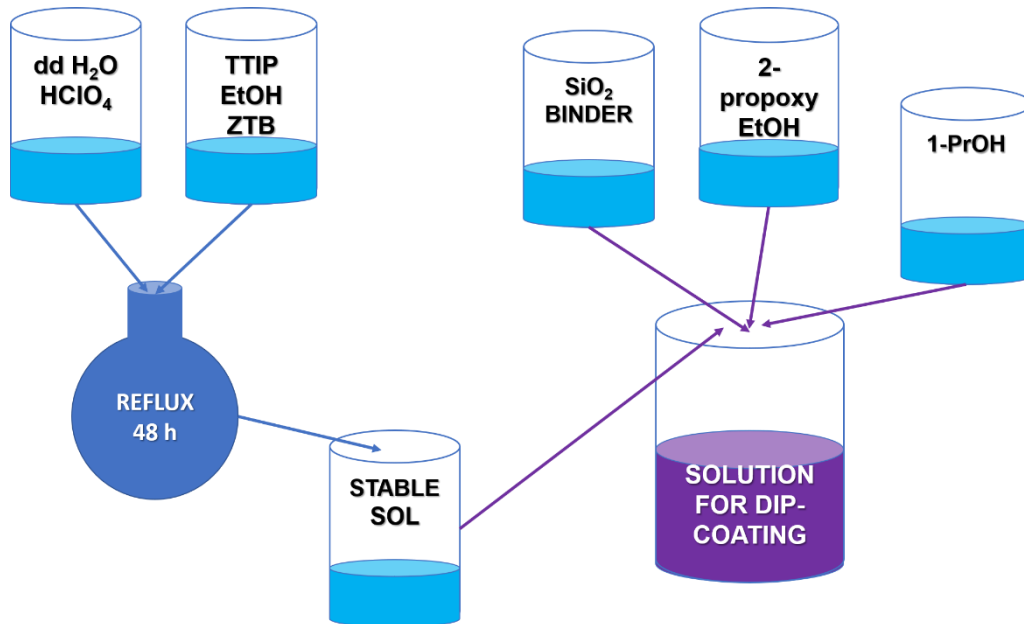
Figure 3.1 Sol-gel synthesis of colloidal solutions for dip-coating deposition.

Flask with the sol solution was then put into fabric heating mantle, heated up to around 85 °C and kept under reflux conditions for 48 hours. During reflux, the solution was continuously stirred, and the temperature was kept constant at around 75 °C. After that, a stable nanocrystalline sol was obtained (Figure 3.2).

Solutions were named by molar concentration of zirconium versus titanium, Ti0Zr – solution without zirconium (0 %), Ti5Zr – solution with 5 % of zirconium, Ti10Zr – solution with 10 % of zirconium and Ti20Zr – solution with 20 % of zirconium.
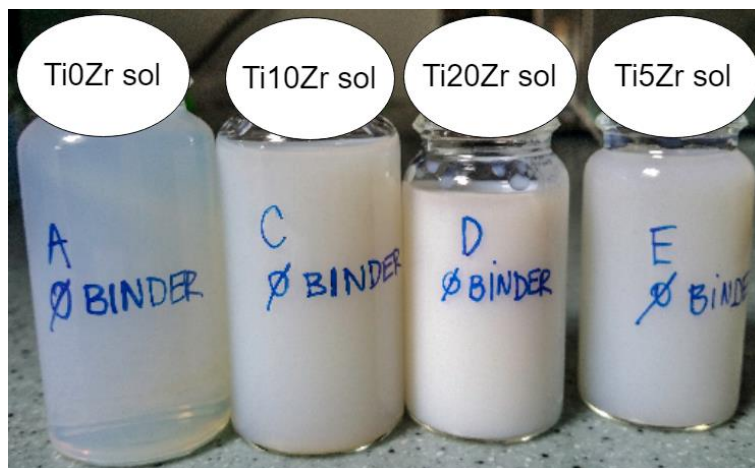
Figure 3.2 Sol solutions of TiO_2 after 48 hours of reflux.

Preparation of SiO₂ binder

SiO₂ binder solution was prepared by mixing 1.11 mL of tetraethyl orthosilicate (TEOS) and 1.7 mL of colloidal silica (Levasil 200/30 %), into which 30 µL of 37 % HCl was added under stirring. After one hour, 5 mL of 2-propanol was added, and the solution was left to stir for at least 12 hours so that TEOS underwent sol-gel reactions. On the contrary to primary titania-zirconia sol, the silica binder solution was not stable for long terms (maximum two weeks) and was therefore freshly prepared for each batch of experiments. The role of silica binder was to provide better mechanical and adhesion properties with higher optical transparency of the thin films.

Preparation of thin films

The final diluted solution for deposition of thin films (Figure 3.3) was prepared with 6 mL of primary sol solution, 6 mL of silica binder, 8 mL of deionized water, 12 mL of 1-propanol and 39 mL of 2-propoxyethanol.

In order to improve thin films quality, SiO₂ binder and various solvents (alcohols) are added. The synthesis protocols described in the dissertation are already results of prior experiments with varying amount of binder and solvent composition to prepare sols that give thin films with best optical quality. Similarly, number of dip-coating depositions and withdrawal speed were varied to find the optimum conditions.
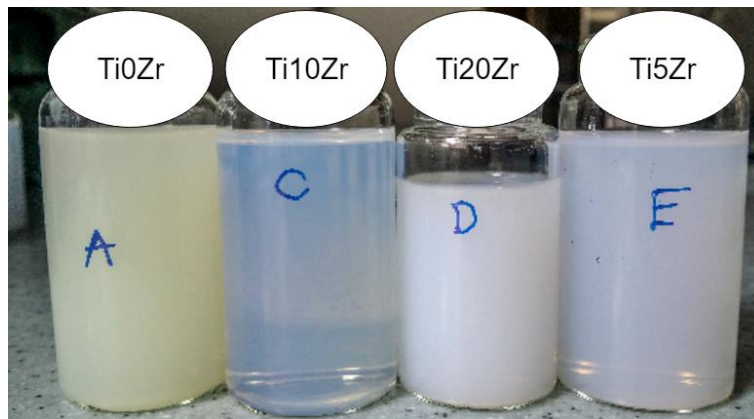
Figure 3.3 The final diluted sol TiO₂-ZrO₂ solutions prepared for the dip-coating.

Before deposition of sols on glass slides, the substrates were thoroughly cleaned using detergent, rinsed with distilled water and ethanol, dried with a blow dryer. Thermosensitive substrates were first cut to dimensions 80 mm × 40 mm and then thoroughly washed in the same manner as glass substrates.

Thin films were deposited by the dip-coating technique. We used a homebuilt dip-coating apparatus; a substrate was fastened with a crocodile clip and submerged with constant speed 100 mm/min into a beaker with the final sol solution. The substrate was pulled out with the same constant speed (100 mm/min) to form a thin film, which was then dried with a blow dryer. Glass samples were put into a furnace (EUP-K 6/1200, Bosio) at 150 °C for one hour, whereas films on thermosensitive materials were fast dried with heat-gun (Black&Decker) for 30 seconds on each side from *ca.* 30 centimeters distance. On every substrate, three layers of photocatalyst were deposited, drying and thermo-fixing were repeated in between each deposition. In the case of glass samples, after the third layer deposition, they were heat treated for 3 hours at 150 °C. Figure 3.4 shows finally deposited films with three layers on glass, PVC and D1 substrates.
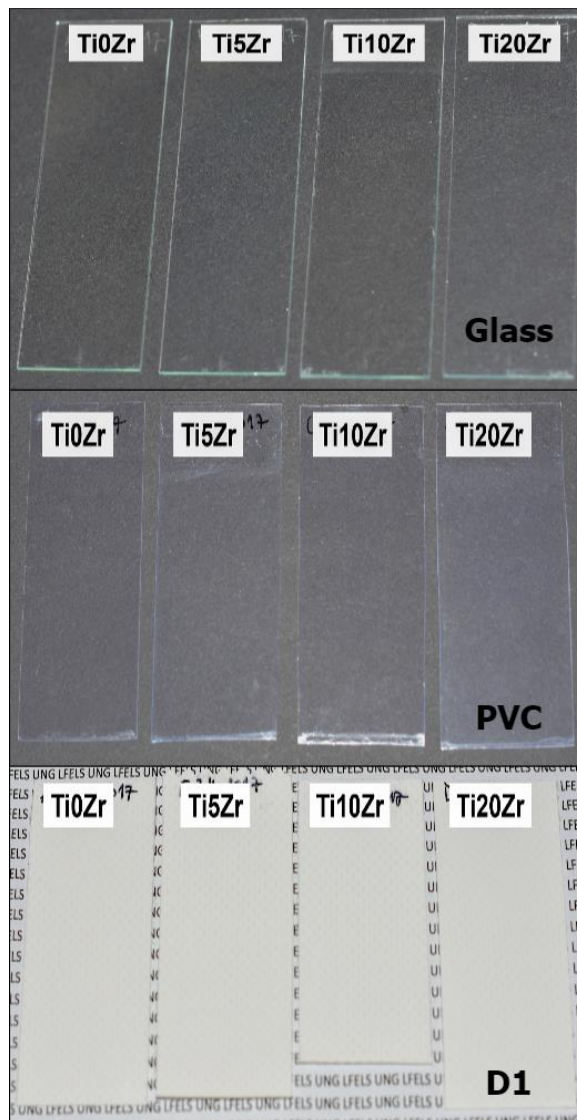
Figure 3.4 Thin films on some of the substrates.

The films were labeled according to their nominal Zr content with respect to Ti, namely TiXZr, where X stands for the molar percentage of Zr vs. Ti (0, 5, 10 or 20). Films labeled TiXZr also contain SiO_2, but it is not specially denoted in labels.

3.3 Materials characterization

3.3.1 X-ray powder diffraction

Powder samples that were used for X-ray powder diffraction analyses were prepared first by drying layers of the sols in Petri dishes at ambient conditions for the excess liquid to evaporate and then by final drying of xerogels at 150 °C for few hours.

X-ray powder diffraction (XRD) patterns were obtained with RIGAKU MiniFlex 600 (Rigaku) apparatus with the copper source, providing X-rays of the wavelength of 1.54 Å. The diffraction data were collected in the 2θ range of 20 – 80 °. For each analysis around 50 mg of powder was used. From the XRD data, size of nanocrystalline anatase particles was calculated by the Scherrer equation (Equation 12).

$$d = K \times \frac{\lambda}{B \cos \theta} \qquad\qquad 12$$

d is crystallite size [nm], λ is a wavelength of the incident beam [nm], B is full width at half maximum (FWHM), θ is Bragg angle [rad], K is Scherrer constant related to crystallite shape (0.89).

3.3.2 Ultraviolet-visible spectroscopy

UV-Vis transmission spectra of transparent substrates and thin films in the range from 200 to 800 nm were collected using LAMBDA 650 UV/Vis spectrophotometer (PerkinElmer). Diffuse reflectance spectroscopy (DRS) measurements of the powder analogs were performed on the same instrument and were used to determine photocatalysts bandgap values. Powder samples were prepared the same way as in the case of XRD measurements.

The indirect bandgap was determined by the Kubelka-Munk model from the plot $(F(R)*h\nu)^{1/2}$ vs. hν, where F(R) is [83–85]:

$$F(R) = \frac{(1 - R_\infty)^2}{2R_\infty} \qquad\qquad 13$$

$$R_\infty = (R_{sample} / R_{standard})$$

3.3.3 Infrared spectroscopy: attenuated total reflection

FTIR is a technique that is used for identification of functional groups present in the liquids or solids by measuring infrared spectra in absorption (or transmission) or reflection mode. FTIR spectrometer converts raw data into a spectrum using Fourier transform. ATR accessory makes FTIR technique user-friendly because there is no need for special sample preparation (*e.g.,* KBr pellets or oil suspensions); it offers fast and easy to-clean accessories – a diamond ATR crystal was used in our case.

Spectra were obtained in the frequency range from 4000 to 400 cm^{-1} by Perkin Elmer 100 with GladiATR™ Single Reflection ATR Accessory (PIKE Technologies). Powder samples, substrates, thin films on substrates, and aged D1 samples were recorded on this instrument.

3.3.4 Laser beam deflection spectroscopy

The laser beam deflection spectroscopy (LBDS) [86] technique was performed using the lab-built experimental setup that is presented in Figure 3.5. The sample is illuminated by intensity modulated light beam (pump beam) [86] from a solid state laser (Coherent, OBIS 455) with 450 nm and 50 mW of output wavelength and power, respectively. It is modulated by mechanical chopper (SCITEC INSTRUMENTS, Control unit model 300C, chopping head model 300CD, chopping disks model 300H, Scitec Instruments Ltd), and heats the sample perpendicularly to its surface. The sample is placed on a three-dimensional (3D) translation stage (CVI, Model 2480M/2488) to vary its position in x, y, and z-direction and to optimize the experimental configuration. The absorbed energy induces temperature oscillations (TOs) not only in the sample but also in its surroundings. The TOs are probed by He-Ne laser beam (probe beam) of 632.8 nm output wavelength and 2 mW output power (Model 25-LGR-393-230, CVI MELLES GRIOT). The interaction of probe beam (PB) with TOs results in PB intensity change that is detected by a quadrant photodiode (Model C30846E, RBM–R. Braumann GmbH) equipped with an interference filter (Edmund Optics) and connected to the lock-in amplifier (Stanford research instruments, Model SR830 DSP).

The amplitude and phase of the signal are collected as a function of the modulation frequency of the pump beam for the samples. Furthermore, both the amplitude and phase of the BDS signal are sensitive to optical properties (energy bandgap) of the examined samples, what allows for determining its value based on the least-squares method of fitting the theoretical curve to the experimental data [86].
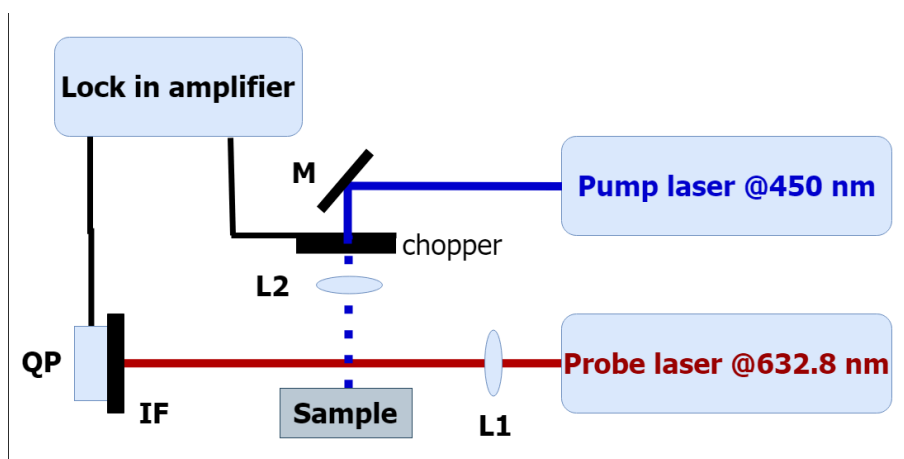
Figure 3.5 Schematic presentation of LBDS experimental setup. L1, L2 - lenses; M - reflecting mirrors; IF - interference filter; QP - quadrant photodiode.

3.3.5   Thermogravimetric analysis – differential scanning calorimetry

For thermogravimetric analysis, the powder analogs were used that were obtained at ambient conditions after releasing solvents (without drying at 150 °C like for all other samples in powders or thin film form). Thermogravimetric curves were recorded from 40 to 600 °C with TGA/DSC 2 STARᵉ System, Mettler Toledo. DSC measurements of the samples were simultaneously performed. Thermogravimetric analysis of thermosensitive substrates was performed on a Mettler Toledo TGA/DSC1 instrument.

3.3.6   Multi-point BET specific surface area

Both dried and heat-treated 150 °C powder samples were measured. However, due to the sample preparation procedure for BET characterization – samples were outgassed under vacuum for 3 hours at 423 K (150 °C) before measurement – there was no significant difference between dried and heat-treated samples of the same kind.

Multi-point BET specific surface area of powder samples was determined with Quantachrome NOVA 2200e, by measuring the nitrogen adsorption-desorption isotherms at 77 K.

3.3.7 Film thickness

Thickness measurements of the films on glass substrates were performed at Rowan University (NJ, United States) on Ambios XP2 Profilometer, Ambios Technology, Inc., during my visit in the frame of the bilateral project (BI-US/15-16-080) with the USA.

3.3.8 Scanning electron microscopy

Images of thin films on glass substrate were taken on scanning electron microscope JEOLJSM 7001 TTLS (FEG) with CL. Samples were sputtered with gold/palladium before scanning. The scanning electron microscope was operating at 20 kV.

Images of films on thermosensitive substrates were obtained on a Zeiss Supra 35 VP microscope (Carl Zeiss NTS GmbH) operating at 1 kV. The samples were pre-coated with carbon (approx. 8 nm).

3.3.9 Pencil hardness test

The mechanical scratch resistance of the films was determined by a pencil hardness test (ISO15184:1998) using Elcometer 501 (Elcometer Instruments). Fourteen pencils were used from very hard 6H to very soft 6B (Faber Castell 9000) (Figure 3.6).
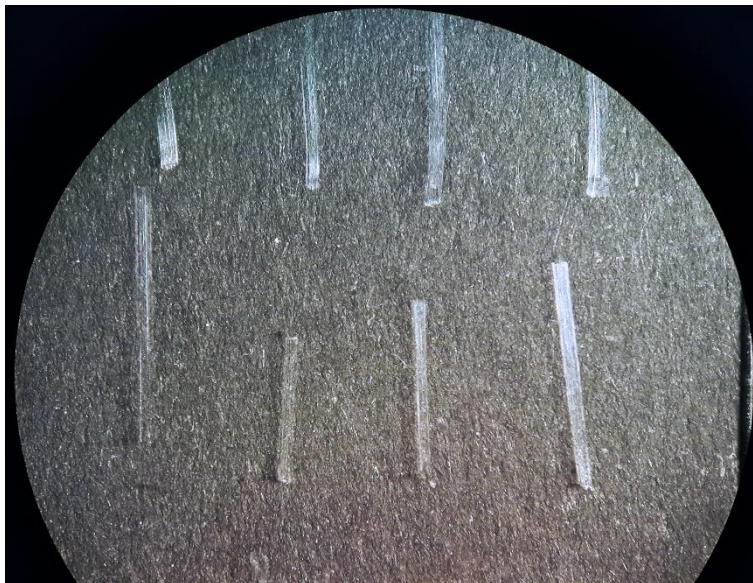
*Figure 3.6 Example of scratches on thin films made with various pencil hardness, under 12×
magnification.*

This test is also known as Wolff-Wilborn method. The sample is placed on a horizontal surface and the pencil is held firmly in the pencil tester against a thin film, at a 45 ° angle. The pencil is then pushed against the surface of thin films, for about 6 mm, and the speed of tester should be between 0.5 and 1 mm/s. Afterward, the surface of the thin film was inspected for scratches or residues and checked by the naked eye and under a magnifying glass. If there was no scratch, the next hardest pencil was used. The test was finished when visible scratch throughout its length was observed.

3.3.10 Water contact angle measurement

Superhydrophilicity of TiO_2 photocatalyst is an important characteristic and can be evaluated by the water contact angle (WCA) on the film surface. These measurements were carried out on Contact Angle Meter CAM-100 (KSV Instrument, Ltd.) (Figure 3.7).

Before measurement thin films were kept in the dark for at least two weeks. Before irradiation, the initial contact angle of this film was measured on at least five different points. Water was then dried off, and samples were placed into UVA chamber ($\lambda_{max} = 365$, irradiance = 2.3 mW/cm^2). The water contact angle was measured until water did not completely spread out and it was not possible to measure CA anymore (under 5 °), or when constant CA was reached.
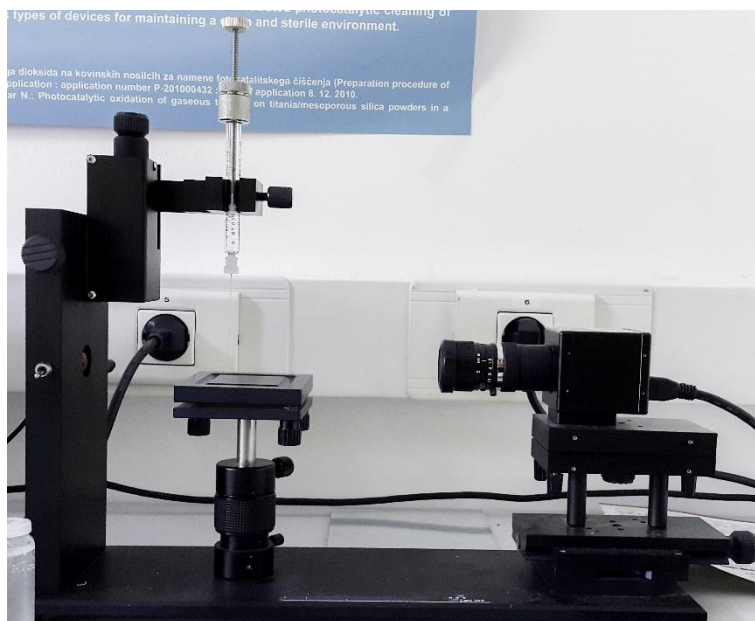
Figure 3.7 Contact angle meter CAM 100.

3.3.11 Aging of plastic substrate (D1)

The bare D1 substrate, a D1 substrate with the Ti10Zr film without binder, and a D1 substrate with the Ti10Zr film with SiO_2 binder were irradiated for 14 days in a Suntest chamber under a daylight filter to determine the possible damage upon irradiation. Suntest XLS+ (Atlas, USA) was operating under following conditions: Xenon light, daylight filter, irradiation intensity 750 W/m^2 (300–800 nm), with UVA fraction of 0.62 W/m^2 (300–400 nm).

Further identification of structural changes in the samples during such an accelerated aging test was conducted by FTIR-ATR.

3.4 Photocatalytic activity measurements

Choosing the appropriate method for determination of photocatalytic activity mainly depends on a shape (powder, thin films, fibers, *etc.*) and application (water or air purification, self-cleaning surfaces, antibacterial coating) of a photocatalyst. For photocatalysts with a self-cleaning application goal, a solid organic compound over the surface is a preferable model contaminant (in a real environment a solid-solid interface is the most common) than a dye-solution (solid-liquid interface). Specific characteristics that change during the photocatalytic process are directly or indirectly followed by several methods described below.

3.4.1   Contact angle measurements: methyl stearate (MS) as a model contaminant

Thin films were, before measurement and deposition of this organic fatty compound, irradiated in UVA chamber for a few hours (λ_{max} = 365 nm, 2.3 mW/cm^2) to remove possible dirt that was accumulated on the surface. Methyl stearate was dissolved in n-hexane (0.2 M) and deposited onto photocatalytic thin film with a dip-coater (withdrawal speed 20 cm/min). A resulting uniform layer was blow-dried to form a frosty looking like film. The initial water contact angle was measured before irradiating the sample (substrate + thin photocatalytic film + methyl stearate layer) in the UVA chamber. Contact angles were measured on at least five different spots. After each measurement, water was removed by drying before the sample was put back in the chamber. The sample was in determined time intervals taken out from UVA

36

chamber, and a water contact angle was measured [61]. Measurements continued until a stable value of contact angle, a contact angle lower than 5 ° or until the initial contact angle of a film was reached.

This method is very time-consuming due to slow degradation process of a solid fatty deposit. It cannot be used for evaluation of possible hydrophobic photocatalytic surfaces and porous substrates or substrates with a rough surface [87]. Instead, the destruction of the organic contaminant film can be followed by FTIR-ATR spectroscopy, which becomes more suitable for previously mentioned samples.
In this work, this method was only used for glass samples, because it showed the same trend as other activity measurements but requires more time.

3.4.2 Fluorescence measurements: terephthalic acid (TPA) as a model contaminant

Photocatalytic oxidation of TPA proceeds through various intermediates and one of them, in the first step of degradation, is fluorescent hydroxyterephthalic acid (Figure 3.8). A coating solution was prepared by mixing Na-terephthalate (0.0031 mol TPA, 0.201 M aqueous solution of NaOH and 96 % ethanol) and hydroxyethyl cellulose (2 wt. % hydroxyethyl cellulose, 96 % ethanol). HEC acts as a polymer host for obtaining a uniform solid organic coating and, additionally, as an electron scavenger for e$^-$ produced by TiO$_2$ during irradiation. Before the deposition samples were irradiated for 1-2 hours in the UVA chamber ($\lambda_{max} = 365$ nm, 2.3 mW/cm^2). TPA layer was deposited by dip-coating with 10 cm/min pulling speed. It is important that the TPA layer itself is stable under UVA radiation. After TPA layer was deposited, PMMA holder (Figure 3.9) with silicone grease was put on top of it (TPA surface of wells was not covered with grease). Silicone grease prevented leaking between wells (hole diameter 9 mm). This system was then put in the UVA chamber and taken out on chosen time intervals. Three wells were washed out with 159 µL mixture of ethanol-water (volume ratio 1:1) each and pipetted into a microtiter plate. The products that might form under TPA degradation are 2-hydroxyterephthalic acid (HTPA), 4-hydroxybenzoic acid, benzoquinone, benzene, acids: formic, acetic, oxalic, maleic, fumaric [88]. HTPA (Figure 3.8) is one of the first products and is highly fluorescent so that it can be easily detected by fluorimetry [89].
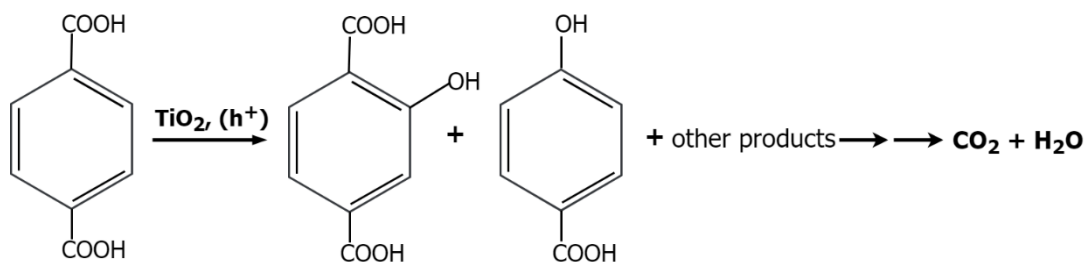
Figure 3.8 Terephthalic acid degradation.

The collected samples were analyzed by microtiter plate reader spectrofluorimeter (Infinite F200 Microplate Reader, Tecan) with an excitation wavelength of 320 nm and an emission wavelength of 430 nm.
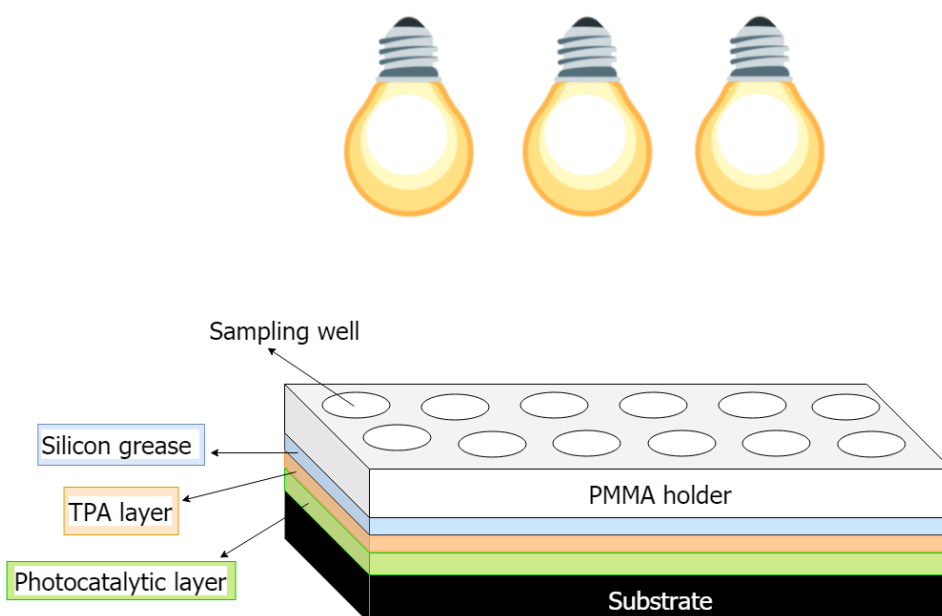
Figure 3.9 Experimental set-up of photocatalytic activity measurement with TPA.

The concentration of HTPA at the beginning is increasing, then it reaches a plateau (formation and degradation rate of HTPA are the same), and after that, it begins to decrease because HTPA is degrading to further products. We only focused on the initial step where the formation of HTPA occurs; these data were used for fitting.

A simplified kinetic model for HTPA formation (k_1 rate constant) and subsequent degradation (k_2 rate constant) was applied [89]:

$$\frac{d[HTPA]}{dt} = k_1 - k_2[HTPA] \qquad 14$$

It leads to an expression used to fit experimental results:

$$[HTPA] = \frac{k_1}{k_2}(1 - e^{-k_2 t}) \qquad 15$$

38

3.4.3 Electron paramagnetic resonance

The EPR experiments were carried out at the Slovak University of Technology in Bratislava (CEEPUS scholarship). In the EMX Plus X-band EPR spectrometer (Bruker) with a High Sensitivity Probe-head (Bruker) using the thin-walled quartz EPR tubes the thin films on glass (dimensions of ~2.5 mm × 25 mm) were inserted. Then 200 µL of the solution of nitroxide free radical Tempone in toluene ($c_{0, Tempone}$ = 10 µM) were added into the tube. The samples were irradiated at 295 K directly in the EPR resonator using UVA LED source (λ_{max} = 365 nm; 19 mW/cm^2; perpendicularly towards the titania on glass), and the EPR spectra were recorded *in situ*. The reference data were obtained via irradiation of Tempone in toluene. In order to obtain more information on the radical species produced upon UVA exposure of titania films in toluene, the analogous experiments were performed with DMPO spin trap. The quartz tube containing film on glass and 250 µL DMPO in toluene (c_{DMPO} =0.04 M) was irradiated and EPR spectra of generated spin-adducts were monitored *in situ*. Due to the high equilibrium concentration of molecular oxygen in toluene (~9 mM [90,91]), the irradiated solution was saturated with argon before the subsequent EPR measurement to get better resolved spectra by suppressing the line-broadening effect of molecular oxygen [92].

The photoinduced generation of hydroxyl radical DMPO spin-adduct ($^•$DMPO-OH) in water was monitored *ex-situ*. Samples (5 mm × 25 mm) were inserted in 2-mm UV cell, 300 µL of DMPO solution in water were added (c_{DMPO} =0.035 M), and samples were irradiated by UV LED source (λ_{max} = 365 nm; 19 mW/cm^2) for 5 minutes. Then the irradiated solution was filled in the small quartz flat cell (WG 808-Q, Wilmad-LabGlass) and the EPR spectrum was recorded two minutes after irradiation was stopped. The reference data were obtained by the irradiation of aqueous DMPO solution in the presence of a microscopic glass slide. The concentration of photogenerated spin-adducts was evaluated from the double-integrated EPR spectra based on the calibration curve obtained from the EPR spectra of Tempol solutions measured under strictly identical experimental conditions.

The g-values (± 0.0001) were determined using a built-in magnetometer. The experimental EPR spectra were analyzed and simulated using the Bruker software (WinEPR) and Winsim2002 software [93].

3.4.4 Photoreduction of resazurin ink

The activity of thin films was also visually assessed with resazurin (Rz) ink test. The Rz solution was prepared by dissolving Rz dye (250 mg) in deionized water (50 mL) and mixed overnight to dissolve the dye completely. A sacrificial agent (*e.g.*, glycerol) for the photogenerated holes was not used, as we wanted to test the wetting of the surface also. Hence, generated holes react with water (or surface –OH) and prevent electron-hole recombination. A drop (0.5 mL) of such prepared Rz solution was put on the surfaces. Samples were then put in the UVA chamber and irradiated by UV light; photos were taken in 15 min intervals for two hours to observe the kinetics.

The color changes are associated with the photoreduction of the resazurin and are presented in Figure 3.10. The initial blue color of resazurin gradually transforms via pink resorufin to the final reduced form, colorless dihydroresorufin.

Figure 3.10 Degradation of resazurin [94].

3.5 Antibacterial assay

Bacteria (*Escherichia coli* and *Staphylococcus aureus*) were taken out of the fridge and put into a tube with nutrient broth. The nutrient broth was prepared by mixing 2.5 g yeast, 5 g peptone, 5 g NaCl and 500 mL deionized water. After 12 hours of incubation at 37 °C, bacteria from the tube were transferred into another tube with nutrient broth and again put into an incubator for 12 hours. After 12 hours, the concentration of bacteria was checked measuring optical density with a spectrophotometer at 600 nm. On glass samples, a silicone barrier was placed around the edges that prevented bacteria solution to leak out of the sample surface. Slides with thin films were put into glass Petri dishes and sterilized at 160 °C for 2 hours. Simultaneously three sets of samples were tested: **i)** glass substrate (without photocatalyst) under UVA; **ii)** photocatalytic thin film on a slide under UVA; **iii)** photocatalytic thin film on a slide in Petri dishes wrapped in aluminum foil to keep in the dark (Figure 3.11). On every sample, 0.5 mL bacteria solution was pipetted.

Experiments were running for 4, 12 or 24 hours; then the bacteria solution was washed out from the sample with a physiological solution and put in a microcentrifuge. Washed solution was diluted if needed and 0.1 mL of it was pipetted onto an agar plate. Agar plate was prepared by pouring a mixture of 2.5 g yeast, 5 g peptone, 5 g NaCl, 500 mL deionized water and 7.5 g agar into a petri dish. Agar plates were incubated overnight at 37 °C. Next day, colonies were counted; we have taken into account only plates with 30 to 300 colonies. Log reduction of bacteria was determined with the following equation:

$$Log\ reduction = log\frac{N_i}{N_t} \hspace{3cm} 16$$

Log reduction of bacteria, N_i is a number of bacteria before starting the experiment, N_t is a number of bacteria at the end of the experiment.

The reduction can also be expressed as a fraction:

$$Percent\ reduction = \frac{(N_i - N_t)}{N_i} \times 100 \hspace{2cm} 17$$

Percent reduction of bacteria, N_i is a number of bacteria before starting the experiment, N_t is a number of bacteria at the end of the experiment.
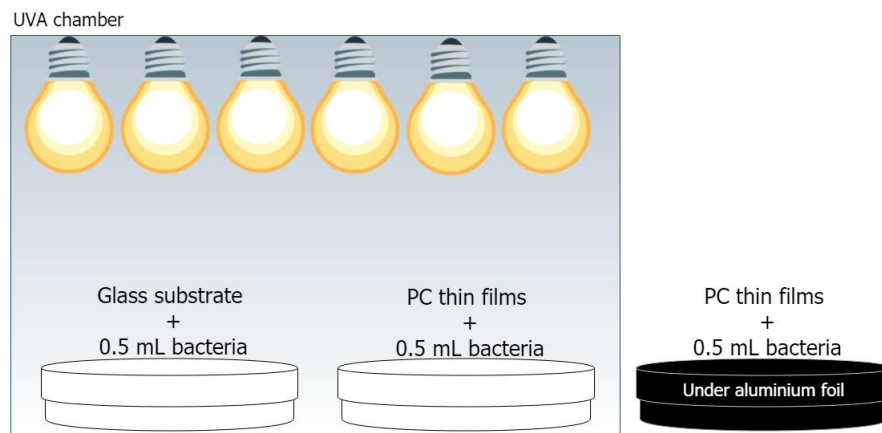
Figure 3.11 Experimental set-up for antibacterial assay.

3.6 Ecotoxicological assay with *Daphnia Magna*

Daphnia magna are small (< 5 mm) freshwater invertebrate species, and they are commonly known also as water flea, because of their typical movement. They are important in the aquatic food web, and their decrease in number would result in an ecosystem-level response. It has also been shown that acute toxicity tests with *Daphnia magna* respond to a variety of chemicals with a higher sensitivity than those with, *e.g., Danio rerio* [95]; therefore, *Daphnia magna* is a good representative for an ecotoxicological test.

Species used in our test were cultivated in the laboratory. For this assay younger species were chosen. A stock solution was prepared by mixing in a 1-liter flask 25 mL of CaCl·2H$_2$O aqueous solution (γ = 11.76 g/L), 25 mL of MgSO$_4$·7H$_2$O solution (γ = 4.93 g/L), 25 mL of NaHCO$_3$ (γ = 2.59 g/L), 25 mL of KCl (γ = 0.23 g/L) and additional water up to 1 L mark.

In a PTFE beaker, a sample with a photocatalyst was immersed in 25 mL of the stock solution, providing a surface contact area of 13.0 cm^2 ± 0.5 cm^2. In each beaker, five appropriate water fleas were inserted (Figure 3.12). In addition to beakers with photocatalyst samples, two sets of beakers were also added: "control" with only fleas and stock solution, and "blank" with glass substrate (without PCA coating) additionally to fleas and stock solution. The assay lasted for 48 hours at ambient conditions and then the number of mobile species was evaluated. For each sample, four repetitions were made.
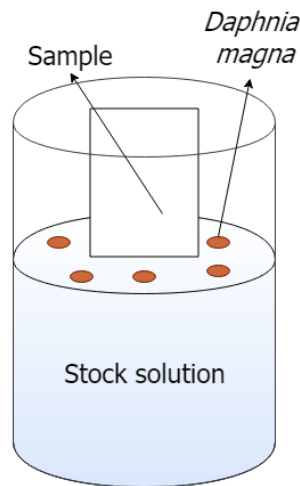
Figure 3.12 Experimental set-up for ecotoxicological assay.

Percent of mobile *Daphnia magna* was calculated by:

$$\% \ of \ mobile \ Daphnia \ magna = \frac{N_m}{N_a} \times 100 \qquad 18$$

N$_m$ - a number of mobile organisms, N$_a$ – initial number of Daphnia magna

3.7 Field test of Ti10Zr thin films on float glass

For a field test, Ti10Zr was chosen as an optimized photocatalyst based on laboratory measurements of activity and mechanical stability. Ti10Zr was prepared almost the same way as for the laboratory samples. The only difference was the thin-film deposition method. In this case, spraying instead of dip coating was used, because

considerably larger surfaces were coated to approach the actual size of windowpanes. The solution was sprayed on float glass from a distance of 15 cm and dried by a heat gun; then the glass was put in 30 cm × 30 cm wooden frame. Three sets of samples (uncoated float glass, Ti10Zr coated float glass, and reference BIOCLEAN glass from Saint Gobain) were exposed in three different tilt conditions of the samples (45 °, 90 ° and 90 ° with a roof) and at three different locations (Nova Gorica, Ljubljana and Žiri). Placement of the samples on each location is shown in Figure 3.13. Samples were exposed to weather conditions for one year and a half.
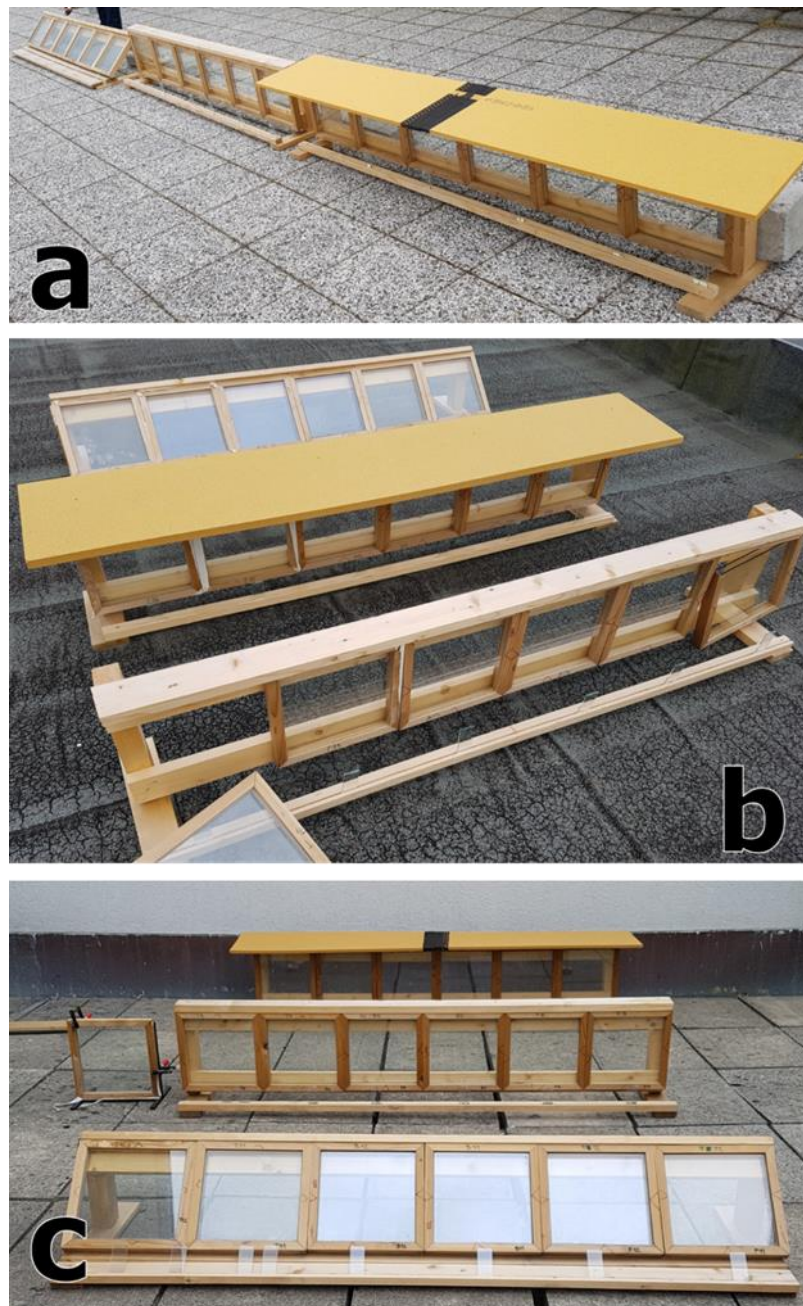
Figure 3.13 Field test of the three sets of samples at three different modes of exposure and locations: a) Ljubljana, b) Žiri, c) Nova Gorica

4 RESULTS AND DISCUSSION

Most of the results with the associated discussion were published in two scientific articles with the titles: "*Transparent titania-zirconia-silica thin films for self-cleaning and photocatalytic applications*" [96] and "*Transparent photocatalytic thin films on flexible polymer substrates*" [94].

4.1 Powder samples

Although the final form of photocatalysts was a thin film, some techniques in materials' characterization require the samples to be introduced in powder form. The corresponding results are shown and discussed in this section.

4.1.1   X-ray powder diffraction

The X-ray powder diffraction patterns of the samples are presented in Figure 4.1. It was observed that all samples are crystalline despite the low-temperature preparation route. The most intense diffraction at 25.3 ° corresponds to (101) Miller indices of anatase reflection plane [97–99]. There are also other common reflections, which are not as intense, at 37.8 °, 47.9 °, 53.9 ° and 62.5 ° and they are ascribed to anatase reflection planes (004), (200), (105), and (204), respectively [97,98].
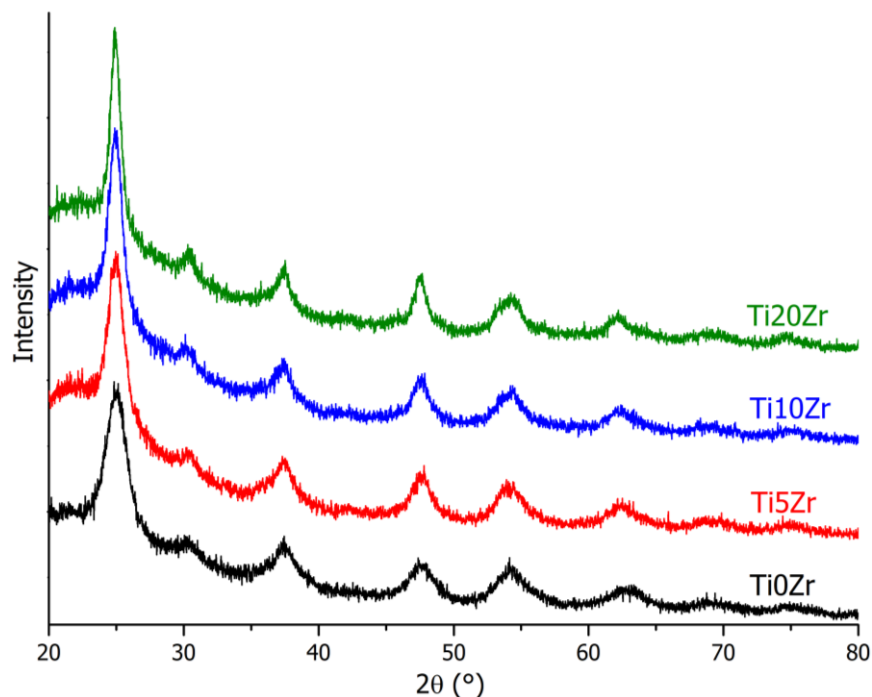
Figure 4.1 X-ray powder diffraction (XRD) patterns.

Thus, XRD results show no major differences among the samples and, the anatase polymorph is clearly seen despite the heat treatment temperature being only 150 °C. Peak around 30 ° is also noticeable, but it is much less intense and can be ascribed to brookite TiO_2 phase reflection plane (121) [100].

Contrary to the expected effect of guest species introduction, all the peaks become sharper and more pronounced with higher loading of zirconium so it can be concluded that introduction of ZrO_2 results in an increase of the anatase crystallites size. As expected, the presence of zirconia and silica was not detected in the diffraction patterns due to the amorphous character of these two phases. Particle sizes from XRD patterns were calculated by using the Scherrer equation based on the full width at the half maximum (FWHM) of the (101) diffraction peak (Equation 12). They fall in the range between 4 and 8 nm (Table 4.1).

From the XRD study, we can conclude that zirconium species had not been substituted into the crystal lattice sites of titania, since this would result in the effect of decreasing the anatase crystal sizes with increased Zr content, due to introduction of disparate boundaries resulting in the inhibition of the growth of TiO_2 crystals [101]. However, increase in particle size with higher Zr content can be explained by higher crystallization or agglomeration rate that occurs during sol preparation. It can be seen from photographs in Figure 3.3 that Ti20Zr sol with the highest Zr content is the most opaque one. Also, a shift of (101) anatase peak into the lower 2θ region due to the differences in the ionic radii of Zr^{4+} and Ti^{4+} was not observed, hence, no inclusion of Zr into anatase lattice occurred.

4.1.2 Infrared spectroscopy (FTIR-ATR)

IR spectra of the powder samples are presented in Figure 4.2. The broad band between 3600 and 3000 cm^{-1} corresponds to O-H stretching vibrations of hydroxylated titania, followed by O-H bending bands at ~1635 cm^{-1} [102–105]. Spectra do not show presence of organic residues, confirming that adopted drying conditions successfully removed major organic components in the sols. In the case of Ti0Zr sample, O-H stretching broad peak is higher in intensity, indicating an even greater amount of hydroxyl groups than in the samples with Zr.

OH groups are important for maintaining superhydrophilicity of the surface, which is essential to the self-cleaning property of TiO_2 thin films [106].
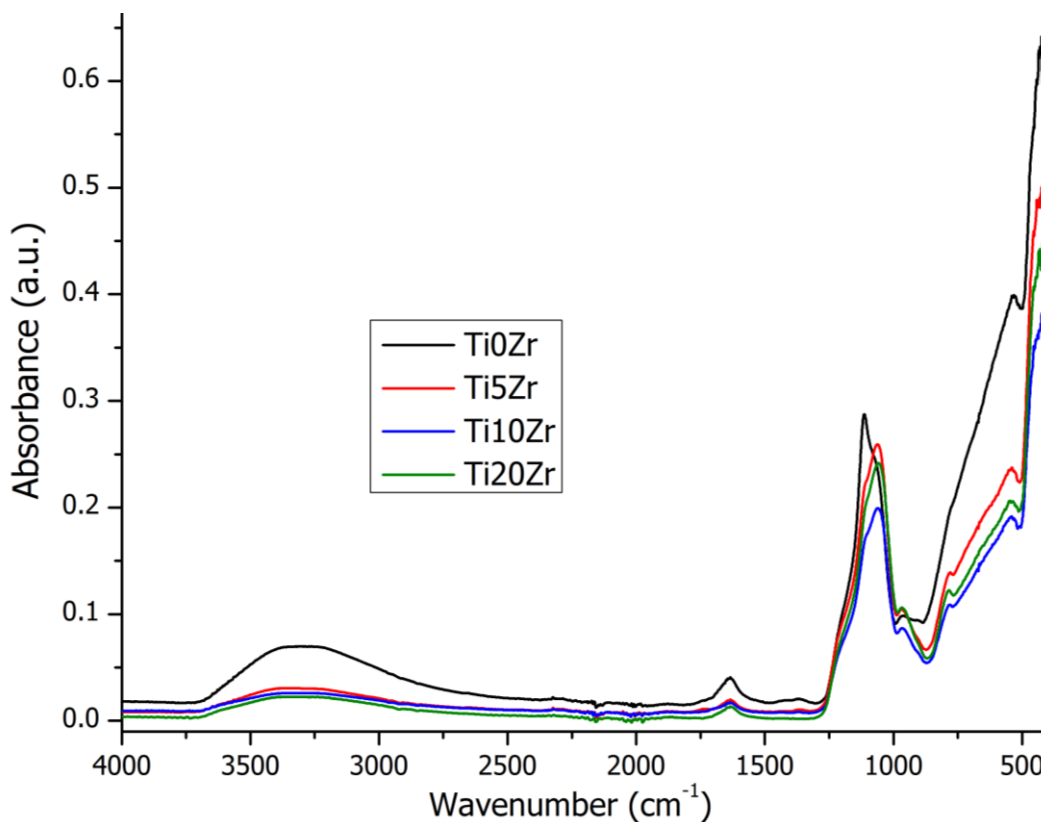
Figure 4.2 FTIR-ATR spectra of powders, dried at 150 °C.

On the spectrum of Ti0Zr sample, a shoulder type peak is presented with a higher intensity peak around 1114 cm^{-1}, which can be assigned to asymmetric Si-O-Si stretching modes with a shoulder at around 1070 cm^{-1} [107]. In spectra of samples with Zr, a shoulder type peak was also observed, but the peak around 1060 cm^{-1} had a higher intensity than the one at 1114 cm^{-1}. The intense peak at 1060 cm^{-1} associated with asymmetric Si-O-Si stretching vibrations is excited by the presence of Zr in its environment [108,109]. Two less intense peaks are present in the samples with Zr, around 970 cm^{-1} and 780 cm^{-1} that can be assigned to symmetric Si-O-Si vibrations, Si-OH and maybe even to Si-O-Zr bonds [109–111] since it is not evident in the case of Ti0Zr sample. The band centered at around 500 cm^{-1} indicates Ti-O bonds in the TiO_2 lattice [104,112].

FTIR study thus implies that the environment of Si is changed upon Zr introduction with the subsequently decreased hydroxylation of the catalyst surface. This could have a negative effect on the photocatalytic activities of Zr-modified samples, as surface

OH groups are important for high hydrophilic effect as well as high production of OH radicals upon irradiation.

4.1.3 UV–Vis diffuse reflectance spectroscopy

Bandgap values of the samples were determined by measuring UV-Vis diffuse reflectance spectra of the powder analogs. Data were then extrapolated using the Kubelka-Munk function for indirect bandgap calculation and the linear part of the onset of the absorption was used to determine the bandgap (Figure 4.3).
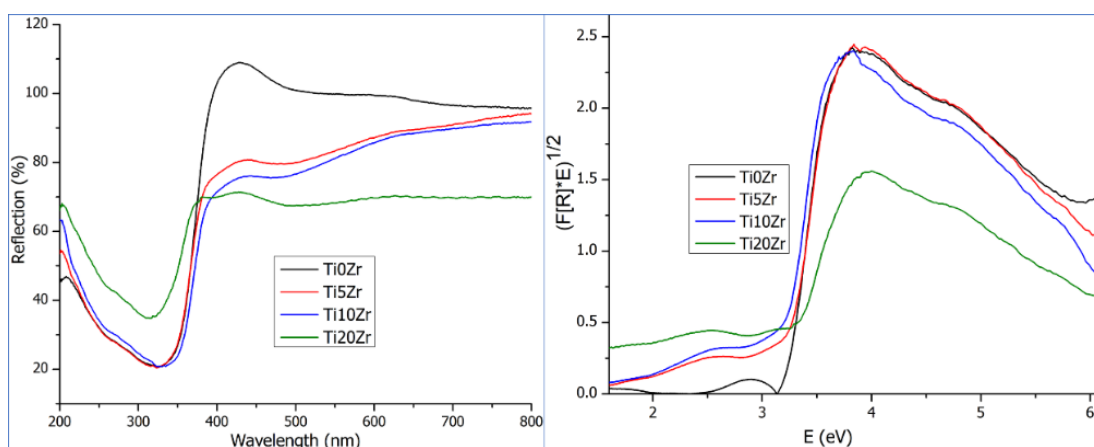
Figure 4.3 UV-Vis reflectance spectra of powders (left) and Kubelka-Munk transformation for estimation of the indirect bandgap values (right).

Bandgap values are listed in Table 4.1. Obtained values showed that with higher loading of Zr, the bandgap energy of samples is decreasing, which is inversely correlating with the anatase particle size (Table 4.1). This phenomenon is related to the quantum size effect and is well agreed with the data reported elsewhere [113].

Table 4.1 Bandgap size determined by DRS and calculated particle size.

Sample	Bandgap - DRS	Anatase Crystallite Size (101)
Ti0Zr	3.23 eV	4.2 nm
Ti5Zr	3.16 eV	5.0 nm
Ti10Zr	3.11 eV	5.8 nm
Ti20Zr	3.09 eV	7.7 nm

In section 4.2.3, a relation between bandgap values obtained from DRS and LBDS will be discussed. These results imply on greater utilization of solar light spectrum in case of Zr-modified TiO_2, which could be beneficial with real long-term exposure.

4.1.4 Thermal analysis (TGA-DSC)

TGA-DSC was performed to follow thermal stability of the as-prepared materials by determination of weight reduction as a function of temperature and heat flow in and out of sample with an increase of temperature. TGA analysis (Figure 4.4) revealed the expected loss of weight, *i.e.*, 19 – 25 % up to 600 °C. Most reduction of mass was observed for sample Ti0Zr, which was also the most hydrated as it can be speculated from these and IR results above. Volatile organics and some of the adsorbed water were removed up to 100 °C; at the DSC curve this corresponds to endothermic peak with a minimum around 90 °C. While at temperatures in the range of 150 – 400 °C, the mass loss can be attributed to the decomposition of OH groups, any residual organic components, and formation of metallic oxo-bridged bonds [103,114,115]. Two of the exothermic peaks are shown in the range between 150 and 300 °C. The more pronounced exothermic peak at approx. 210 – 230 °C can be attributed to the combustion of organic constituents in the sols (from TTIP and ZTB precursors). The weight of the samples decreased up to approx. 450 °C after which there was no evidence for further mass loss nor any signs of exothermic peaks.
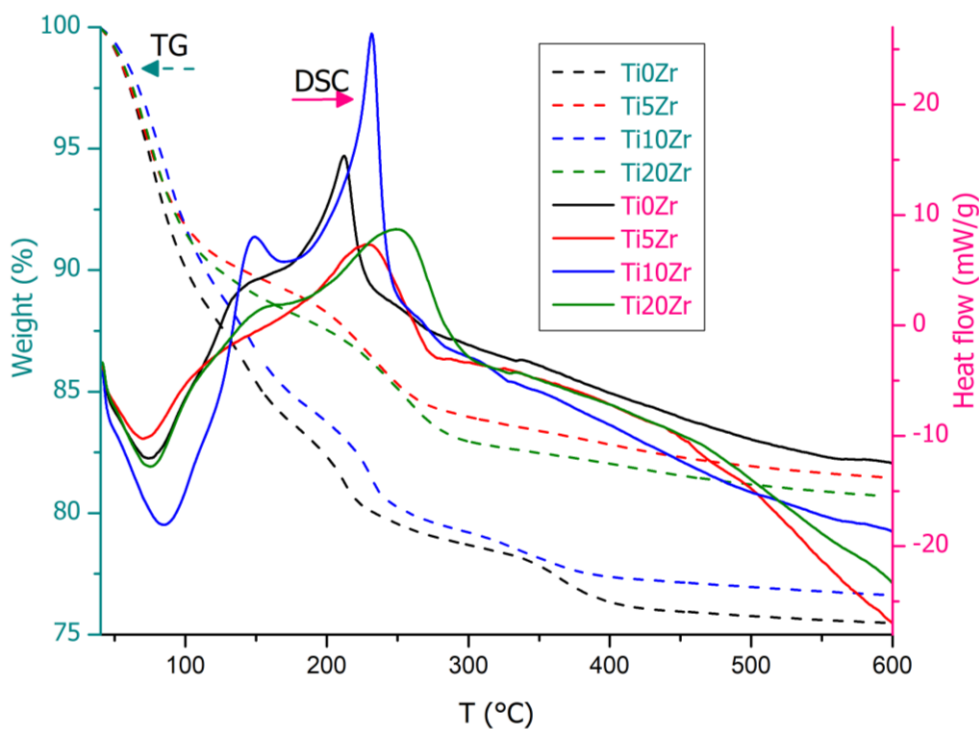
Figure 4.4 Thermal analysis of the powder samples.

4.1.5 BET specific surface area

Specific surface area (Figure 4.5) of samples gradually decreased with a higher percent of Zr, except in the case of the highest Zr loading, where Ti20Zr showed higher surface area than expected concerning the largest grain sizes derived from XRD and SEM results. Apart from this unclear deviation, reduction of the specific surface area is in good agreement with the growth of anatase crystallite size upon an increasing amount of zirconia in the composite materials (Table 4.1).
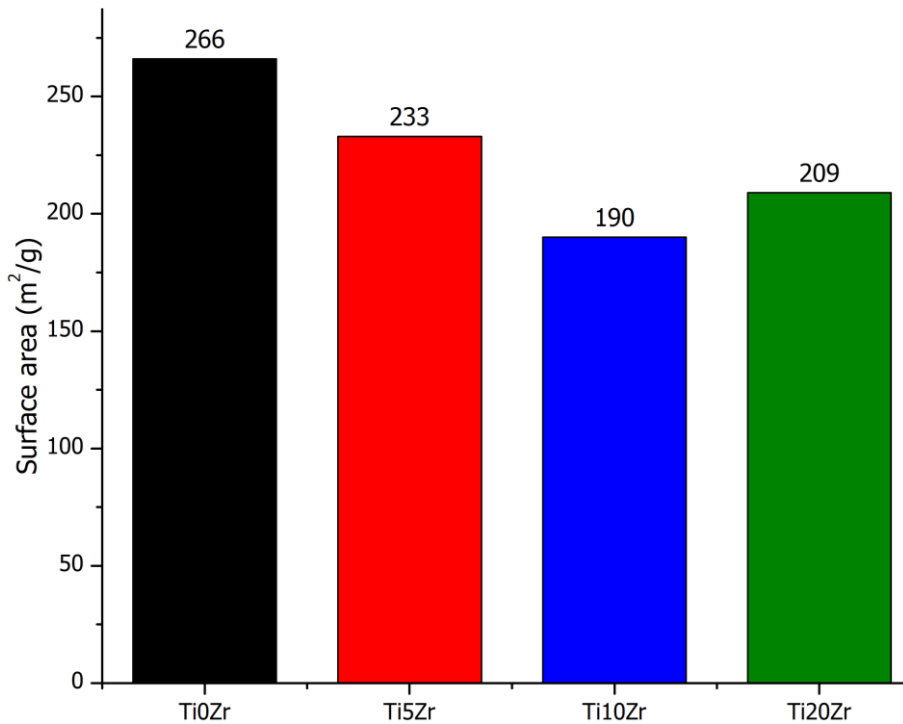
Figure 4.5 Specific surface area of powder samples.

The surface areas of samples are considerably high for titania; it is a consequence of the presence of the amorphous phase, which was deduced from XRD patterns, and of course, the small particle size. The low-temperature process did not remove all of the residues and fully arranged structure was not achieved. Surface area also affects photocatalytic activity, the larger the surface area more active sites are accessible and that usually results in higher photocatalytic activity. The correlation between surface area values and activities are discussed in the following chapters.

4.2 Thin films on glass substrate

The results obtained with instrumental techniques which are suitable for thin films characterization are discussed below. The samples for these techniques were deposited on glass substrates, dried at elevated temperature as described in the experimental section and analyzed without further treatments.

4.2.1   UV-Vis transmittance

Thin films on glass substrate were highly transparent, and they did not alter the transparency of the glass. UV-Vis transmission spectra of thin films on a glass substrate are showing high optical transmittance in the visible region (Figure 4.6).
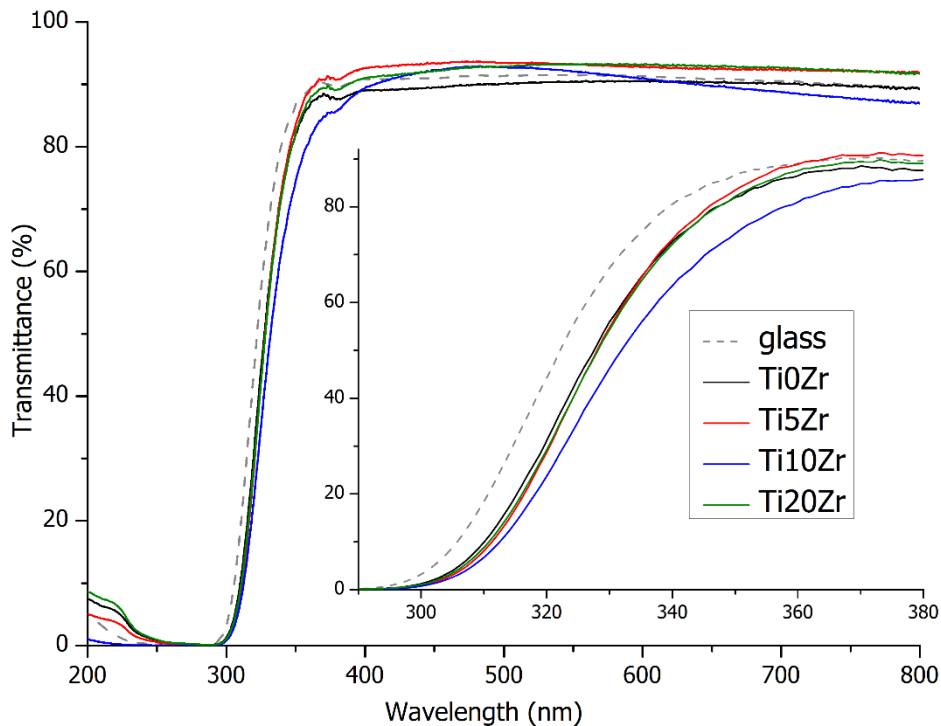
Figure 4.6 UV-Vis transmittance measurements of thin films on a glass substrate and a bare glass substrate.

The transmittance of visible light of the thin films in the visible region exceeds even that of the bare glass substrate; this phenomenon is known as the antireflective properties of silica [116,117]. The refractive index of titania is ca. 2.6, while for applications a better value would lie between 1.23 and 1.27 [118]. Thus, in order to decrease the refractive index of the layer, an effective medium is consisting of high-index particles (TiO_2 & SiO_2) and low-index pores can be created, where the pores are formed by incorporation of mesoporous silica.

However, in the UV region, samples transmit less light compared to the glass substrate (Figure 4.6, inset), because titania absorbs UV light. The lowest transmittance in the range of 300 – 380 nm has the sample with 10 % of zirconia (Ti10Zr). Differences in the transmittance among the thin films are not significant and can easily be assigned to the variations in film thickness, particles, surface area, and/or bandgap value.

Therefore, the results as obtained with the UV-Vis spectroscopy show that the films deposited on glass have the mesoporous structure and high transparency suitable for construction applications (as windows or coatings on mirrors) and the absorbance in the UV region clearly shows on the presence of titania phase which should be active under UV-light and thus exhibit self-cleaning effect.

4.2.2 Infrared spectroscopy (FTIR-ATR)

FTIR-ATR analysis was also performed on glass samples (Figure 4.7). From obtained spectra, it can be concluded that the influence of substrate is very high and most of the bands related to thin films are masked. The strong observed influence of the substrate is a consequence of the thickness of the films; they are thin (less than 140 nm), and the infrared beam penetrates through the film to a substrate.
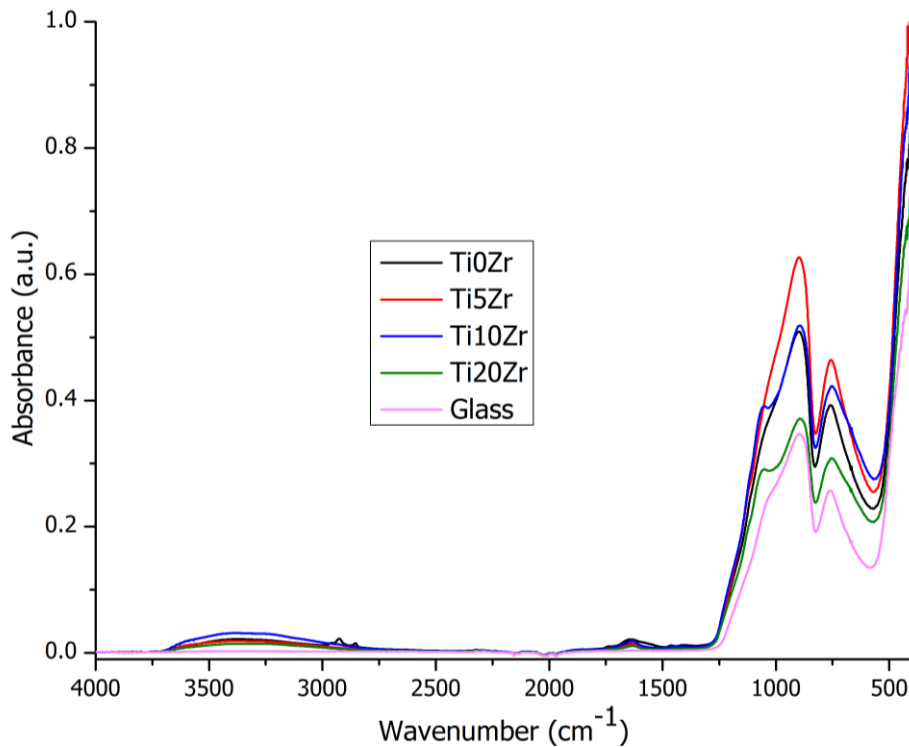
Figure 4.7 FTIR-ATR spectra of thin films on a glass substrate and bare glass.

The presence of thin film is indicated by broad band at 3600 – 3000 cm^{-1} and band around 1630 cm^{-1}, which are assigned to O-H stretching and bending vibrations, respectively. Also, the characteristic band of samples with Zr, at 1060 cm^{-1} is evident on thin film spectra and is related to asymmetric Si-O-Si stretching vibrations promoted by Zr-addition.

Characteristic bands of glass (Si-O-Si vibrations) are around 895 and 760 cm^{-1}; it can be speculated that because of these two bands other characteristic bands of Si and Ti species that were found in powder samples, are masked. The comparison between spectra of Ti10Zr powder, Ti10Zr thin film on glass substrate and bare glass substrate is shown in Figure 4.8 and confirmed our prediction that glass substrate is masking most of the characteristic thin films bands. In spite of this, the presence of OH groups and typical vibration at 1060 cm^{-1} (ascribed to Si-O-Si in the environment of Zr) is clearly visible in both, powder and thin film form of the sample.
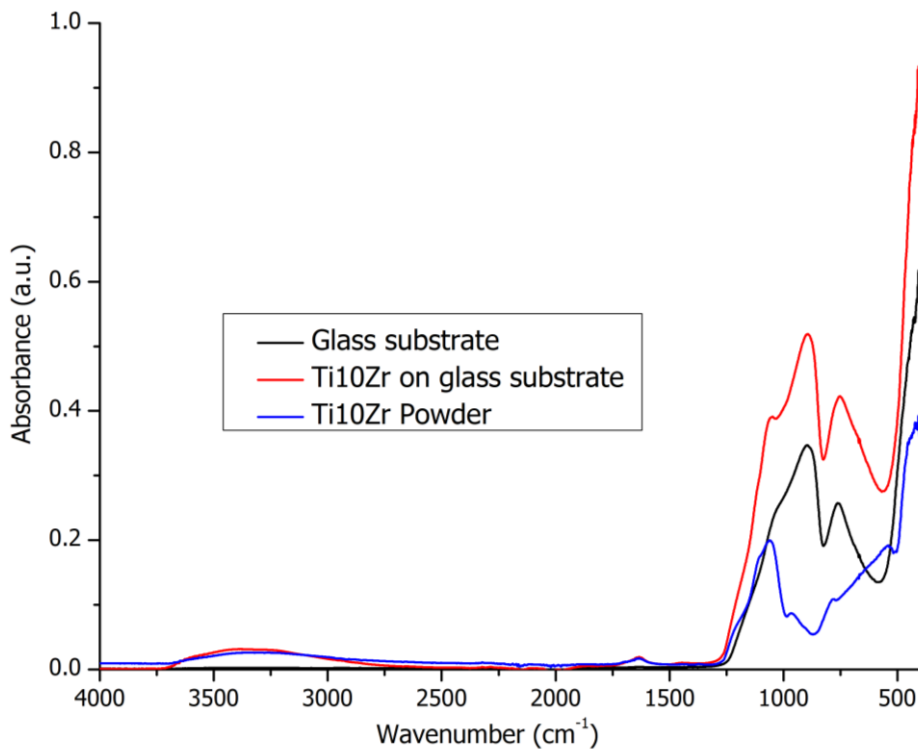
Figure 4.8 FTIR-ATR spectra of bare glass substrate compared to a Ti10Zr thin film on glass substrate and Ti10Zr powder.

4.2.3 Laser beam deflection spectroscopy

The bandgap values of the samples in thin film form were measured with laser beam deflection spectroscopy. The amplitude and phase of the signal are collected as a

function of the modulation frequency of the pump beam for the samples [86] (Figure 4.9). It is evident that the signal falls off exponentially with the increase in the modulation frequency of the TOs. Thus, to optimize the experimental conditions, the probe beam is tightly focused and carefully aligned close to the sample surface, to skim it. For that reason, the measurement is performed on flat samples with small lateral dimensions.
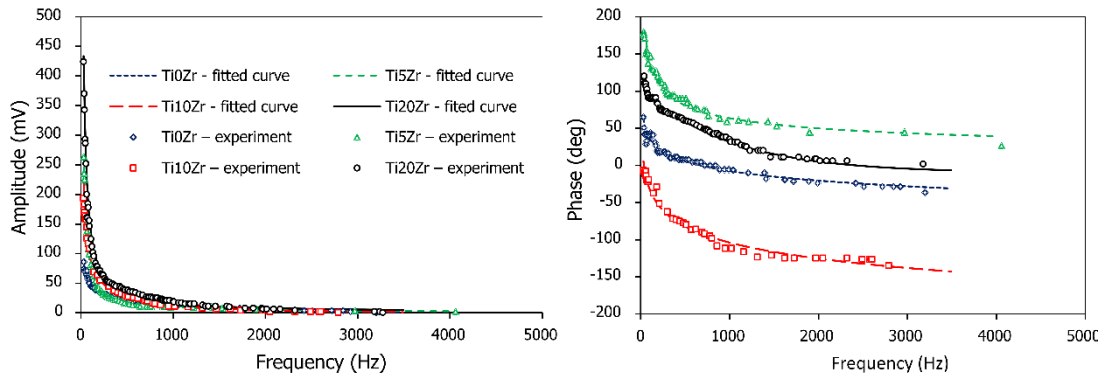
Figure 4.9 The amplitude (left) and phase of BDS signal (right) for thin films. Points represent the experimental data, whereas continuous lines the best fitting.

The best theoretical fittings to the obtained experimental data for the bandgap values are presented in Table 4.2. The variation in the value of the energy bandgap that was caused by the introduction of ZrO_2 into the TiO_2 material is rather low (approximately 5 %), and it can be attributed to the effective value of the whole composite and its changes in composition. With higher loadings of Zr, the bandgap energy is decreasing, which is inversely correlating with the anatase particle size (Table 4.2, Table 4.1).

Table 4.2 Bandgap value, fitted and determined by LBDS and film thicknesses.

Sample	Bandgap value	Thickness
Ti0Zr	3.30 eV	125 nm
Ti5Zr	3.20 eV	130 nm
Ti10Zr	3.15 eV	129 nm
Ti20Zr	3.05 eV	132 nm

Comparing the two methods, DRS for powders (Table 4.1) and LBDS applied for thin films (Table 4.2), the values match very well, and the trend is the same while using both methods. With higher loadings of Zr the band gap energy is decreasing, which is inversely correlating with the anatase particle size; Ti0Zr has the smallest and Ti20Zr the biggest particles. Moreover, it is also well agreed with the data reported elsewhere [113] and it can be described by the quantum size effect. Lin H. et al. [113] reported that

when decreasing anatase particle size from 29 nm to 17 nm bandgap decreases, but when particle size diminishes from 17 nm to 3.8 nm the bandgap value increases.

4.2.4   Film thicknesses

In Table 4.2, the thicknesses of films as measured with the profilometer are also presented. Significant differences among samples were not observed (five percent range of deviation). It seems that the thickness a little bit increases with the amount of Zr added, considering measurements precision of about $\pm$ 1 nm. Since dip-coating conditions were the same and their rheological properties are almost identical (see Appendix), the small differences can be a consequence of the small differences in the size of particles.

The thickness of films can also impact the activity of photocatalyst, but more importantly, thickness affects the transparency of films and consequently, the substrate's appearance.

Thin films were homogeneously deposited and because of the particle size, film thickness and porosity of the films, transparency was maintained. The most visually noticeable is Ti20Zr film, it had slightly milkier appearance than the others (Figure 3.4), even the colloidal solution for deposition of Ti20Zr was not as translucent as the others (Figure 3.3). Such an appearance is a consequence of high ZrO_2 concentration that obviously leads to bigger particles/agglomerates.

4.2.5   Scanning electron microscopy

SEM images of thin films on glass substrates are shown in Figure 4.10. The mesoporous structure, which gives rise to the antireflective properties, is clearly visible in all films. Gradual progress in morphology can be observed from the sample without addition of Zr to the sample with 20 mol. % of Zr; that is a higher content of the zirconium results in more spherical and larger particles. Progression in particle size was also confirmed by XRD diffraction and DRS with lower bandgap values. By comparing images of Ti0Zr and Ti20Zr, this difference in morphology can clearly be seen.
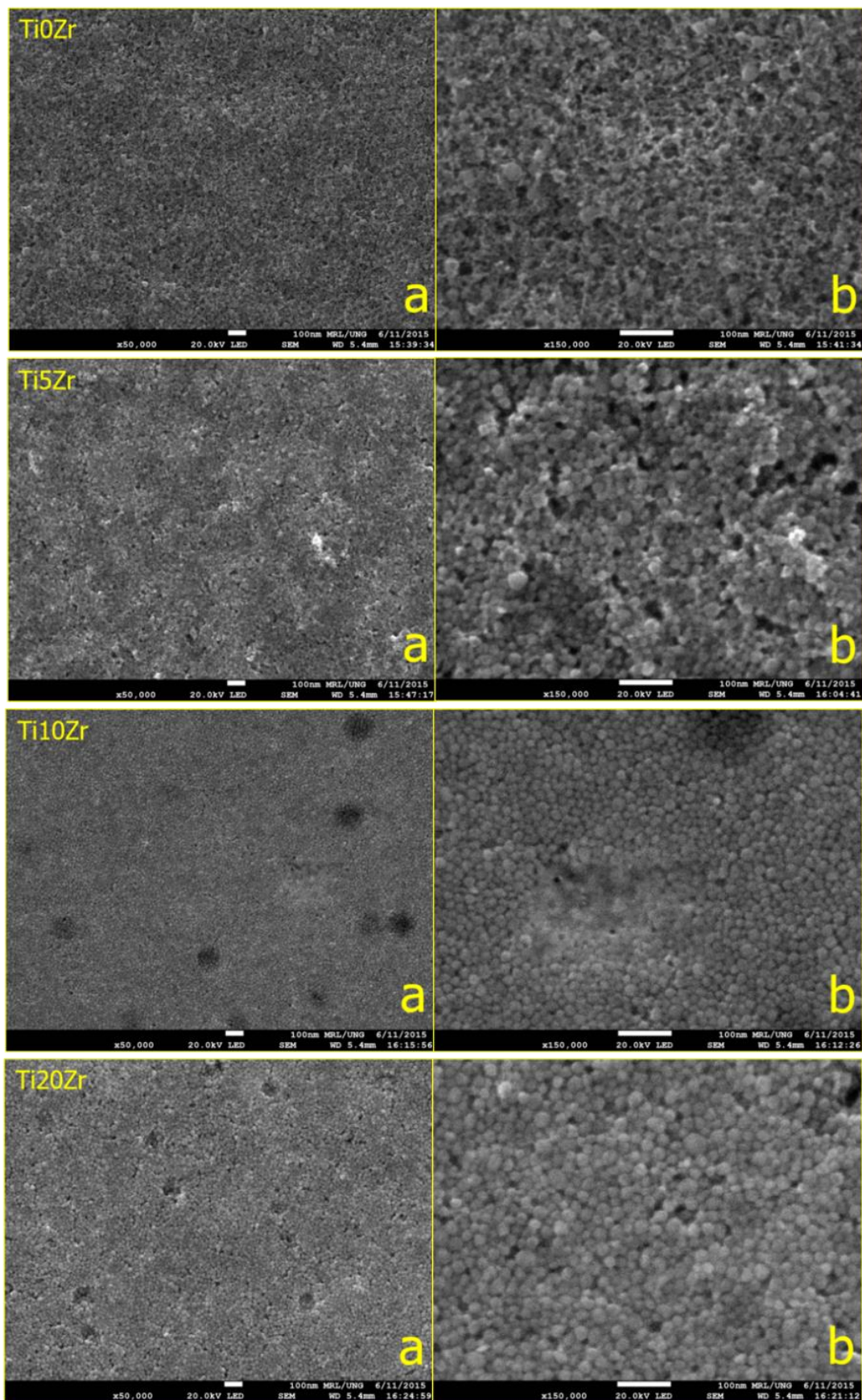
Figure 4.10 Plain-view SEM images of thin films on a glass substrate (a – low magnification, b – high magnification). Images of samples are in the following order: Ti0Zr, Ti5Zr, Ti10Zr and Ti20Zr.

56

4.2.6 Pencil hardness test

Hardness pencil test was performed on newly prepared ("new") and aged ("old") samples. New samples were considered those tested two weeks after preparation. Old samples were stored in the dark at room conditions for at least one year. From Figure 4.11, it can be concluded that samples lost mechanical stability upon aging, except the sample with the highest loading of zirconia (Ti20Zr). On both fresh and aged samples Ti20Zr and the new one Ti10Zr, pencil with hardness 6H (the highest) did not make any visible scratch.
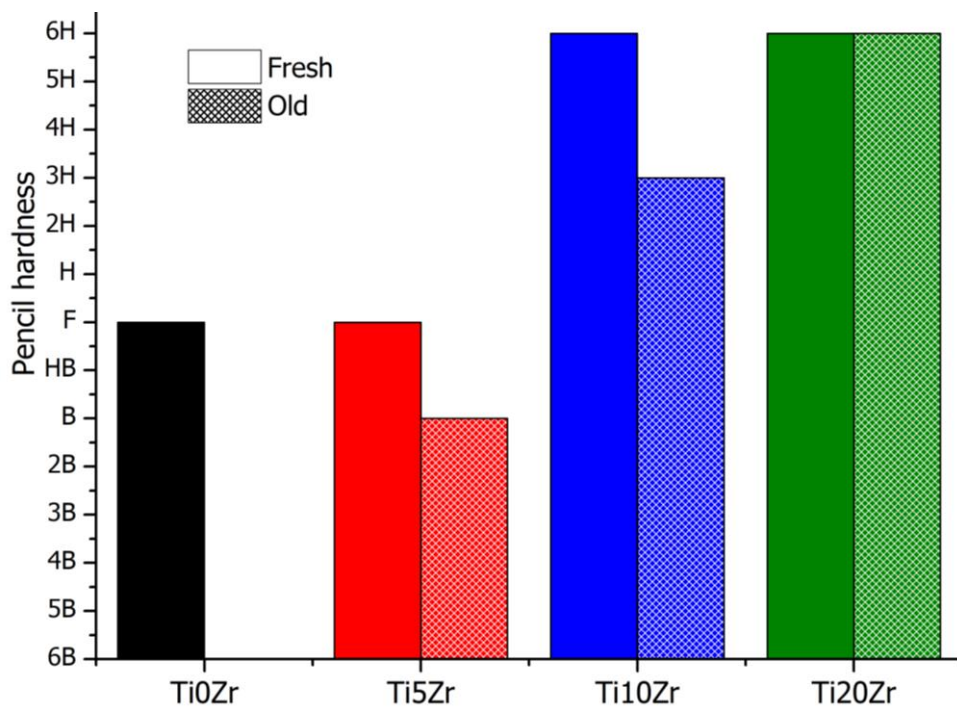
Figure 4.11 Hardness achieved for different thin films.

The most unstable was the sample without zirconia (Ti0Zr), where even the softest pencil 6B made a visible scratch on the old sample. The exact reason for obviously better mechanical stability of Zr containing thin films is not yet fully understood. It is reasonable to speculate that progressive morphology development of surface with the addition of Zr, evidenced by SEM images, beneficially influences mechanical properties of the film. Also, lower content of OH groups could mean that more of these reacted and resulted in a higher number of M—O—M bonds, thus hardening the composite. Ti-O-Zr bonds and ZrO_2 on it is own has a great chemical and mechanical stability [119,120].

4.2.7 Contact angle measurements

An important aspect of self-cleaning performance of TiO_2 is photoinduced superhydrophilicity that occurs after TiO_2 surface is exposed to UV light (Figure 4.12); the phenomenon is a consequence of surface structure modification of the semiconductor film by the action of UV irradiation. After 3 hours of exposure, the sample with 5 % of ZrO_2 reached the lowest contact angle value and has together with Ti0Zr sample the highest reduction in contact angle from the initial value (before UV irradiation).

Although no clear trends between Zr content and WCA kinetics / final value can be drawn, it is clear, that all samples were hydrophilic by nature and showed superhydrophilicity upon UV irradiation; even the Ti20Zr sample came close to 10 ° after 3 h of illumination.
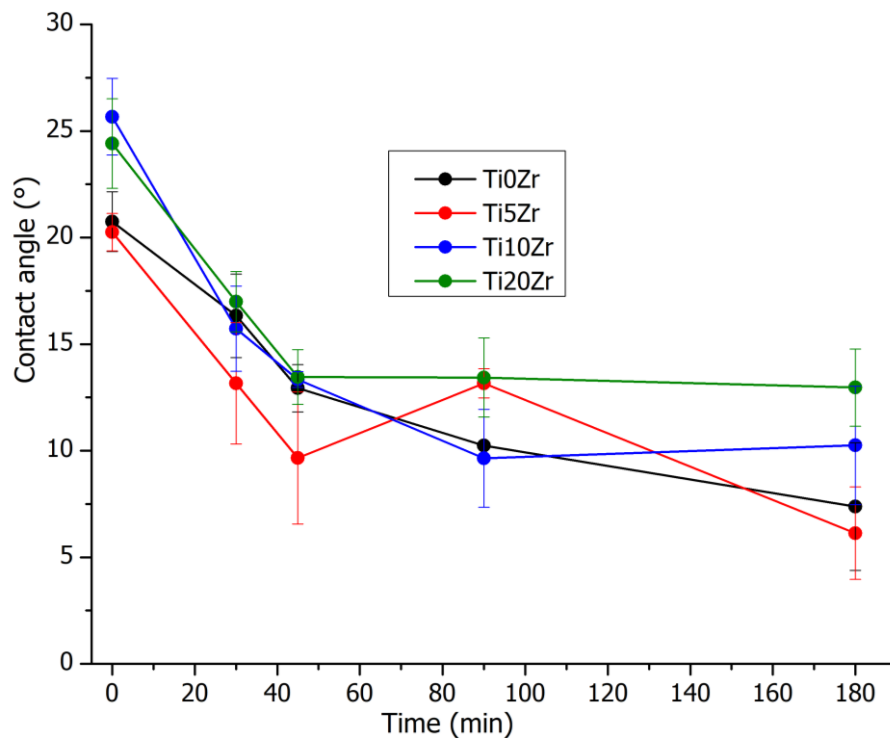
Figure 4.12 Water contact angle measurements on thin films on a glass substrate as a function of UVA irradiation time.

4.2.8 Photocatalytic activity measurements

Contact angle measurement: methyl stearate as a model contaminant

The contact angles are related to the degradation degree of methyl stearate. Initial contact angles that were measured after deposition of methyl stearate layer and before UV irradiation are relatively high (from 75 to 95 °, Figure 4.13) as expected from the surface covered with the fatty compound. Measurements were stopped when the contact angle was below 10 °. Ti0Zr first reached contact angle below 10 ° at 1200 min, Ti5Zr at 1680 min and Ti10Zr at 2640 min. The contact angle of Ti20Zr even after 2880 min did not decrease below 10 ° and was still relatively high, around 30 °. Although no kinetic model could be applied to these data, the results show that all samples were photocatalytically active towards methyl stearate degradation and that the sample with the highest amount of Zr was the least active, concurring with the trend seen in the previous (hydrophilic) test.
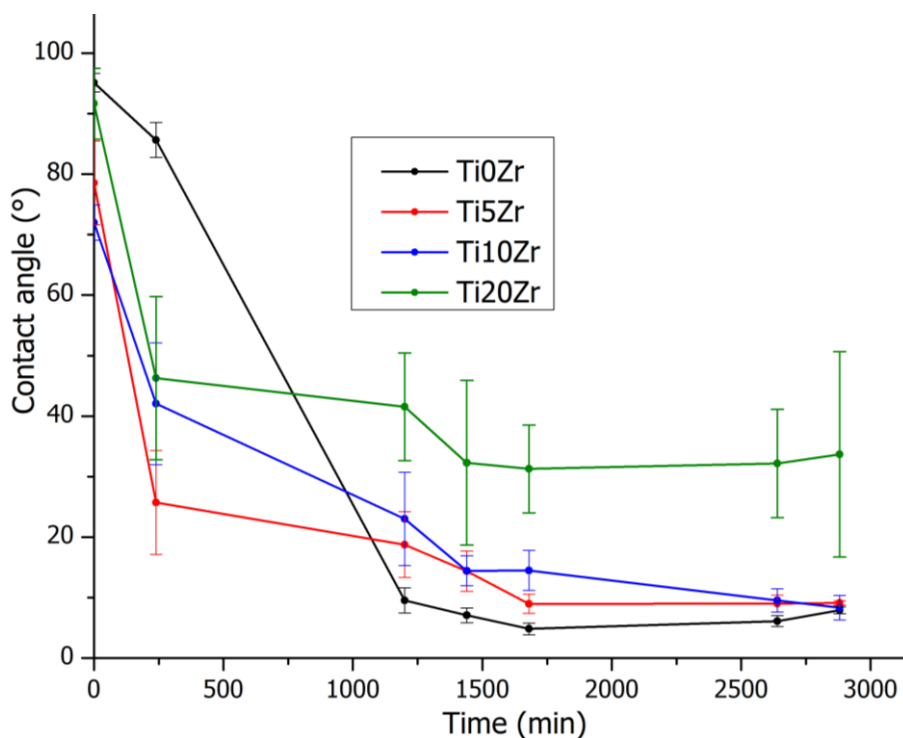
Figure 4.13 Photocatalytic activity determined by the degradation of methyl stearate coating, measuring water contact angle on the surface as a function of irradiation time.

Fluorescence measurements: TPA as model contaminant

The experimental results and corresponding curves after fitting to Equation 15 are represented in Figure 4.14. HTPA formation rate constants (k_1) of the samples decreased from 0 to 20 % addition of Zr as follows: Ti0Zr 84×10^{-9} M/min; Ti5Zr 54×10^{-9} M/min; Ti10Zr 48×10^{-9} M/min and Ti20Zr 12×10^{-9} M/min.
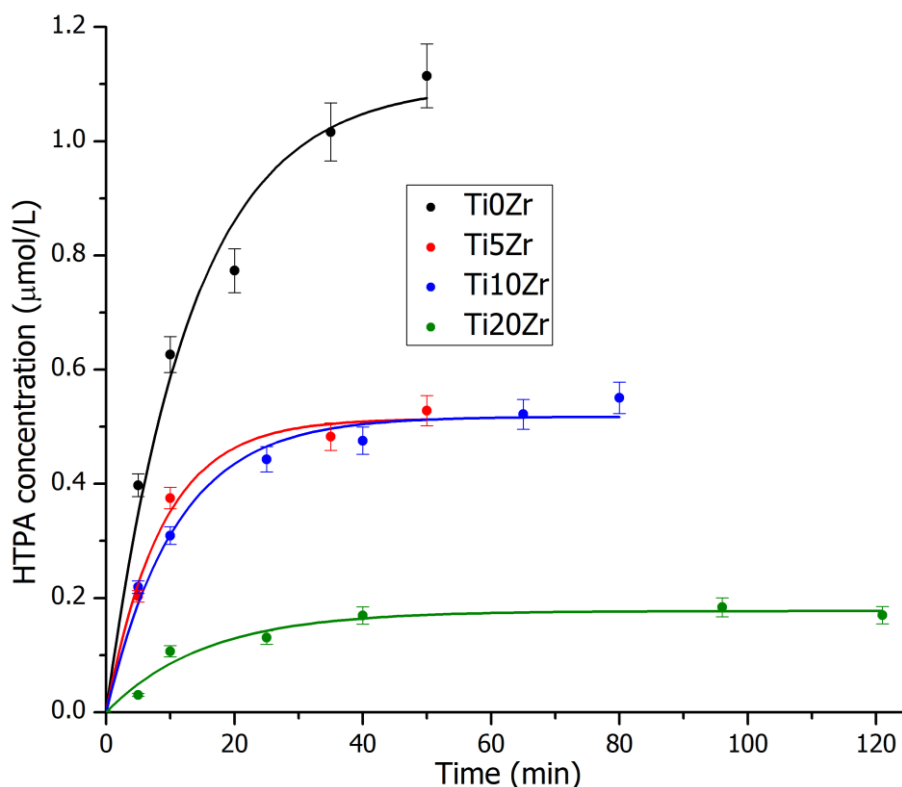
Figure 4.14 Photocatalytic activity determined by the degradation of terephthalic acid, measuring the formation concentration of HTPA.

Similarly to the results of contact angle measurements, Ti0Zr exhibited the highest activity. Photocatalytic activity gradually decreases with increasing content of zirconia; the lowest activity has the sample Ti20Zr again. The activity of thin film with 5 % Zr is half as active as Ti0Zr, but it is still 3-times more active than Ti20Zr. Interestingly, the samples modified with 5 and 10 % Zr showed almost the same kinetics, yet the concentration of Zr being doubled in the latter sample.

By comparing contact angle values and measured photocatalytic activities by TPA, we can conclude that they cannot be exactly related, because the mechanism behind WCA measurement involves the creation of oxygen defects, but not necessarily radical species which would be involved in the degradation of model compounds; yet, some conclusions can be drawn. The difference between the WCA before irradiation and

WCA after 180 min is almost the same for all films (Figure 4.12). Nevertheless, Ti0Zr and Ti5Zr reach the lowest WCA and they are also more photoactive than Ti10Zr and Ti20Zr. Maybe under longer exposure, the correlation between photoactivity and hydrophilicity would be more expressed.

The Ti0Zr sample has the highest surface area, which is one of the main reasons why it is the most active, maybe surface-to-surface ratio between substrate and contaminant is high enough to be more effective than other three films. Another possibility is that ZrO_2 suppresses the activity of TiO_2, due to its amorphous nature and the fact that it induces formation of larger TiO_2 particles.

The measurements with monitoring degradation of MS were time-consuming and gave comparable results with fluorescence measurements; that is why they were not applied in further investigations.

Because the structure-activity relationship after the above tests still proved to be elusive, a deeper look was taken by measuring the active species (OH radicals) by means of EPR technique. Being complementary to h^+ activity measurement (HTPA formation rate) these results should provide additional insights into the mechanism of action of such materials.

EPR measurements

In situ UV irradiation of films on a glass in the toluene solution of DMPO led to the formation of broad-line EPR signals of spin-adducts superimposed on the broad low-intensity signal attributed to the paramagnetic metal ions (*e.g.,* Fe(III)), present in the glass slide. Consequently, to obtain the spectra suitable for the identification of spin-adduct parameters, the saturation of the exposed sample with argon was necessary. The experimental EPR spectrum was recorded immediately after a post-irradiation argon-saturation along with its simulation. The complex experimental spectrum was simulated as a superposition of three individual spin-adducts. The dominant twelve-line signal with spin Hamiltonian parameters $a_N = 1.280$ mT, $a_H^\beta = 0.642$ mT, $a_H^\gamma = 0.184$ mT; $g = 2.0059$ was attributed to the alkoxyl radical spin-adduct, produced *via* interaction of reactive oxygen species (ROS) with toluene [121,122]. Further signals were assigned to •DMPO-O_2^- ($a_N = 1.372$ mT, $a_H^\beta = 1.113$ mT; $g = 2.0057$) and •DMPO-OH ($a_N = 1.381$ mT, $a_H^\beta = 1.361$ mT, $a_H^\gamma = 0.131$ mT; $g = 2.0057$) spin-adducts [121,122],

in good accordance with the photoactivation of TiO_2 in toluene under oxygenated conditions [123].

The *ex situ* photoexcitation of titania in the aqueous solutions in the presence DMPO followed by the measurement of EPR spectra confirmed the generation of •DMPO-OH spin-adduct with spin Hamiltonian parameters a_N = 1.493 mT, a_H^β = 1.475 mT; g = 2.0057 [92]. The highest concentration of •DMPO-OH was found for the Ti0Zr, the presence of 5 or 10 % of ZrO_2 lowers its concentration, and only a negligible amount was detected for the sample Ti20Zr (Figure 4.15).
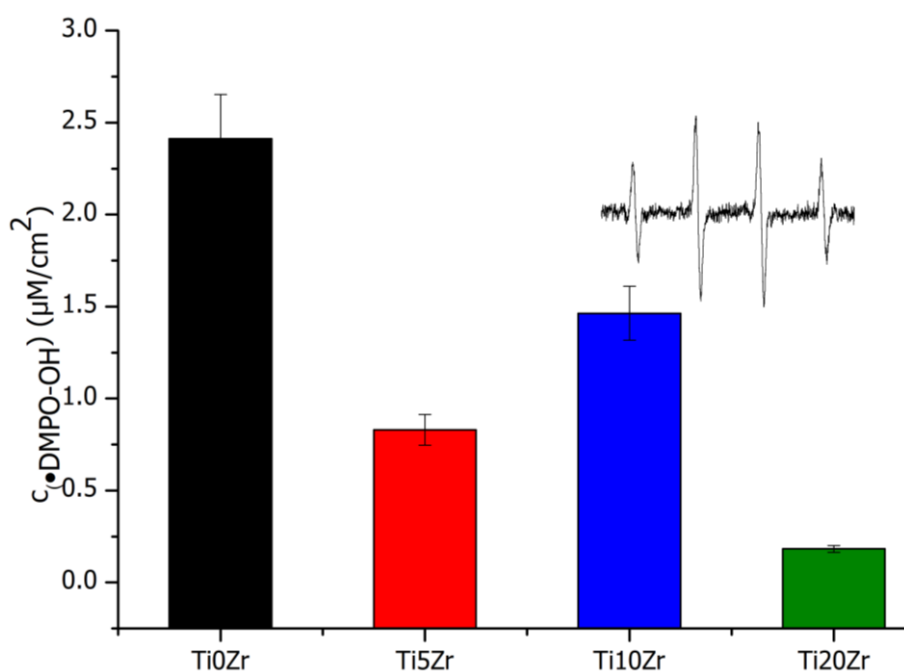
Figure 4.15 Concentration of •DMPO-OH evaluated by the double-integration of EPR spectra obtained upon ex situ irradiation of samples in the aerated aqueous DMPO solutions ($c_{0,DMPO}$ = 0.035 M). Inset: Experimental EPR spectrum obtained upon ex situ irradiation of Ti0Zr.

Figure 4.16 shows the sets of individual EPR spectra of Tempone in aerated toluene monitored upon irradiation, as well as upon exposure in the presence of Ti0Zr or Ti10Zr film on the glass. The results obtained demonstrate sufficient photostability of Tempone under experimental conditions, as well as the impact of immobilized photocatalysts on the elimination of Tempone.
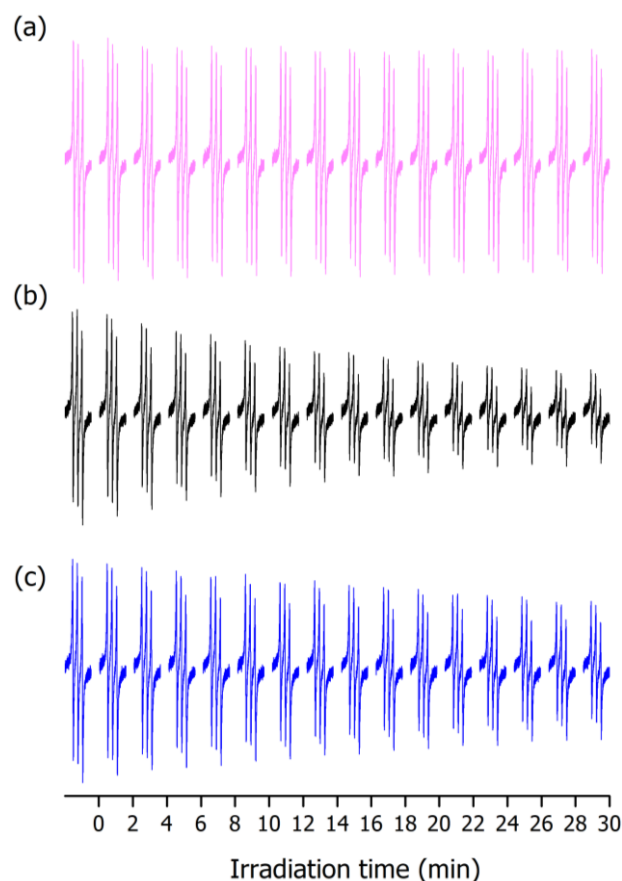
Figure 4.16 The sets of individual EPR spectra (SW = 8 mT) of nitroxide radical Tempone in aerated toluene monitored upon continuous UVA irradiation: (a) Reference; (b) Ti0Zr; (c) Ti10Zr.

The decrease of Tempone relative concentration was described using formal first-order kinetics (Figure 4.17, left), and the formal first-order rate constant was recalculated considering the irradiated surface of the photocatalyst (Figure 4.17, right).
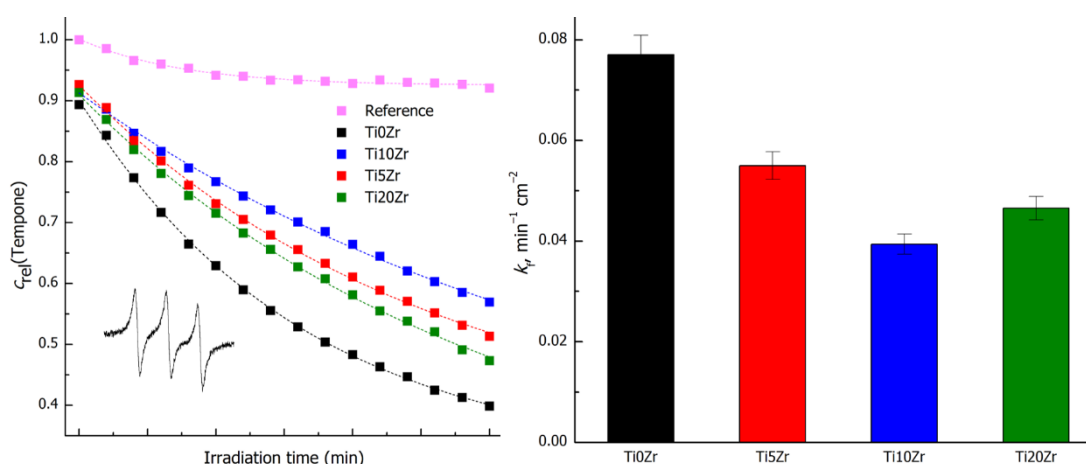
Figure 4.17 Left: Relative Tempone concentration measured upon continuous UVA photoexcitation. The inset represents the EPR spectrum of Tempone (SW = 6 mT, $c_{0, Tempone} = 10 \ \mu M$). Right: The formal first-order rate constant of Tempone degradation obtained upon in situ irradiation.

The results thus confirm the catalytic trends as were observed with the TPA technique. The sample without modification (Ti0Zr) was the most active in all activity tests and the samples with addition of Zr were considerably less active. Interestingly, as the TPA test showed practically the same activity of 5 and 10 % modification, also measuring the concentration of ·DMPO-OH spin-adduct showed a similar trend, thus concurring the two techniques.

Photoreduction of resazurin ink

Resazurin ink test was used for visual evaluation of the activity (Figure 4.18). The test relies on the reduction of the Rz ink by e$^-$ from the excited catalyst.
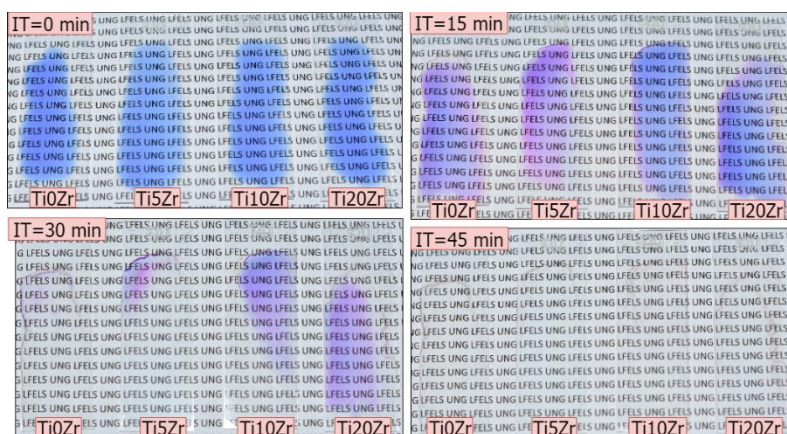
Figure 4.18 Degradation of the resazurin ink under UV light on different films deposited on a glass substrate; (IT – irradiation time).

The bare substrate is not shown, but there was no change in appearance under UVA irradiation. However, all the films show some wetting properties, that is, even at the very beginning, drops of water wet the surface to a certain degree (Figure 4.18, IT = 0). This observation concurs nicely with the WCA measurements, where the modified samples showed faster kinetics for decreasing the WCAs (5 % > 10 % > 20 %) compared to the Ti0Zr sample; while the unmodified sample showed the lowest final WCA. After 15 minutes, there is an obvious change in resazurin color on the Ti0Zr and Ti5Zr into pink (resorufin); thinner edges of the droplet on Ti10Zr and Ti20Zr also begin to change color. After 30 minutes, Ti0Zr and Ti5Zr become almost transparent (Rz ink is transformed into dihydroresorufin); meanwhile, Ti10Zr and Ti20Zr are still colored. After 45 minutes of irradiation, resazurin is almost completely discolored and transformed into dihydroresorufin. The same trend was observed as in other methods, Ti0Zr is the most active and with a higher content of Zr activity decreases.

4.2.9 Antibacterial assay

Microbial log reductions (Equation 16) of thin films on glass for *Escherichia coli* are shown in Figure 4.19. Three different irradiation times of experiments were chosen, 4, 12, and 24 hours. From the values on y-axis, we can see that logs reduction were small, less than 1-log reduction. Percents of reduction (Equation 17) of *E.coli* are also low (Table 4.3), which means that photocatalysts have insignificant efficiency on *Escherichia coli* inhibition [73].
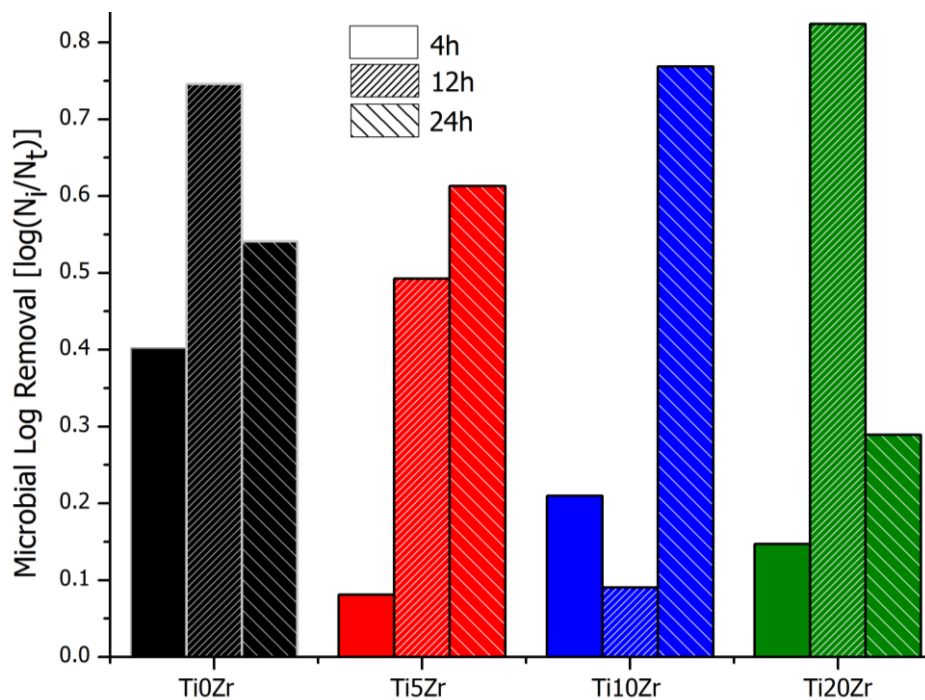
Figure 4.19 Microbial log reduction of Escherichia coli.

Figure 4.20 represents a log reduction of *Staphylococcus aureus* on thin films, experiments were held for 12 and 24 hours. Reduction of *S. aureus* on thin films was significantly higher in comparison to *E. coli*. It is interesting that reduction was the lowest in the case of Ti0Zr and that is entirely contrary to previous results of photocatalytic activity. The highest antibacterial efficiency has Ti10Zr. In Table 4.3, percent of reduction of *S. aureus* are shown, and it can be concluded that films have a powerful antibacterial effect against chosen bacteria.
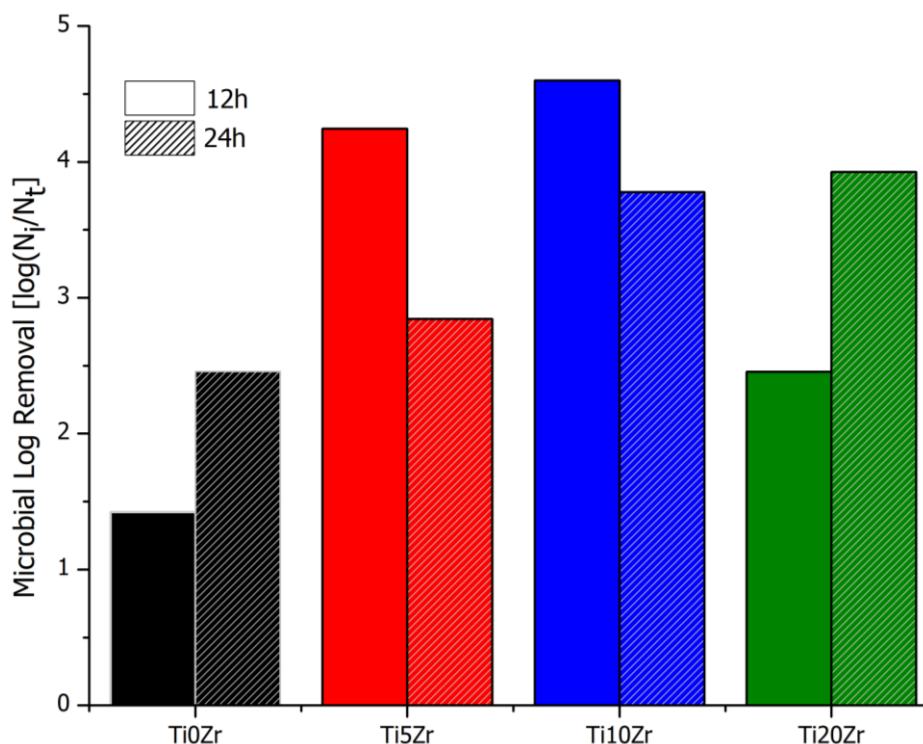
Figure 4.20 Microbial log reduction of Staphylococcus aureus.

Photokilling of bacteria is also significantly affected by light intensity, using greater intensity the TiO_2 reduction of bacteria is more successful [124]. One of many other conditions that also affect the reduction of microbes on thin films is the contact between surface and microbes [124]. Larger contact surface area is harder to achieve in case of photocatalytic thin film and therefore antibacterial activity is usually lower than in case of a particle-shaped photocatalyst in a liquid medium. The conclusion here is that low light intensity and poor contact area were the two major reasons for low activity in the case of *E. coli*.

Table 4.3 Percent reduction of E. coli and S. aureus.

	Escherichia coli			*Staphylococcus aureus*	
	4 h	12 h	24 h	12 h	24 h
Ti0Zr	60.38	82.05	71.22	96.22	99.71
Ti5Zr	17.04	67.83	75.63	99.99	99.86
Ti10Zr	38.29	18.85	82.97	99.99	99.98
Ti20Zr	28.76	85.00	48.61	99.65	99.99

No obvious relation between the concentration of zirconium and reduction of bacteria was found. It is interesting that Ti10Zr was the most effective against *S. aureus* and the surface area is the lowest. Also, in some cases reduction of bacteria was higher after 12 hours than after 24 hours. Colony count method has poor accuracy and

sensitivity; method provides the number of viable cells, which are able to form colonies and provides no information about cell impairments that could recover and grow in delay in smaller colonies [2,72].

Nevertheless, a striking difference between both types of bacteria chosen for antibacterial activity test could be explained. Bacteria cell structure and their wall thickness also play an important part in bacteria reduction. It seems that *E. coli* has a simple cell membrane, which interacts with and covers titania, thus shading the reactive surface of the photocatalyst, but opposite to *E. coli*, *Staphylococcus aureus* has a complex multilayered membrane, that cannot cover TiO_2 and activation of bacteria can thus be more successful [73].

4.2.10 Ecotoxicological assay with *Daphnia magna*

The ecotoxicological assay was conducted to see if TiO_2 process has any possible detrimental effects on the ecological parameters. The adverse effects could arrive from particles fouling from the immobilized catalyst surface into the water body or the degradation products which are formed during the photocatalytic oxidation and can be toxic to aquatic flora and/or fauna. *Daphnia magna* organisms were used in our case in order to test if the photocatalyst is detaching from the surface and if there is a toxicological effect of such process. Since the experiment did not include any organic pollutants, the effect of any intermediates being formed on/near the TiO_2 surface (apart from the ROS themselves) can be excluded. After 24 hours of the experiment, the number of mobile organisms was checked and no differences were observed. Results of the experiment after 48 hours of exposure *Daphnias* to photocatalytic films are presented in Figure 4.21.

In control (flask with a stock solution and water fleas, without photocatalyst), all organisms were still mobile. In the case of uncoated glass 95 % organisms were still mobile, the same as in the case of Ti10Zr sample. The other samples did not cause any effect on the organisms (100 % mobility was seen). It can be concluded that photocatalytic films were efficiently immobilized to the glass support, preventing possible nanotoxicity to *Daphnia magna*.
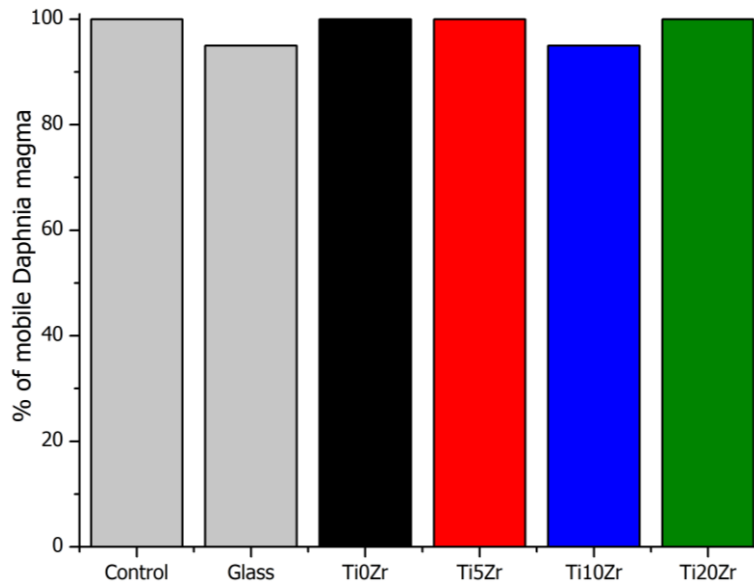
Figure 4.21 Mobile Daphnia magna after 48 hours of being exposed to photocatalytic thin films.

4.2.11 Field test of Ti10Zr thin films on float glass with a demonstration of their anti-fogging effect

Real-time experiments in real environments are important because usually, laboratory measurements differ from a field test since more variables impact on the activity of the test subject. Hence, we chose three locations across Slovenia and three different configurations (45° and 90° inclination and 90° inclination under roof) for testing of windows with photocatalytic layers applied [125]. For transparent photocatalytic films characteristics like haze, transparency and color are crucial; that is why they were regularly monitored during the experiment.

Samples chosen for this test were:

- Float glass: reference glass surface, without any layer or modification;
- BIOCLEAN™: reference photoactive glass from Saint-Gobain;
- Ti10Zr: float glass plus coating with the best compromise between long-term mechanical stability, hydrophilic effect and photocatalytic activities found in laboratory tests.

As expected from the real conditions which involve many parameters – some of them unfriendly to the nature of the photocatalytic process – Bioclean and Ti10Zr were not as effective as they were in laboratory conditions. Inclination angle had a considerable effect on self-cleaning activity. It seems that placement with the 90 ° tilt without roof

shows the highest transmittance and self-cleaning effect. This set of samples were at the end of the experiment the cleanest mainly due to the access to rain, sunlight and the possibility of dirt to slide down with water droplets. Based on the patterns of the crucial weather parameters and field measurements, it was concluded that raining patterns also had an influence. Results of lux, haze and CIELab measurements are shown in APPENDIX.

Anti-fogging properties were tested in the laboratory; samples were pressed against a cold aluminum block (cooled to -15 °C). Firstly, large droplets that scatter light and reduce the transparency of glass were formed on bare glass samples, shortly after those droplets were also formed on Bioclean sample and at the latest on the Ti10Zr coated float glass (see APPENDIX). Anti-fogging properties of our coatings were also observed on the office window at Faculty of Chemistry and Chemical Technology, University of Ljubljana. Figure 4.22 is a photo of window coated with Ti0Zr and Ti10Zr; it was taken one month after application (at the end of October, when morning temperatures were low). The difference between uncoated and coated area is easily visible, and it is in line with photocatalytic activity results. Even the difference between Ti0Zr and Ti10Zr is noticeable, demonstrating the higher anti-fogging activity of the sample without Zr addition on this relatively short time scale. After longer exposure, the difference became smaller and on a long-time scale, it is expected that the beneficial effect of improved durability of Ti10Zr over higher activity of Ti0Zr will prevail. It is important to state that the reason for antifogging properties of these films lies not only in the superhydrophilicity but also in the decreased emissivity of such coatings; every film that is deposited onto bare glass generally decreases the emissivity (float glass has $\varepsilon = 0.94$), the extent of which was not determined experimentally for our materials, due to the lack of equipment for such measurements.
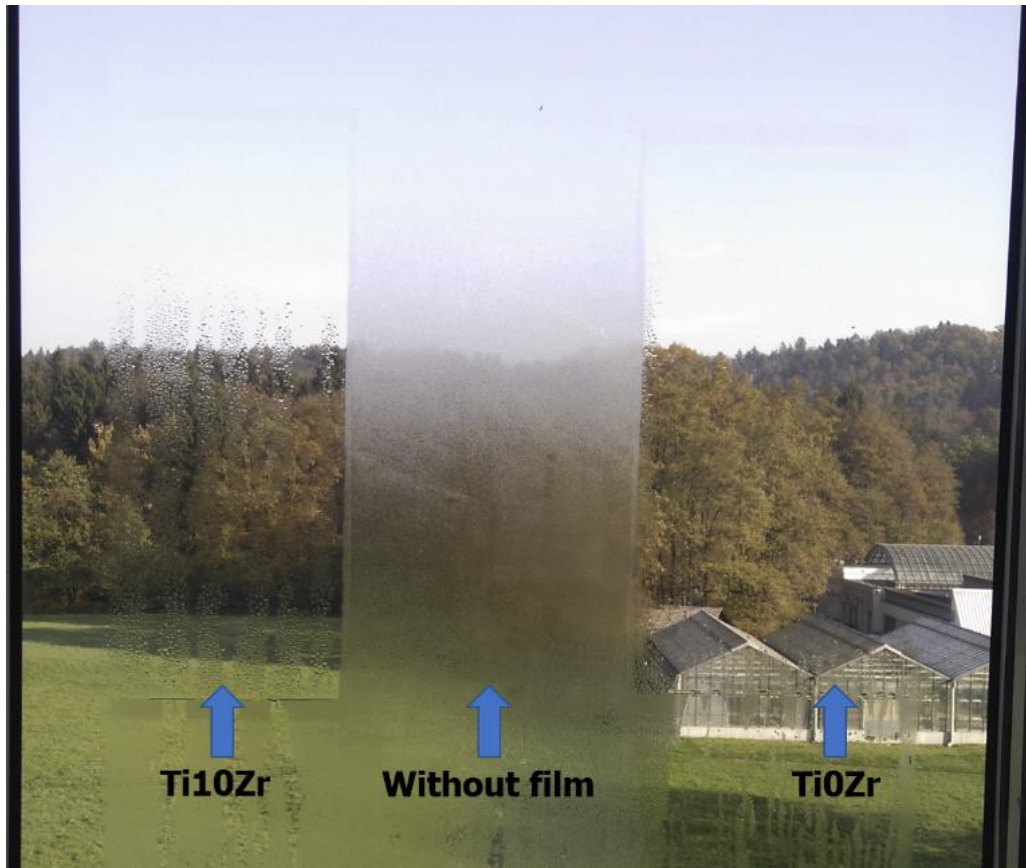
Figure 4.22 The anti-fogging effect of Ti10Zr and Ti0Zr thin film on a window. The photo was taken one month after application.

4.3 Thin films on thermosensitive substrates

The thin films that were used on glass were also deposited on thermosensitive substrates. These kinds of plastics are used in all kind of application and sometimes they even replace the glass material, because of more suitable properties or easier maintenance.

Four different substrates were chosen:
- PVC
- PMMA
- D1
- D2

Detailed descriptions of used substrates are given in section 3.1. They are thermally stable up to approximately 200 °C (see corresponding thermogravimetric analysis in Appendix).

4.3.1   UV-Vis transmittance

The transmittance of samples was recorded on transparent substrates PMMA (Figure 4.23) and PVC (Figure 4.24), while D1 and D2 substrates are not transparent, so UV-Vis transmission was not measured. Figures confirm high visible transparency of the samples. Again, samples with thin films generally showed higher transmittance than bare substrates in the visible region because films contain SiO_2, which has an antireflective property [116,117,126,127]. Nanostructured silica has a low refractive index and the thin film on substrate reduces reflection and improves light transmission, due to the presence of pores in the mesoporous silica-titania composite as described in previous chapters [128].
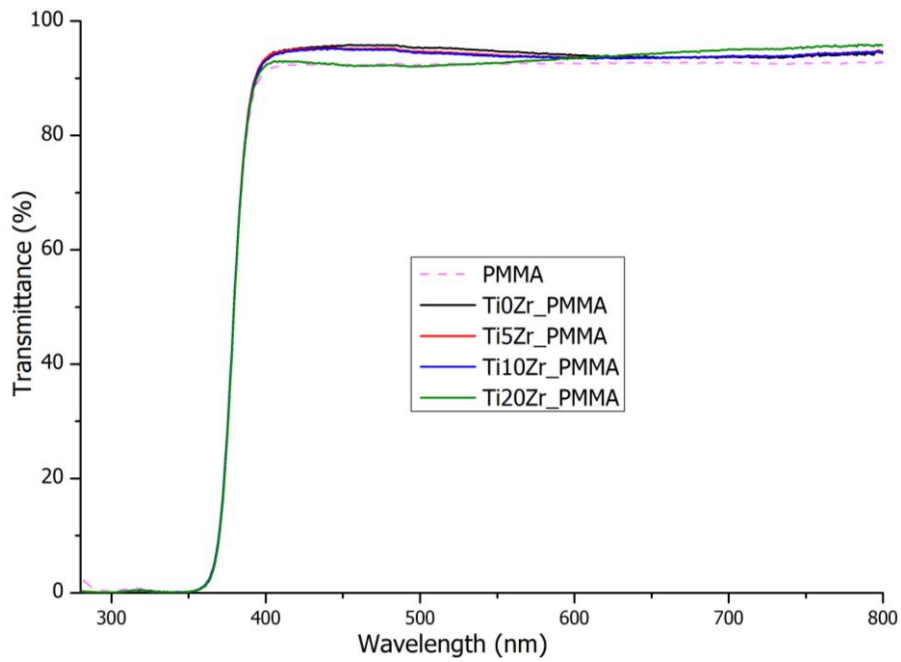
Figure 4.23 Transmission spectra of thin films on PMMA.

Differently to PMMA, bare PVC substrate transmits a part of the UV light, and the transmittance variation is noticeable among samples. The substrate starts to absorb at λ < 320 nm, but in case of thin film samples the transmittance shifts to higher wavelengths, *i.e.,* 350 nm (inset in Figure 4.24), which is close to the absorption edge of TiO_2.
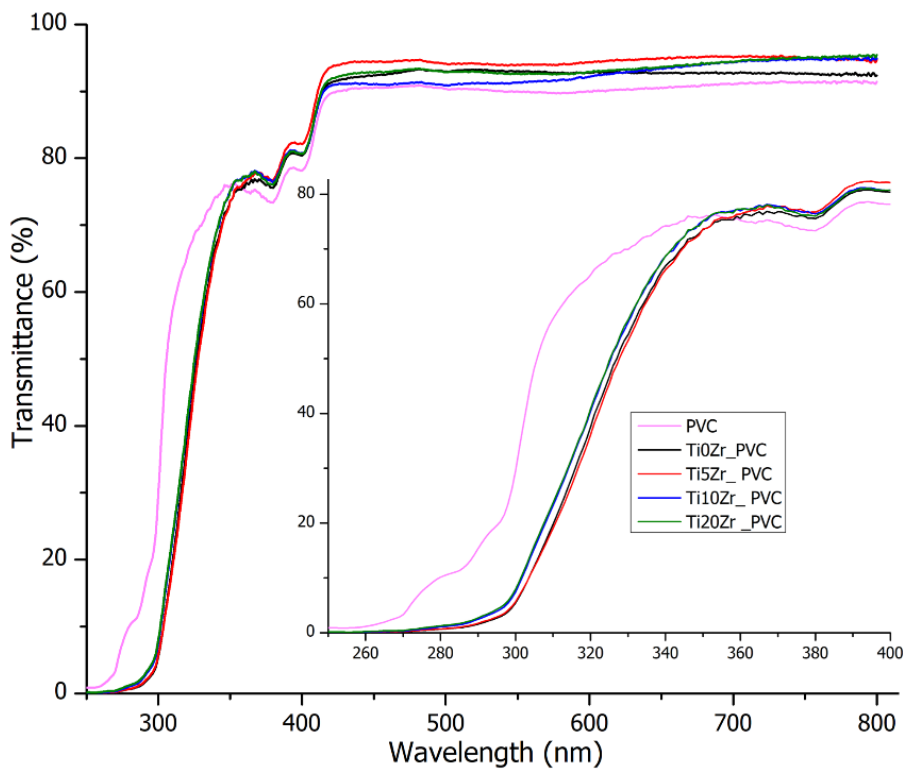
Figure 4.24 Transmission spectra of thin films on PVC.

72

4.3.2 Infrared spectroscopy (FTIR-ATR)

FTIR-ATR spectra of thin films on thermosensitive substrates (Figure 4.25) show a significant influence of the substrate, but distinguished bands of the films are also present. Bands around 2950 cm^{-1}, 2915 cm^{-1} and 2854 cm^{-1} that appear in all bare thermosensitive substrates can be assigned to C-H stretches. Bands around 1721-1725 cm^{-1} are assigned to C=O stretch and around 1433 cm^{-1} to CH$_2$ bending vibration [129]. All these bands appear in all four bare substrates. PMMA substrates have some additional characteristic peaks at 1386 cm^{-1}, 1238 cm^{-1}, 985 cm^{-1}, 964 cm^{-1} and 750 cm^{-1}, which are assigned to CH$_3$ bend, C-O stretch, CH$_3$ rock, C-H bend and CH$_2$ rock, C=O bend, respectively [129].

A characteristic broad band from 3600 and 3000 cm^{-1} for the OH groups is seen in all spectra with a thin film, whereas this broad band is of course not present on the substrate spectra. Also, Si-O-Si peaks around 1114 cm^{-1} and 1060 cm^{-1} are seen and the one assigned to Ti-O around 500 cm^{-1} is observed in all samples with thin films.
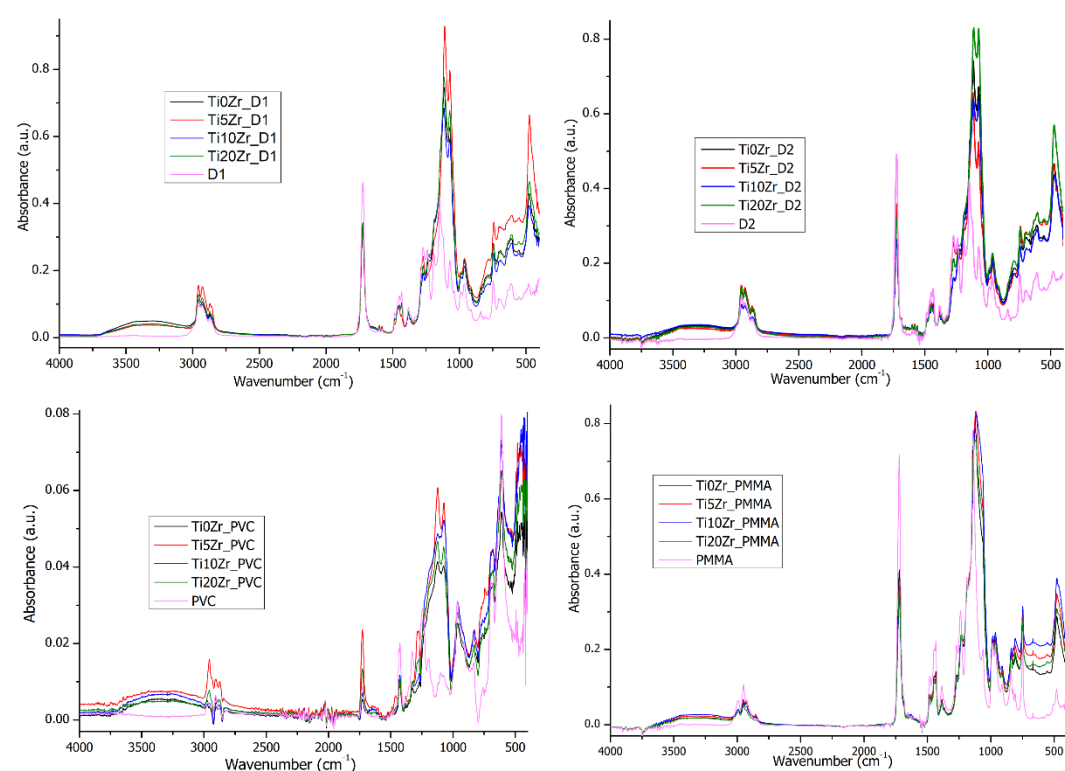
Figure 4.25 FTIR-ATR spectra of thin films on thermosensitive substrates. The graph on the top left D1, top right D2; bottom left PVC and bottom right PMMA.

4.3.3 Scanning electron microscopy

In Figure 4.26 SEM images of the Ti0Zr and Ti10Zr thin films on PVC, D1 and PMMA substrates are presented. Similary to the samples on glass substrate, the growth of the particles size and a trend towards better-resolved shapes can be seen in the 0 to 10 % Zr sample series. Also, the structure of the films is rougher upon Zr introduction, which is in agreement with our other characterization methods. As the size of anatase particles is progressively increasing upon Zr introduction, this manifests also in development of more granulated morphology of the films (Figure 4.10 and Figure 4.26) and films become rougher.
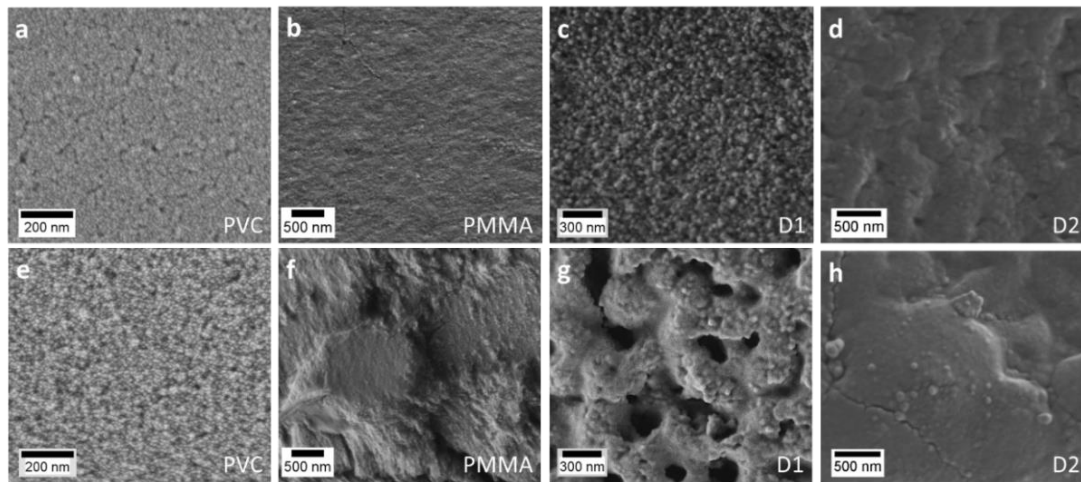
Figure 4.26 Scanning electron microscopy (SEM) images of Ti0Zr film (a – d) and Ti10Zr film (e – h) on four thermosensitive substrates: PVC, PMMA, D1, and D2.

4.3.4 Pencil hardness test

Pencil hardness tests were not possible to be conducted on substrates D1 and D2, because of the rough texture (PES fabric). Mechanical stability of PVC and PMMA specimen (Figure 4.27) show that the highest stability was obtained for the sample with the highest Zr content on both substrates, while sample without Zr was the least mechanically stable. Interestingly, although the trend of higher scratch resistance with higher Zr concentrations is present in both substrates, lower Zr loadings (0 and 5 %) performed better on PVC substrate, while TI10Zr shows higher stability with PMMA substrate. A scratch test was also performed on one-year-old PVC films stored in the dark (Figure 4.27, middle group). The Ti20Zr retained the stability, but the other three films lost their mechanical stability for one or two pencil hardness, which is in agreement with the measurements on glass substrates described in section 4.2.6 [96].
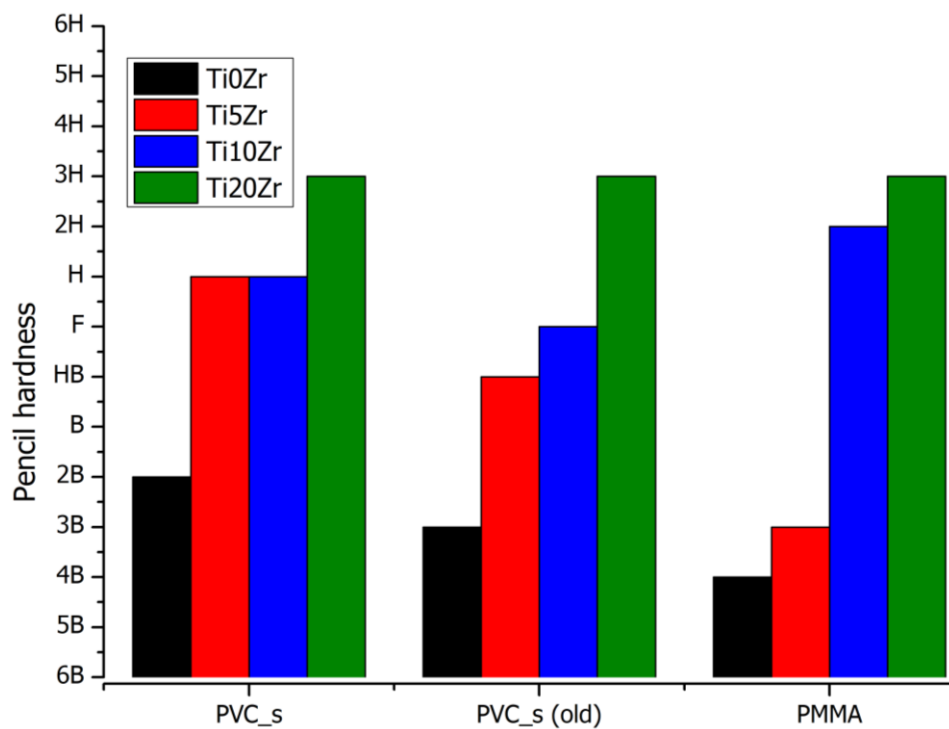
Figure 4.27 Results of the pencil hardness test.

4.3.5 Contact angle measurements

Surface wettability and the hydrophilic character were evaluated by measuring water contact angles (WCA), and they are shown in Figure 4.28. The WCAs of bare substrates were approximately 85 ° (PVC and D2) except for PMMA it was lower (65 °) and for D1 higher (95 °). The high WCA of D1 is a consequence of the presence of fluorine in the PVDF top layer, which is absent in the D2 bare substrate. The WCAs of all bare substrates do not show significant change after 3 h of UV irradiation. On the other hand, coating the surfaces with TiO_2 films showed much lower initial WCAs in case of PVC (15 - 25 °) and PMMA (15 - 20 °) substrates; it did not, however, affect the D1 and D2 initial WCAs - they remained relatively high, *i.e.*, 70 ° and 80 ° for D2 and D1 substrate, respectively. Upon irradiation, the WCAs decreased on PVC and PMMA samples, although no clear correlation can be deduced with the concentration of Zr in the TiO_2 film. Interestingly, the WCAs of films on D1 and D2 substrates increased upon irradiation, although mostly not in a statistically significant manner. From these observations, it seems that the films are highly active on PVC and PMMA substrates but not on acryl coated PES substrates.
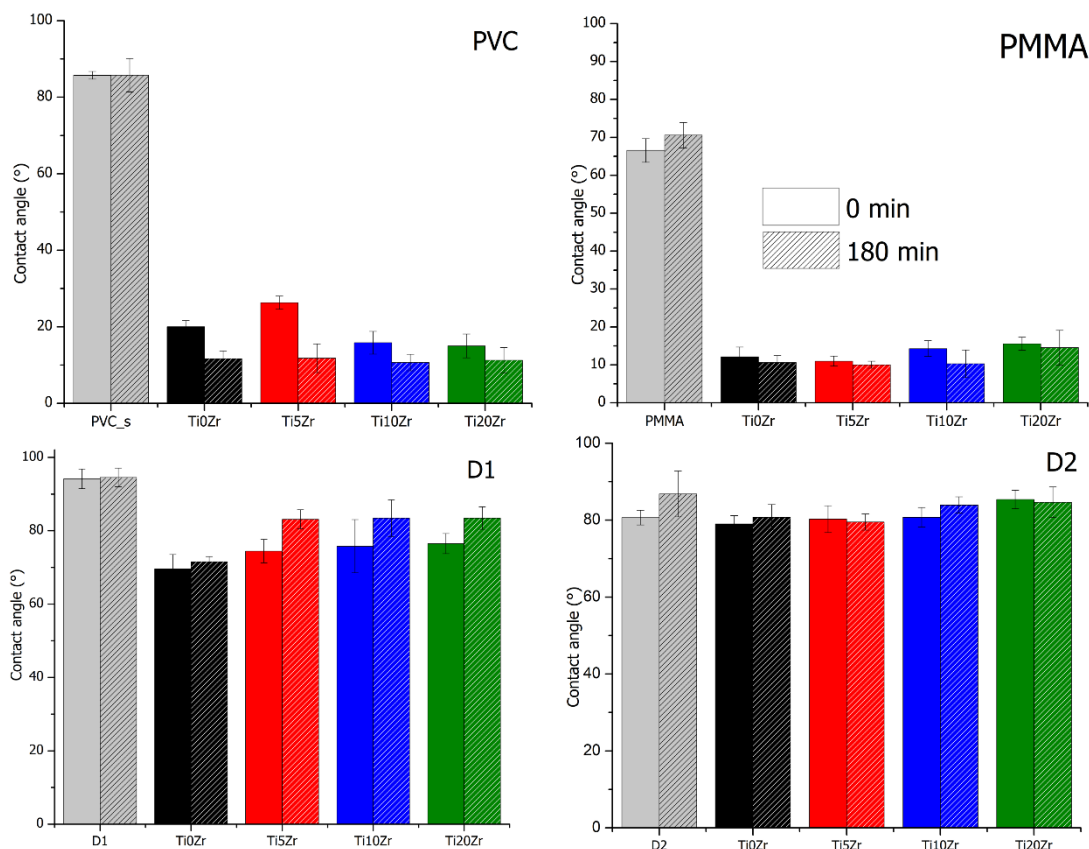
Figure 4.28 Contact angle measurement of thin films on thermosensitive materials, not-patterned columns are initial contact angles before irradiation; patterned columns are contact angles after 180 min of irradiation.

4.3.6 Photocatalytic activity

Photocatalytic activity of thin films on flexible substrates was measured, similarly to glass substrates, by two methods; measuring formation constant of HTPA and by a more visually oriented method with resazurin ink. The importance of measuring the activity again – although the interface (solid-solid for HTPA and solid-liquid for resazurin) remains the same – arises from the fact that the substrate could have a great influence on the behavior of films, either due to its different texture, chemical composition or optical properties, which, for example, reflect part of the incoming light back to the film in case of white polymer substrates such as D1 and D2.

Fluorescence measurements: TPA as a model contaminant

To determine photocatalytic activities, measurements of the HTPA formation rate on films were conducted (Figure 4.29). The addition of zirconium decreased the photoactivity of the films, regardless of the substrate used. These results are in

accordance with the study on glass substrates described previously and the reason for such a trend can be attributed to larger crystal size and consequently lower surface area, together with an increasing portion of inactive amorphous zirconia phase. Interestingly, the decrease in the activity of Ti20Zr films is similar at all of the substrates (~ 70 % decrease), except for D2 substrate where activity was lowered for only 44 % (and not statistically significant). However, this sample also showed the lowest activity in general. The reasons for this are still unclear.
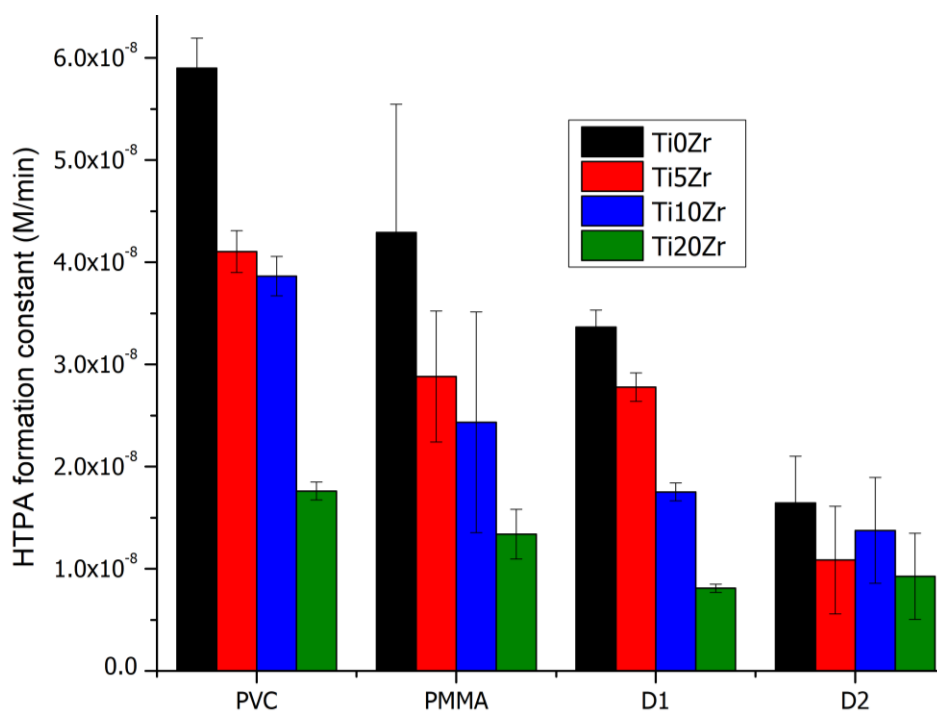
Figure 4.29 Photocatalytic activities determined by the rate constant of hydroxyterephthalic acid formation.

Films on PMMA and PVC substrates seem to be in general more active than films on D1 and D2; which was indicated already by WCA measurement shown above; activities of films on PVC are comparably high to the activities of films on glass (Figure 4.14).

Photoreduction of resazurin ink

The second and more visible-oriented photocatalytic test was the reduction of resazurin ink on the surface of the materials (Figure 4.30). Clearly, the neat substrates showed no discoloration of the ink and also substrates themselves were stable, even though the irradiation source was UV-light.
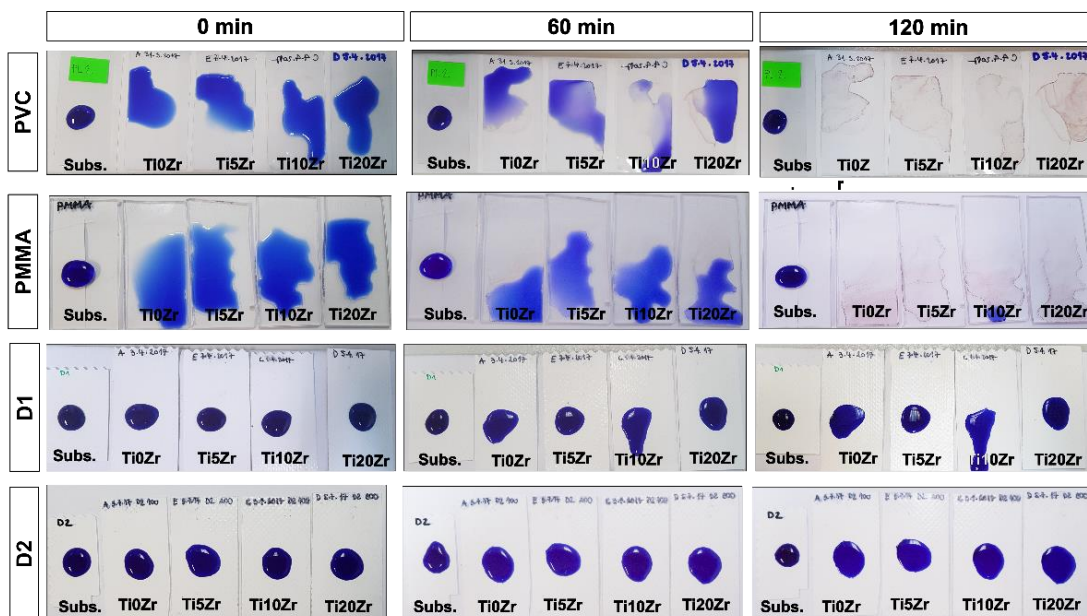
Figure 4.30 Degradation of the resazurin ink under UV light for thin films on substrates PVC, PMMA, D1, and D2. 0, 60 and 120 minute irradiation times are shown.

The wetting of the surface with increasing irradiation times was observable in the case of PVC and PMMA substrates, while for D1 and D2 substrates this effect was not seen, thus confirming their less hydrophilic nature when compared to PMMA and PVC. Between the latter two, PMMA is showing faster wetting of the surface with the resazurin, which is following the measurements of WCAs on these substrates, *i.e.*, PMMA showed more hydrophilic nature. Regarding the reduction of resazurin, only PVC and PMMA substrates showed a remarkable reduction of resazurin to resorufin (pink) and even further to dihydroresorufin (colorless) (Figure 3.10), as shown in Figure 4.30. PMMA, however, showed slightly higher discoloration at the final irradiation times. Generally, a higher percentage of Zr produced smaller discoloration in PVC and PMMA substrates, while D1 and D2 samples were much less active, and such a trend was not possible to observe.

Basically, samples have the same trend in activity at both methods, with TPA and resazurin, and the trend is also the same as in the case of glass substrates. Thermosensitive substrate gives better insight on the relation between the hydrophobic-hydrophilic character of a substrate and photocatalytic activity of the deposited films on them. Films on D1 and D2 are the least active and from Resazurin assay, it can be concluded that because of the hydrophobic surface droplet of Rz ink did not spread over the film. This had a consequence of smaller contact area and hence lesser chance for discoloration, which was not detected on these two samples. While

films on PVC and PMMA were more hydrophilic, consequently the TPA degradation was faster and after 120 min of irradiation, a droplet of Rz ink was almost completely discolored. It is also important to stress that formation constant of HTPA on films on PVC substrate can be comparable to films on a glass substrate, again much higher than on D1 and D2 substrates. The result is rather surprising, as the white color of D1 and D2 shows that at least a portion of the visible light gets reflected back and, if anything, this should boost the activity of films on such substrates. Clearly, the chemical composition of these substrates plays a role as well as their surface roughness. However, most importantly, the hydrophilic nature of films deposited on D1 and D2 is much lower, which means lower contact area and that results in lower production of OH radicals on the surface.

4.3.7 Accelerated aging of D1

Although the activity of photocatalytic films on D1 and D2 substrates was not comparable to other ones (especially glass and PVC), their large shaping capabilities and extreme anti-wear resistance have made them extremely applicable. Therefore, they nevertheless represent a possible substrate for application of such films in the future. The instability of acrylic coatings in the presence of TiO_2 and UV-irradiation has been described in the literature [130]. The resistance of PVDF membranes has also been investigated, especially for application in electronic devices [131]. Degradation of the chosen polymeric substrates could be expected due to the formation of the highly reactive radicals or h^+ themselves by the photocatalyst layer, as confirmed by the HTPA test. Hence, a simulated aging experiment was performed; the bare D1 substrate, a D1 substrate with the Ti10Zr film without binder, and a D1 substrate with the Ti10Zr film with SiO_2 binder were irradiated for 14 days (336 hours) in a Suntest chamber with a daylight filter applied. Figure 4.31 shows that the bare substrate (stable under UVA/B irradiance) and film with SiO_2 binder were stable after such prolonged exposure to light in the accelerated aging experiment.
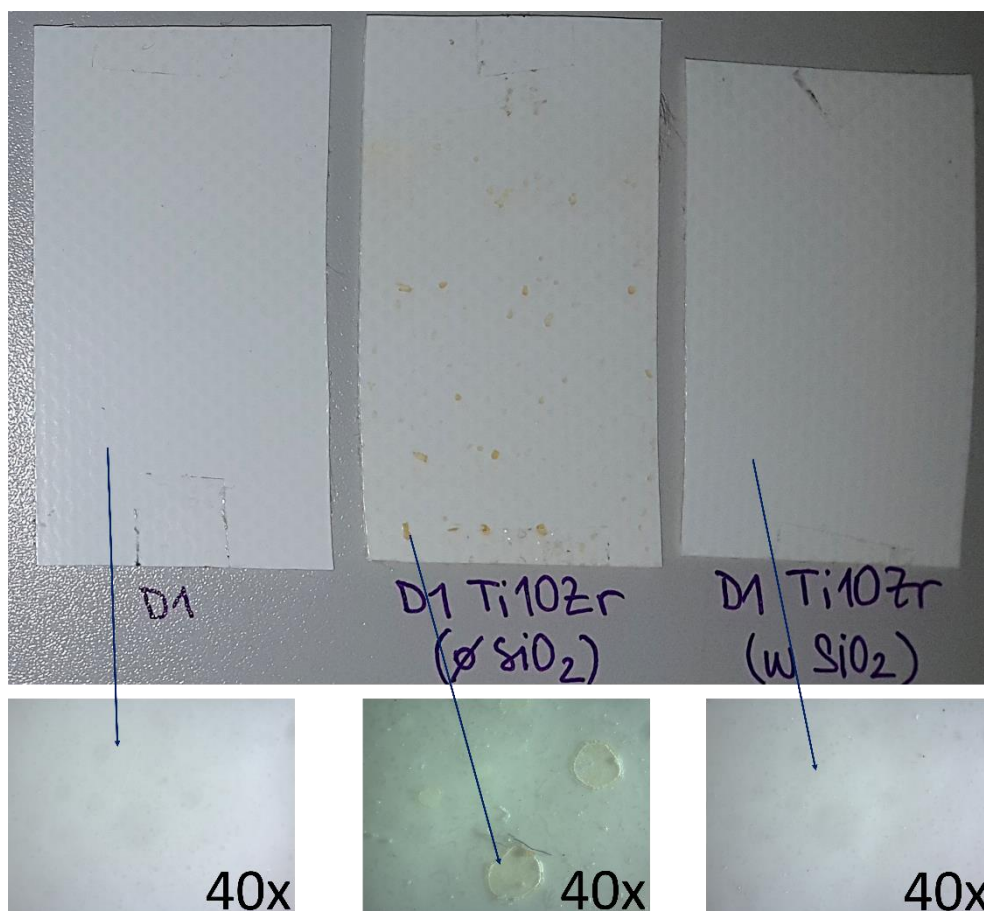
Figure 4.31 D1 samples exposed to accelerated aging in Suntest chamber under a daylight filter for 14 days. Left: a bare substrate; middle: Ti10Zr film without SiO₂ binder; right: Ti10Zr with SiO₂ and their appearance under higher magnification (below).

On the contrary, yellow spots appeared on the sample with the photocatalytic layer, lacking the SiO_2 binder (Figure 4.31, middle). A closer look (Figure 4.31, below) showed crater-like surface structures on the substrate surface, which additionally caused part of the photocatalytic layer to detach at such spots. Further identification of changes in the samples was conducted by FTIR-ATR (Figure 4.32). The semi-crystalline polymer which sits on top of the acryl-painted PES fabric shows a complex structure and can present several distinct crystalline phases that are related to different chain conformations; commonly α-, β-, and γ-phase. The β-phase is characterized by a peak at 1273 cm^{-1} [132], while α-phase was detected at 612, 967, and 1383 cm^{-1}. The presence of γ-phase was also evidenced by the peak at 1240 cm^{-1}, thus confirming the presence of a mixture of α-, β-, and γ-phase PVDF on the surface of the polymer support, as stated by the producer [133].
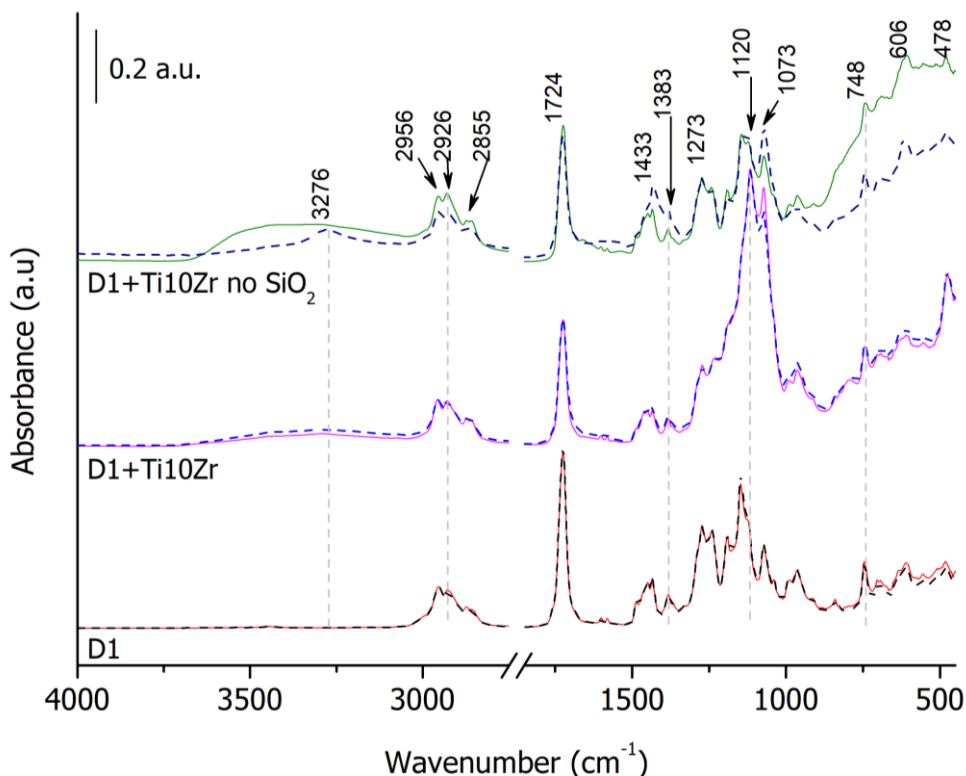
Figure 4.32 ATR-FTIR spectra of fresh (solid lines) and samples irradiated in Suntest for 14 days (dashed lines).

The TiO$_2$-coated samples show ν(OH) at 3600 – 3200 cm^{-1}, indicating on a more hydroxylated surface, which is in accordance with the CA measurements. It can be observed, however, that the TiO$_2$ films without SiO$_2$ showed even more hydroxylated surface versus Ti10Zr that contains SiO$_2$ binder. The wide absorption around 700 – 400 cm^{-1} is ascribed to δ(OTiO), due to the presence of TiO$_2$ in the coating layer. Upon simulated aging, several features in the spectra of TiO$_2$ coated D1 sample (without SiO$_2$ binder) appeared, *i.e.*, in the sample that exhibited photo-yellowing. In FTIR spectra pointed at the yellow spot a reduction of absorption bands in the 900 – 400 cm^{-1} range – vibrations of TiO$_2$ lattice – is seen; it indicates the TiO$_2$ active layer was masked, probably by organics from the D1 polymer. Also, the 1073 cm^{-1} peak increased, which could be ascribed to ν(CF) [134,135], suggesting the higher exposure of the C–F bonds. The peak at 1383 cm^{-1} also increased together with 1431 cm^{-1} band; the latter belongs to α-phase of PVDF [132]. Indeed, the α-phase has a more open structure, thus rendering the detection of C–F in a higher number. Second, an increase in the peak at 3266 cm^{-1} was seen together with a decrease of the ν(OH) band. Absorptions at such high frequencies are characteristic for OH, FH, and NH stretching vibrations [135]. Nasef et al. [131] claimed that the mechanism upon electron beam

81

irradiation-mediated degradation of PVDF membrane involved the elimination of HF upon crosslinking. This explains the presence of ν(FH) in the aged films as HF becomes trapped in-between the PVDF and TiO_2 layer.

Additionally, Dzinun et al. [136] studied the prolonged UV-stability of TiO_2/PVDF dual-layer hollow fiber membranes. Similar observations with respect to the aging of the PVDF were reported and ascribed to a higher number of carbon-carbon double bonds (–CF=CH–) formed due to the dehydrofluorination, *i.e.*, the elimination of an H–F unit, resulting in the formation of a carbon-carbon double bond. They also attributed the appearance of yellow color after prolonged UV-exposure to the consequence of the mentioned phenomenon. Our data suggest a partially distorted structure of the PVDF polymer and an increase in the α-phase fraction; hence, crosslinking probably appeared to some degree, while the yellow color suggests the formation of double bonds in –(CF=CH)– units. These results corroborate with the WCA measurements, where D1 coated with TiO_2 layer showed increased hydrophobic nature. That layer included a SiO_2 binder—this layer (shown in Figure 4.32), however, also showed a slightly decreased band at 3266 cm^{-1} (ν(OH) band). Hence, the low activity of this substrate can be explained by the decreased concentration of surface –OH species upon irradiation.

However, the presence of SiO_2 binder inhibited this process, which was proved by the FTIR spectra and photographs (Figure 4.31) before and after the aging experiment, and thus it acts beneficially not only at improving the mechanical and optical properties of the films but also extending the stability of the support.

5 CONCLUSIONS

TiO$_2$ sol solutions were prepared by the low-temperature sol-gel method with alkoxide precursors. There were four different sols prepared with the various concentration of zirconium content. Sols with 0, 5, 10 and 20 molar percent of Zr according to Ti were produced. Upon prolonged reflux, suspension with amorphous precipitate transformed into a colloidal solution with semi-crystalline particles. Zirconia was added to titania to improve its performance and/or to improve TiO$_2$ response to visible light. Thin films were deposited by dip-coating technique.

Coupling TiO$_2$ with amorphous ZrO$_2$ (Zr oxo-clusters probably formed on titania surface through Zr-modification) did not result in improvement of photocatalytic activity; actually, it was substantially reduced. Lower surface area and larger particle sizes of the modified titania can be one of the reasons for that. However, TiO$_2$-ZrO$_2$ nanocomposite had better mechanical stability, which was maintained during long-term aging. The reasons for this lied in the changed surface morphology of the modified samples. We assume that amorphous zirconia with higher scratch resistance protects active titania phase in the composite material.

Silica sol was added after the first trials to deposit TiO$_2$-ZrO$_2$ solutions on the glass in order to get uniform films. SiO$_2$ provides preferable mechanical and optical properties, and in the case of the organic substrate, it protects the substrate. TiO$_2$ can deteriorate organic substrates, as shown in this work with the aging experiment on PVDF substrate (D1). Long term exposure of D1 sample with TiO$_2$ (sample without SiO$_2$) damaged the surface, while the sample with TiO$_2$ and silica showed no visible damage to the substrate. We were able to explain the structural changes on such surface that accompanied the damage under accelerated aging conditions.

X-ray powder diffraction confirmed the presence of crystalline anatase phase, which is generally accepted as the most active TiO$_2$ phase. The particle sizes (obtained from the (101) anatase reflection) increased with increased zirconium content. Particles in Ti20Zr sample were almost twice the size (7.7 nm) of the particles in the sample without Zr (4.2 nm). XRD data were well correlated to the measurements of the specific surface area, showing that samples with smaller particles have a higher surface area and *vice versa*. Although the low-temperature heat treatment was chosen, we were interested in the thermal behavior of the prepared solution-derived powders. Results

show that no further crystallization occurred, nor in titania, nor in zirconia and that the exothermic peaks could be attributed to the combustion of the residual organic matter from the precursors.

SEM images of the films on glass substrate also confirmed the XRD measurements; a gradual transformation of the film's morphology with a higher content of zirconium was observed. Particles on the surface became more spherical, well defined and larger. The same trend was also observed on organic substrates; thin films with Zr had a rougher surface.

UV-Vis technique performed on the films deposited on transparent substrates showed high optical quality in addition to antireflective properties of such films and also confirmed the presence of titania phase with the absorption edge below 400 nm.

Complementary, bandgap values of the samples were determined by two methods: powders were measured with UV-Vis diffuse reflectance spectroscopy and thin films on a glass substrate with laser beam deflection spectroscopy. Both methods showed the same trend, though values that were measured by the LBDS technique are slightly higher. The largest bandgap was measured with Ti0Zr sample, following by Ti5Zr, Ti10Zr, and Ti20Zr. Reduction in bandgap with a higher concentration of zirconium may be related to a particle size, which increases by the content of zirconium.

Superhydrophilic phenomenon of TiO_2 which happens under UV irradiation, was measured by the water contact angle (WCA). WCAs before irradiation were the lowest on glass substrate while thermosensitive substrates showed higher WCAs. The impact of substrates was pronounced, especially in the case of D1 and D2. Under irradiation, WCAs decreased.

Photocatalytic activity measurements with methyl stearate contaminant showed that after UV exposure Ti0Zr sample was the most active sample, followed by Ti5Zr and Ti10Zr and the least active was Ti20Zr. The same trend was also observed with all the other photocatalytic activity tests.

Another solid-solid interface activity measurement method of films was a fluorescence method with the terephthalic acid probe. Activities of the films differed according to a substrate. Thus, films on glass were the most active, followed by PVC samples, PMMA samples, D1, and the lowest activity was seen with films on D2 substrates. Probably, films on hydrophobic substrates have low activity because of the influence

of substrate and possibly deposition of more layers would minimize the influence of the substrate. On each substrate, films had the same trend with Ti0Zr as the most active film, and activity decreasing with increased zirconium content.

Visually oriented, more qualitative activity test with an aqueous solution of resazurin dye was also used. Under UV irradiation, resazurin in the presence of TiO_2 transforms to resorufin and later on into colorless dihydroresorufin. The discoloration of resazurin happened the fastest on films on glass substrates, followed by PVC and PMMA, whereas because of the hydrophobic nature of D1 and D2 there was only a slight discoloration observed on these samples.

Scratch resistance was evaluated by a pencil hardness test. It was performed on glass, PVC, PMMA and not on D1 and D2 because of their rough surface. Films on glass substrate had better resistance compared to PMMA and PVC samples that showed lower stability. The strength of films increased with the content of zirconium and Ti20Zr was the most mechanically stable coating in all cases. The integrity of films was also checked after one year, during which they were stored in the dark at ambient conditions. Ti0Zr, Ti5Zr, and Ti10Zr lost their stability after one year for a few pencil hardness rates, where Ti0Zr suffered the highest loss. Surprisingly, Ti20Zr thin films did not lose their stability and mechanical integrity at all, confirming strong positive effect of Zr addition.

Thus, the best compromise between mechanical stability and photocatalytic activity was found in sample Ti10Zr. That is why this sample was tested in the outdoor setting in the course of 1.5 years. It was shown that the self-cleaning efficiency was comparable to that of the commercial glass, although much lower than reported in the lab results. On the other hand, the antifogging effect of such layers was highly expressed even in prolonged installment times and offers a promising route for commercialization of such materials.

6 SCIENTIFIC CONTRIBUTIONS

Journal articles:

Transparent titania-zirconia-silica thin films for self-cleaning and photocatalytic applications; Nives Vodišek, Kandalam Ramanujachary, Vlasta Brezová, Urška Lavrenčič Štangar; Catalysis Today 287 (2017) 142 - 147.

Transparent photocatalytic thin films on flexible polymer substrates; Nives Vodišek, Andraž Šuligoj, Dorota Korte and Urška Lavrenčič Štangar; Materials 11 (2018) 1945 - 1961.

WO_3-decorated ZnO nanostructures for light-activated applications; Alberto Gasparotto, Giorgio Carraro, Chiara Maccato, Cinzia Sada, José Balbuena, Manuel Cruz-Yusta, Luis Sánchez, Nives Vodišek, Urška Lavrenčič Štangar, Davide Barreca; CrystEngComm 20 (2018) 1282 - 1290.

Field test of self-cleaning TiO_2-SiO_2 films on glass with demonstration of their anti-fogging effect; Andraž Šuligoj, Olena Pliekhova, Nives Vodišek, Mohor Mihelčič, Angelja K. Surca, Roman Kunič, Barbara Šubic, Jernej Starman, Aleš Ugovšek, Urška Lavrenčič Štangar; Materials 12 (2019) 2196.

Conference contributions:

Low-temperature TiO_2/ZrO_2/SiO_2 photoactive thin films on glass; Nives Vodišek and Urška Lavrenčič Štangar, 2015, International Scientific Conference on Nanomaterials & Applications "Nanoapp" (2; 2015; Maribor)

Transparent titania-zirconia thin films for self-cleaning and photocatalytic application; Nives Vodišek, Kandalam Ramanujachary, Vlasta Brezová, Urška Lavrenčič Štangar, European Meeting on Solar Chemistry and Photocatalysis: Environmental Applications "SPEA" (9; 2016; Strasbourg)

Self-cleaning and photoactive TiO_2-ZrO_2-SiO_2 films on thermosensitive and glass substrates; Nives Vodišek, Urška Lavrenčič Štangar, 2017, International Scientific Conference on Nanomaterials & Applicationsc"Nanoapp" (3; 2017; Maribor)

Antibacterial and photocatalytically active titania-zirconia-silica thin films; Nives Vodišek, Urška Lavrenčič Štangar, 2017, International Conference on New Photocatalytic Materials for Environment, Energy and Sustainability (2; 2017; Ljubljana)

Transparent thin films with self-cleaning efficiency and improved durability prepared at low temperatures; [invited lecture]: Urška Lavrenčič Štangar, Nives Vodišek, 2017. International Conference on New Photocatalytic Materials for Environment, Energy and Sustainability (2; 2017; Ljubljana)

Titania-silica based nanostructured films for photocatalysis in solid, aqueous and gaseous phase; [oral presentation]: Urška Lavrenčič Štangar, Andraž Šuligoj, Nives Vodišek, Olena Pliekhova, Nataša Novak Tušar; Solid state ionics: 21st International Conference, June 18-23, 2017, Padua, Italy: program guide and abstracts.

Transparent titania-based thin films with silicate binder for self-cleaning and photocatalytic applications [invited lecture]; Urška Lavrenčič Štangar, Nives Vodišek, Andraž Šuligoj; International Conference on Modern Materials and Technologies (14; 2018; Perugia); International Ceramics Congress (14; 2018; Perugia); Forum on New Materials (8; 2018; Perugia).

7 TRANSFER OF KNOWLEDGE

The simple idea is to have a self-cleaning surface that would with the help of sun and rain or an occasional splash of water, clean itself (Figure 7.1).

The synthesized photocatalysts (Ti0Zr and Ti10Zr) were deposited on window glass in the frame of applied research project Thermo-and Photo-Active Coatings for Windows (project partners: University of Nova Gorica, National Institute of Chemistry; University of Ljubljana, Faculty of Chemistry and Chemical Technology and Faculty of Civil and Geodetic Engineering; M SORA d.d.).

These solutions have the potential to be used in a bigger industrial scale, except the deposition method should be changed and optimized into a more suitable method for coating large areas, for example, spray coating. One of the interesting characteristics is that a coating can also be applied on the already built-in surface and does not need a high fixing temperature (on site it can be treated by a blow dryer, heat gun or even just sunlight).

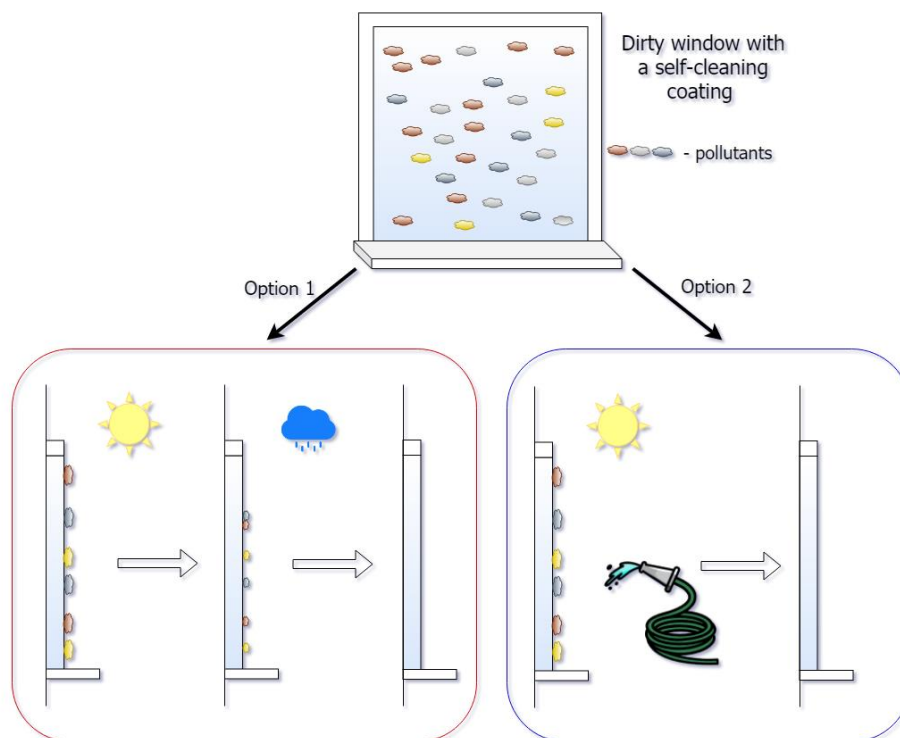
Figure 7.1 Basic idea of an outdoor self-cleaning surface with TiO₂.

Figure 7.1 shows two theoretical options of outdoor self-cleaning. Water is not a condition but is accelerating the photocatalysis of pollutants on the self-cleaning surface.

8 REFERENCES

[1]   F. Fresno, R. Portela, S. Suárez, J.M. Coronado, Photocatalytic materials: recent achievements and near future trends, J. Mater. Chem. A. 2 (2014) 2863–2884.

[2]   U. Žvab, U. Lavrenčič Štangar, M. Bergant Marušič, Methodologies for the analysis of antimicrobial effects of immobilized photocatalytic materials, Appl. Microbiol. Biotechnol. 98 (2014) 1925–1936.

[3]   R. Nakano, M. Hara, H. Ishiguro, Y. Yao, T. Ochiai, K. Nakata, T. Murakami, J. Kajioka, K. Sunada, K. Hashimoto, A. Fujishima, Y. Kubota, Broad Spectrum Microbicidal Activity of Photocatalysis by TiO_2, Catalysts. 3 (2013) 310–323.

[4]   D. Mukherjee, S. Barghi, A. Ray, Preparation and Characterization of the TiO_2 Immobilized Polymeric Photocatalyst for Degradation of Aspirin under UV and Solar Light, Processes. 2 (2013) 12–23.

[5]   T. Ochiai, A. Fujishima, Photoelectrochemical properties of TiO_2 photocatalyst and its applications for environmental purification, J. Photochem. Photobiol. C Photochem. Rev. 13 (2012) 247–262.

[6]   H. Park, Y. Park, W. Kim, W. Choi, Surface modification of TiO_2 photocatalyst for environmental applications, J. Photochem. Photobiol. C Photochem. Rev. 15 (2013) 1–20.

[7]   R. Dastjerdi, M. Montazer, A review on the application of inorganic nano-structured materials in the modification of textiles: Focus on anti-microbial properties, Colloids Surfaces B Biointerfaces. 79 (2010) 5–18.

[8]   M. Pelaez, N.T. Nolan, S.C. Pillai, M.K. Seery, P. Falaras, A.G. Kontos, P.S.M. Dunlop, J.W.J. Hamilton, J.A. Byrne, K. O'Shea, M.H. Entezari, D.D. Dionysiou, A review on the visible light active titanium dioxide photocatalysts for environmental applications, Appl. Catal. B Environ. 125 (2012) 331–349.

[9]   R. Saravanan, F. Gracia, A. Stephen, Basic Principles, Mechanism, and Challenges of Photocatalysis, in: M.M. Khan, D. Pradhan, Y. Sohn (Eds.), Nanocomposites Visible Light. Photocatal., Springer International Publishing, 2017: pp. 19–40.

[10]   A. Mattsson, C. Lejon, S. Bakardjieva, V. Štengl, L. Österlund, Characterisation, phase stability and surface chemical properties of photocatalytic active Zr and Y co-doped anatase TiO_2 nanoparticles, J. Solid State Chem. 199 (2013) 212–223.

[11]   K. Pirkanniemi, M. Sillanpää, Heterogeneous water phase catalysis as an environmental application: a review, Chemosphere. 48 (2002) 1047–1060.

[12]   A. Khataee, G.A. Mansoori, Nanostructured Titanium Dioxide Materials, World Scientific Publishing Co., 2011.

[13]   M.W. Kadi, R.M. Mohamed, Enhanced Photocatalytic Activity of ZrO_2-SiO_2 Nanoparticles by Platinum Doping, Int. J. Photoenergy. 2013 (2013) 1–7.

[14]   R.M. Mohamed, D.L. McKinney, W.M. Sigmund, Enhanced nanocatalysts, Mater. Sci. Eng. R Reports. 73 (2012) 1–13.

[15]   L. Zhang, R. Dillert, D. Bahnemann, M. Vormoor, Photo-induced hydrophilicity and self-cleaning: models and reality, Energy Environ. Sci. 5 (2012) 7491.

[16]   Y. Nosaka, A. Nosaka, Introduction to Photocatalysis: From Basic Science to Applications, The Royal Society of Chemistry, Cambridge UK, 2016.

[17]   M. Castellote, N. Bengtsson, Principles of TiO_2 Photocatalysis, in: Appl. Titan. Dioxide Photocatal. to Constr. Mater., Springer Netherlands, Dordrecht, 2011: pp. 5–10.

[18] R. Wang, K. Hashimoto, A. Fujishima, M. Chikuni, E. Kojima, A. Kitamura, M. Shimohigoshi, T. Watanabe, Light-induced amphiphilic surfaces, Nature. 388 (1997) 431–432.

[19] A. Fujishima, X. Zhang, D.A. Tryk, TiO_2 photocatalysis and related surface phenomena, Surf. Sci. Rep. 63 (2008) 515–582.

[20] H. Zhang, J.F. Banfield, Understanding Polymorphic Phase Transformation Behavior during Growth of Nanocrystalline Aggregates: Insights from TiO_2, J. Phys. Chem. B. 104 (2000) 3481–3487.

[21] K. Fischer, A. Gawel, D. Rosen, M. Krause, A. Abdul Latif, J. Griebel, A. Prager, A. Schulze, Low-Temperature Synthesis of Anatase/Rutile/Brookite TiO_2 Nanoparticles on a Polymer Membrane for Photocatalysis, Catalysts. 7 (2017) 209.

[22] T. Luttrell, S. Halpegamage, J. Tao, A. Kramer, E. Sutter, M. Batzill, Why is anatase a better photocatalyst than rutile? - Model studies on epitaxial TiO_2 films, Sci. Rep. 4 (2015) 4043.

[23] H. Yang, S. Zhu, N. Pan, Studying the mechanisms of titanium dioxide as ultraviolet-blocking additive for films and fabrics by an improved scheme, J. Appl. Polym. Sci. 92 (2004) 3201–3210.

[24] K. Schilling, B. Bradford, D. Castelli, E. Dufour, J.F. Nash, W. Pape, S. Schulte, I. Tooley, J. van den Bosch, F. Schellauf, Human safety review of "nano" titanium dioxide and zinc oxide, Photochem. Photobiol. Sci. 9 (2010) 495.

[25] D. Adak, S. Ghosh, P. Chakrabarty, A. Mondal, H. Saha, R. Mukherjee, R. Bhattacharyya, Self-cleaning $V-TiO_2:SiO_2$ thin-film coatings with enhanced transmission for solar glass cover and related applications, Sol. Energy. 155 (2017) 410–418.

[26] J. He, Self-cleaning Coatings: Structure, Fabrication and Application, RSC smart, Cambridge: Royal Society of Chemistry, Cambridge, 2017.

[27] J.-Z. Wang, J.-P. Zhou, Y. Wang, N. Miao, Z.-Q. Guo, Y.-X. Lei, The surface reactivity and structural properties of anatase TiO_2 (001), (100), (101) and (105) surface researched with DFT, Proc. Natl. Acad. Sci. India Sect. A Phys. Sci. 2 (2018).

[28] J. Lukáč, M. Klementová, P. Bezdička, S. Bakardjieva, J. Šubrt, L. Szatmáry, Z. Bastl, J. Jirkovský, Influence of Zr as TiO_2 doping ion on photocatalytic degradation of 4-chlorophenol, Appl. Catal. B Environ. 74 (2007) 83–91.

[29] Q. Luo, Q. Cai, X. Li, Z. Pan, Y. Li, X. Chen, Q. Yan, Preparation and characterization of ZrO_2/TiO_2 composite photocatalytic film by micro-arc oxidation, Trans. Nonferrous Met. Soc. China. 23 (2013) 2945–2950.

[30] C. McManamon, J.D. Holmes, M.A. Morris, Improved photocatalytic degradation rates of phenol achieved using novel porous ZrO_2-doped TiO_2 nanoparticulate powders, J. Hazard. Mater. 193 (2011) 120–127.

[31] M. Hirano, C. Nakahara, K. Ota, O. Tanaike, M. Inagaki, Photoactivity and phase stability of ZrO_2-doped anatase-type TiO_2 directly formed as nanometer-sized particles by hydrolysis under hydrothermal conditions, J. Solid State Chem. 170 (2003) 39–47.

[32] M.D. Hernández-Alonso, I. Tejedor-Tejedor, J.M. Coronado, J. Soria, M.A. Anderson, Sol–gel preparation of TiO_2–ZrO_2 thin films supported on glass rings: Influence of phase composition on photocatalytic activity, Thin Solid Films. 502 (2006) 125–131.

[33] B. Neppolian, Q. Wang, H. Yamashita, H. Choi, Synthesis and characterization of ZrO_2-TiO_2 binary oxide semiconductor nanoparticles: Application and interparticle

electron transfer process, Appl. Catal. A Gen. 333 (2007) 264–271.

[34]   Y. Gnatyuk, N. Smirnova, O. Korduban, A. Eremenko, Effect of zirconium incorporation on the stabilization of TiO_2 mesoporous structure, Surf. Interface Anal. 42 (2010) 1276–1280.

[35]   S.H. Elder, Y. Gao, X. Li, J. Liu, D.E. McCready, C.F.J. Windisch, Zirconia-Stabilized 25-Å TiO_2 Anatase Crystallites in a Mesoporous Structure, Chem. Mater. 10 (1998) 3140–3145.

[36]   J.H. Schattka, D.G. Shchukin, J. Jia, M. Antonietti, R. a Caruso, Photocatalytic Activities of Porous Titania and Titania / Zirconia Structures Formed by Using a Polymer Gel Templating Technique, Polymer (Guildf). 14 (2002) 5103–5108.

[37]   Navío, Hidalgo, G. Colón, S.G. Botta, M.I. Litter, Preparation and Physicochemical Properties of ZrO_2 and Fe/ZrO_2 Prepared by a Sol−Gel Technique, Langmuir. 17 (2001) 202–210.

[38]   H. Koohestani, S. Khatiboleslam Sadrnezhaad, Improvement in TiO_2 photocatalytic performance by ZrO_2 nanocompositing and immobilizing, Desalin. Water Treat. 57 (2016) 28450–28459.

[39]   S.G. Botta, J.A. Navío, M.C. Hidalgo, G.M. Restrepo, M.I. Litter, Photocatalytic properties of ZrO_2 and Fe/ZrO_2 semiconductors prepared by a sol–gel technique, J. Photochem. Photobiol. A Chem. 129 (1999) 89–99.

[40]   K. Maver, U. Lavrenčič Štangar, U. Černigoj, S. Gross, R. Cerc Korošec, Low-temperature synthesis and characterization of TiO_2 and TiO_2–ZrO_2 photocatalytically active thin films, Photochem. Photobiol. Sci. 8 (2009) 657.

[41]   S.J. Pfleiderer, D. Lützenkirchen-Hecht, R. Frahm, Crystallization behaviour of TiO_2–ZrO_2 composite nanoparticles, J. Sol-Gel Sci. Technol. 64 (2012) 27–35.

[42]   J.Y. Kim, C.S. Kim, H.K. Chang, T.O. Kim, Effects of ZrO_2 addition on phase stability and photocatalytic activity of ZrO_2/TiO_2 nanoparticles, Adv. Powder Technol. 21 (2010) 141–144.

[43]   W. Stöber, A. Fink, E. Bohn, Controlled growth of monodisperse silica spheres in the micron size range, J. Colloid Interface Sci. 26 (1968) 62–69.

[44]   U. Lavrenčič Štangar, U. Černigoj, P. Trebše, K. Maver, S. Gross, Photocatalytic TiO_2 Coatings: Effect of Substrate and Template, Monatshefte Für Chemie - Chem. Mon. 137 (2006) 647–655.

[45]   V.S. Smitha, K.A. Manjumol, K. V. Baiju, S. Ghosh, P. Perumal, K.G.K. Warrier, Sol-gel route to synthesize titania-silica nano precursors for photoactive particulates and coatings, J. Sol-Gel Sci. Technol. 54 (2010) 203–211.

[46]   R.E. Ramírez-García, J.A. González-Rodríguez, M. Arroyo-Ortega, S.A. Pérez-García, L. Licea-Jiménez, Engineered TiO_2 and SiO_2-TiO_2 films on silica-coated glass for increased thin film durability under abrasive conditions, Int. J. Appl. Ceram. Technol. 14 (2017) 39–49.

[47]   A. Eshaghi, A. Eshaghi, Investigation of superhydrophilic mechanism of titania nano layer thin film-Silica and indium oxide dopant effect, Bull. Mater. Sci. 35 (2012) 137–142.

[48]   M.A.M.L. de Jesus, J.T. da S. Neto, G. Timò, P.R.P. Paiva, M.S.S. Dantas, A. de M. Ferreira, Superhydrophilic self-cleaning surfaces based on TiO_2 and TiO_2/SiO_2 composite films for photovoltaic module cover glass, Appl. Adhes. Sci. 3 (2015) 5.

[49]   T.T. Duc, N.T.M. Huong, V.T. Bich, N.D. Dung, N.T. Tinh, T.X. Hoai, The Effect of SiO_2 Addition in Hydrophilic Property of TiO_2 Films, in: D.T. Cat, A. Pucci, K.

Wandelt (Eds.), Phys. Eng. New Mater., Springer Berlin Heidelberg, Berlin, Heidelberg, 2009: pp. 185–192.

[50]   M. Momeni, H. Saghafian, F. Golestani-Fard, N. Barati, A. Khanahmadi, Effect of SiO2 addition on photocatalytic activity, water contact angle and mechanical stability of visible light activated TiO_2 thin films applied on stainless steel by a sol gel method, Appl. Surf. Sci. 392 (2017) 80–87.

[51]   D.M. Tobaldi, A. Tucci, A. Sever Škapin, L. Esposito, Effects of SiO_2 addition on TiO_2 crystal structure and photocatalytic activity, J. Eur. Ceram. Soc. 30 (2010) 2481–2490.

[52]   Y. Xu, W. Zheng, W. Liu, Enhanced photocatalytic activity of supported TiO_2: dispersing effect of SiO_2, J. Photochem. Photobiol. A Chem. 122 (1999) 57–60.

[53]   Aqueous and Nonaqueous Sol-Gel Chemistry, in: Met. Oxide Nanoparticles Org. Solvents Synth. Form. Assem. Appl., Springer London, London, 2009: pp. 7–18.

[54]   S. Watson, D. Beydoun, J. Scott, R. Amal, Preparation of nanosized crystalline TiO_2 particles at low temperature for photocatalysis, J. Nanoparticle Res. 6 (2004) 193–207.

[55]   S.M. Attia, J. Wang, G. Wu, J. Shen, J. Ma, Review on Sol-Gel Derived Coatings: Process, Technique an Optical Applications, J. Mater. Sci. Technol. 18 (2009) 211–217.

[56]   A.E. Danks, S.R. Hall, Z. Schnepp, The evolution of 'sol–gel' chemistry as a technique for materials synthesis, Mater. Horizons. 3 (2016) 91–112.

[57]   A. Chládová, J. Wiener, J.M. Luthuli, V. Zajícová, Dyeing of glass fibres by the sol gel method, AUTEX Res. J. 11 (2011) 18–23.

[58]   C.J. Brinker, G.W. Scherer, Sol-Gel Science: The Physics and Chemistry of Sol-Gel Processing, Elsevier, 1990.

[59]   B. Babiarczuk, A. Szczurek, A. Donesz-Sikorska, I. Rutkowska, J. Krzak, The influence of an acid catalyst on the morphology, wettabillity, adhesion and chemical structure properties of TiO_2 and ZrO_2 sol-gel thin films, Surf. Coatings Technol. 285 (2016) 134–145.

[60]   V.A. Ganesh, H.K. Raut, A.S. Nair, S. Ramakrishna, A review on self-cleaning coatings, J. Mater. Chem. 21 (2011) 16304.

[61]   U. Lavrenčič Štangar, M. Tasbihi, F. Fresno, M. Kete, A. Gasparotto, C. Maccato, D. Barreca, Self-Cleaning and Anti-Fogging Surfaces Based on Nanostructured Metal Oxides, Adv. Sci. Technol. 91 (2014) 39–47.

[62]   K. Hashimoto, H. Irie, A. Fujishima, TiO_2 Photocatalysis: A Historical Overview and Future Prospects, Jpn. J. Appl. Phys. 44 (2005) 8269–8285.

[63]   A. Fujishima, K. Hashimoto, T. Watanabe, TiO_2 Photocatalysis Fundamentals and Applications, 1st ed., BKC Inc., Tokyo, 1999.

[64]   J. Chen, C. Poon, Photocatalytic construction and building materials: From fundamentals to applications, Build. Environ. 44 (2009) 1899–1906.

[65]   S. Pişkin, A. Palantöken, M.S. Yılmaz, Antimicrobial Activity of Synthesized TiO_2 Nanoparticles, in: Int. Conf. Emerg. Trends Eng. Technol., 2013: pp. 91–94.

[66]   J. Xie, Y.-C. Hung, UV-A activated TiO_2 embedded biodegradable polymer film for antimicrobial food packaging application, LWT - Food Sci. Technol. 96 (2018) 307–314.

[67]   A. Kubacka, M.S. Diez, D. Rojo, R. Bargiela, S. Ciordia, I. Zapico, J.P. Albar, C.

Barbas, V.A.P. Martins dos Santos, M. Fernández-García, M. Ferrer, Understanding the antimicrobial mechanism of TiO_2-based nanocomposite films in a pathogenic bacterium, Sci. Rep. 4 (2014) 4134.

[68]   H. Bodaghi, Y. Mostofi, A. Oromiehie, Z. Zamani, B. Ghanbarzadeh, C. Costa, A. Conte, M.A. Del Nobile, Evaluation of the photocatalytic antimicrobial effects of a TiO_2 nanocomposite food packaging film by in vitro and in vivo tests, LWT - Food Sci. Technol. 50 (2013) 702–706.

[69]   A.M.W. Downing, T.P. Blunt, J. Marshall, III. Researches on the effect of light upon Bacteria and other organisms, Proc. R. Soc. London. 26 (1878) 488–500.

[70]   P.H. Quek, J. Hu, Indicators for photoreactivation and dark repair studies following ultraviolet disinfection, J. Ind. Microbiol. Biotechnol. 35 (2008) 533–541.

[71]   K.-J. Shieh, M. Li, Y.-H. Lee, S.-D. Sheu, Y.-T. Liu, Y.-C. Wang, Antibacterial performance of photocatalyst thin film fabricated by defection effect in visible light, Nanomedicine Nanotechnology, Biol. Med. 2 (2006) 121–126.

[72]   U. Žvab, M. Bergant Marušič, U. Lavrenčič Štangar, Microplate-based assays for the evaluation of antibacterial effects of photocatalytic coatings, Appl. Microbiol. Biotechnol. 96 (2012) 1341–1351.

[73]   S. Armin, Z. Estekhraji, S. Amiri, Sol–gel preparation and characterization of antibacterial and self-cleaning hybrid nanocomposite coatings, J. Coatings Technol. Res. 14 (2017) 1335–1343.

[74]   S.M. Taghavi, M. Momenpour, M. Azarian, M. Ahmadian, F. Souri, S.A. Taghavi, M. Sadeghain, M. Karchani, Effects of Nanoparticles on the Environment and Outdoor Workplaces., Electron. Physician. 5 (2013) 706–12.

[75]   B. Nowack, T.D. Bucheli, Occurrence, behavior and effects of nanoparticles in the environment, Environ. Pollut. 150 (2007) 5–22.

[76]   S.C. Lenaghan, Y. Li, H. Zhang, J.N. Burris, C.N. Stewart, L.E. Parker, M. Zhang, Monitoring the Environmental Impact of TiO_2 Nanoparticles Using a Plant-Based Sensor Network, IEEE Trans. Nanotechnol. 12 (2013) 182–189.

[77]   X. Chang, Y. Zhang, M. Tang, B. Wang, Health effects of exposure to nano-TiO_2: A meta-analysis of experimental studies, Nanoscale Res. Lett. 8 (2013) 1–10.

[78]   C. Rompelberg, M.B. Heringa, G. van Donkersgoed, J. Drijvers, A. Roos, S. Westenbrink, R. Peters, G. van Bemmel, W. Brand, A.G. Oomen, Oral intake of added titanium dioxide and its nanofraction from food products, food supplements and toothpaste by the Dutch population, Nanotoxicology. 10 (2016) 1404–1414.

[79]   H. Shi, R. Magaye, V. Castranova, J. Zhao, Titanium dioxide nanoparticles: a review of current toxicological data, Part. Fibre Toxicol. 10 (2013) 15.

[80]   I. Iavicoli, V. Leso, A. Bergamaschi, Toxicological Effects of Titanium Dioxide Nanoparticles: A Review of In Vivo Studies , J. Nanomater. 2012 (2012) 1–36.

[81]   Technical Information Polycasa® Cast, (2014) 1–27.

[82]   Y.J. Yun, J.S. Chung, S. Kim, S.H. Hahn, E.J. Kim, Low-temperature coating of sol–gel anatase thin films, Mater. Lett. 58 (2004) 3703–3706.

[83]   A.B. Murphy, Band-gap determination from diffuse reflectance measurements of semiconductor films, and application to photoelectrochemical water-splitting, Sol. Energy Mater. Sol. Cells. 91 (2007) 1326–1337.

[84]   P. Kubelka, New Contributions to the Optics of Intensely Light-Scattering Materials Part I, J. Opt. Soc. Am. 38 (1948) 448.

[85] R. López, R. Gómez, Band-gap energy estimation from diffuse reflectance measurements on sol-gel and commercial TiO_2: A comparative study, J. Sol-Gel Sci. Technol. 61 (2012) 1–7.

[86] D. Korte, M. Franko, Application of complex geometrical optics to determination of thermal, transport, and optical parameters of thin films by the photothermal beam deflection technique, J. Opt. Soc. Am. A. 32 (2015) 61–74.

[87] U. Lavrenčič Štangar, M. Kete, U. Černigoj, V. Ducman, Testing of Photocatalytic Activity of Self-Cleaning Surfaces, Adv. Sci. Technol. 68 (2010) 126–134.

[88] X.H. Lin, S.N. Lee, W. Zhang, S.F.Y. Li, Photocatalytic degradation of terephthalic acid on sulfated titania particles and identification of fluorescent intermediates, J. Hazard. Mater. 303 (2016) 64–75.

[89] U. Černigoj, M. Kete, U. Lavrenčič Štangar, Development of a fluorescence-based method for evaluation of self-cleaning properties of photocatalytic layers, Catal. Today. 151 (2010) 46–52.

[90] L.R. Field, E. Wilhelm, R. Battino, The solubility of gases in liquids 6. Solubility of N_2, O_2, CO, CO_2, CH_4, and CF_4 in methylcyclohexane and toluene at 283 to 313 K, J. Chem. Thermodyn. 6 (1974) 237–243.

[91] N.J. Turro, V. Ramamurthy, V. Ramamurthy, J.C. Scaiano, Principles of Molecular Photochemistry: An Introduction, University Science Books, 2009.

[92] D. Dvoranová, Z. Barbieriková, V. Brezová, Radical intermediates in photoinduced reactions on TiO_2 (An EPR spin trapping study), Molecules. 19 (2014) 17279–17304.

[93] D.R. Duling, Simulation of Multiple Isotropic Spin-Trap EPR Spectra, J. Magn. Reson. Ser. B. 104 (1994) 105–110.

[94] N. Vodišek, A. Šuligoj, D. Korte, U. Lavrenčič Štangar, Transparent Photocatalytic Thin Films on Flexible Polymer Substrates, Materials (Basel). 11 (2018) 1945.

[95] J. Martins, L. Oliva Teles, V. Vasconcelos, Assays with Daphnia magna and Danio rerio as alert systems in aquatic toxicology., Environ. Int. 33 (2007) 414–25.

[96] N. Vodišek, K. Ramanujachary, V. Brezová, U. Lavrenčič Štangar, Transparent titania-zirconia-silica thin films for self-cleaning and photocatalytic applications, Catal. Today. 287 (2017) 142–147.

[97] K. Thamaphat, P. Limsuwan, B. Ngotawornchai, Phase Characterization of TiO_2 Powder by XRD and TEM, Nat. Sci. 42 (2008) 357–361.

[98] C.H. Kwon, H. Shin, J.H. Kim, W.S. Choi, K.H. Yoon, Degradation of methylene blue via photocatalysis of titanium dioxide, Mater. Chem. Phys. 86 (2004) 78–82.

[99] A. Soklič, M. Tasbihi, M. Kete, U. Lavrenčič Štangar, Deposition and possible influence of a self-cleaning thin TiO_2/SiO_2 film on a photovoltaic module efficiency, Catal. Today. 252 (2015) 54–60.

[100] A. Di Paola, M. Bellardita, L. Palmisano, Brookite, the Least Known TiO_2 Photocatalyst, Catalysts. 3 (2013) 36–73.

[101] O. Pliekhov, O. Pliekhova, Y.O. Donar, A. Sınağ, N. Novak Tušar, U. Lavrenčič Štangar, Enhanced photocatalytic activity of carbon and zirconium modified TiO_2, Catal. Today. 284 (2017) 215–220.

[102] N. Veronovski, M. Sfiligoj-Smole, Functionalization of lyocell fibers with TiO_2, SiO_2, and GLYMO, Fibers Polym. 11 (2010) 545–550.

[103] C.-S. Wu, Synthesis of polyethylene-octene elastomer/SiO_2-TiO_2 nanocomposites via in situ polymerization: Properties and characterization of the hybrid, J. Polym. Sci.

Part A Polym. Chem. 43 (2005) 1690–1701.

[104] Y. Gao, Y. Masuda, W.S. Seo, H. Ohta, K. Koumoto, TiO_2 nanoparticles prepared using an aqueous peroxotitanate solution, Ceram. Int. 30 (2004) 1365–1368.

[105] X. Yan, J. He, D. G. Evans, X. Duan, Y. Zhu, Preparation, characterization and photocatalytic activity of Si-doped and rare earth-doped TiO_2 from mesoporous precursors, Appl. Catal. B Environ. 55 (2005) 243–252.

[106] K. Guan, Relationship between photocatalytic activity, hydrophilicity and self-cleaning effect of TiO_2/SiO_2 films, Surf. Coatings Technol. 191 (2005) 155–160.

[107] R. Poliah, S. Sreekantan, Characterization and photocatalytic activity of enhanced copper-silica-loaded titania prepared via hydrothermal method, J. Nanomater. 2011 (2011).

[108] A. Kumar, S. Singhal, S. Aggarwal, R.P. Badoni, A.K. Sharma, Influence of Synthetic Approach of SiO_2-ZrO_2 Materials, Catal. Sustain. Energy. 5 (2018) 34–40.

[109] H. Wu, Y. Yang, H. Suo, M. Qing, L. Yan, B. Wu, J. Xu, H. Xiang, Y. Li, Effects of ZrO_2 promoter on physic-chemical properties and activity of Co/TiO_2-SiO_2 Fischer-Tropsch catalysts, J. Mol. Catal. A Chem. 396 (2015) 108–119.

[110] S. Kongwudthiti, P. Praserthdam, W. Tanakulrungsank, M. Inoue, The influence of Si–O–Zr bonds on the crystal-growth inhibition of zirconia prepared by the glycothermal method, J. Mater. Process. Technol. 136 (2003) 186–189.

[111] W.-D. Li, J. Gao, L. Wang, Enhancement of durable photocatalytic properties of cotton/polyester fabrics using TiO_2/SiO_2 via one step sonosynthesis, J. Ind. Text. 46 (2017) 1633–1655.

[112] R. Beranek, H. Kisch, Tuning the optical and photoelectrochemical properties of surface-modified, Society. (2008) 40–48.

[113] H. Lin, C. Huang, W. Li, C. Ni, S. Ismat Shah, Y.-H. Tseng, Size dependency of nanocrystalline TiO_2 on its optical property and photocatalytic reactivity exemplified by 2-chlorophenol, Appl. Catal. B Environ. 68 (2006) 1–11.

[114] G.M. Ingo, C. Riccucci, G. Bultrini, S. Dirè, G. Chiozzini, Thermal and microchemical characterisation of sol-gel SiO_2, TiO_2 and $xSiO_2$-$(1-x)TiO_2$ ceramic materials, J. Therm. Anal. Calorim. 66 (2001) 37–46.

[115] N. Nakayama, T. Hayashi, Preparation of TiO_2 nanoparticles surface-modified by both carboxylic acid and amine: Dispersibility and stabilization in organic solvents, Colloids Surfaces A Physicochem. Eng. Asp. 317 (2008) 543–550.

[116] G. Helsch, J. Deubener, Compatibility of antireflective coatings on glass for solar applications with photocatalytic properties, Sol. Energy. 86 (2012) 831–836.

[117] R. Prado, G. Beobide, A. Marcaide, J. Goikoetxea, A. Aranzabe, Development of multifunctional sol–gel coatings: Anti-reflection coatings with enhanced self-cleaning capacity, Sol. Energy Mater. Sol. Cells. 94 (2010) 1081–1088.

[118] K.H. Nielsen, T. Kittel, K. Wondraczek, L. Wondraczek, Optical breathing of nano-porous antireflective coatings through adsorption and desorption of water, Sci. Rep. 4 (2015) 6595.

[119] J. Song, X. Wang, J. Yan, J. Yu, G. Sun, B. Ding, Soft Zr-doped TiO2 Nanofibrous Membranes with Enhanced Photocatalytic Activity for Water Purification, Sci. Rep. 7 (2017) 1636.

[120] J. Nawrocki, M. Rigney, A. McCormick, P.W. Carr, Chemistry of zirconia and its use in chromatography, J. Chromatogr. A. 657 (1993) 229–282.

[121] K. Reszka, P. Bilski, R.H. Sik, C.F. Chignell, Photosensitized Generation of Superoxide Radical in Aprotic Solvents: an EPR and Spin Trapping Study, Free Radic. Res. Commun. 19 (1993) s33–s44.

[122] K. Reszka, C.F. Chignell, Spin-Trapping of the Superoxide Radical in Aprotic Solvents, Free Radic. Res. Commun. 14 (1991) 97–106.

[123] T.A. Konovalova, J. Lawrence, L.D. Kispert, Generation of superoxide anion and most likely singlet oxygen in irradiated TiO_2 nanoparticles modified by carotenoids, J. Photochem. Photobiol. A Chem. 162 (2004) 1–8.

[124] T. Verdier, M. Coutand, A. Bertron, C. Roques, Antibacterial Activity of TiO_2 Photocatalyst Alone or in Coatings on E. coli: The Influence of Methodological Aspects, Coatings. 4 (2014) 670–686.

[125] A. Šuligoj, O. Pliekhova, N. Vodišek, M. Mihelčič, A. Surca, R. Kunič, B. Šubic, J. Starman, A. Ugovšek, U. Lavrenčič Štangar, Field Test of Self-Cleaning Zr-Modified-TiO2-SiO2 Films on Glass with a Demonstration of Their Anti-Fogging Effect, Materials (Basel). 12 (2019) 2196.

[126] M. Righeira Carnegie, A. Sherine, D. Sivagami, S. Sakthivel, Anti-reflection coatings with enhanced abrasion and scratch resistance properties, J. Sol-Gel Sci. Technol. 78 (2016) 176–186.

[127] R. Li, M. Boudot, C. Boissière, D. Grosso, M. Faustini, Suppressing Structural Colors of Photocatalytic Optical Coatings on Glass: The Critical Role of SiO_2, ACS Appl. Mater. Interfaces. 9 (2017) 14093–14102.

[128] M. Keshavarz Hedayati, M. Elbahri, Antireflective Coatings: Conventional Stacking Layers and Ultrathin Plasmonic Metasurfaces, A Mini-Review, Materials (Basel). 9 (2016) 497.

[129] M.R. Jung, F.D. Horgen, S. V. Orski, V. Rodriguez C., K.L. Beers, G.H. Balazs, T.T. Jones, T.M. Work, K.C. Brignac, S.J. Royer, K.D. Hyrenbach, B.A. Jensen, J.M. Lynch, Validation of ATR FT-IR to identify polymers of plastic marine debris, including those ingested by marine organisms, Mar. Pollut. Bull. 127 (2018) 704–716.

[130] A. Mirabedini, S.M. Mirabedini, A.A. Babalou, S. Pazokifard, Synthesis, characterization and enhanced photocatalytic activity of TiO_2/SiO_2 nanocomposite in an aqueous solution and acrylic-based coatings, Prog. Org. Coatings. 72 (2011) 453–460.

[131] M.M. Nasef, H. Saidi, K.Z.M. Dahlan, Investigation of electron irradiation induced-changes in poly(vinylidene fluoride) films, Polym. Degrad. Stab. 75 (2002) 85–92.

[132] X. Cai, T. Lei, D. Sun, L. Lin, A critical analysis of the α, β and γ phases in poly(vinylidene fluoride) using FTIR, RSC Adv. 7 (2017) 15382–15389.

[133] G. Zrim, M. Mihelčič, L. Slemenik Perše, B. Orel, B. Simončič, R. Kunič, Light distribution in air-supported pneumatic structures: Comparison of experimental and computer calculated daylight factors, Build. Environ. 119 (2017) 110–127.

[134] J. Coates, Interpretation of Infrared Spectra, A Practical Approach, in: Encycl. Anal. Chem., John Wiley & Sons, Ltd, Chichester, UK, 2006: pp. 1–23.

[135] Kazuo Nakamoto, Infrared and Raman Spectra of Inorganic and Coordination Compounds, Wiley, 2009.

[136] H. Dzinun, M.H.D. Othman, A.F. Ismail, M.H. Puteh, M.A. Rahman, J. Jaafar, Stability study of PVDF/TiO2 dual layer hollow fibre membranes under long-term UV irradiation exposure, J. Water Process Eng. 15 (2017) 78–82.

9 APPENDIX

Thermal analysis of PVC, D1 and D2 substrates

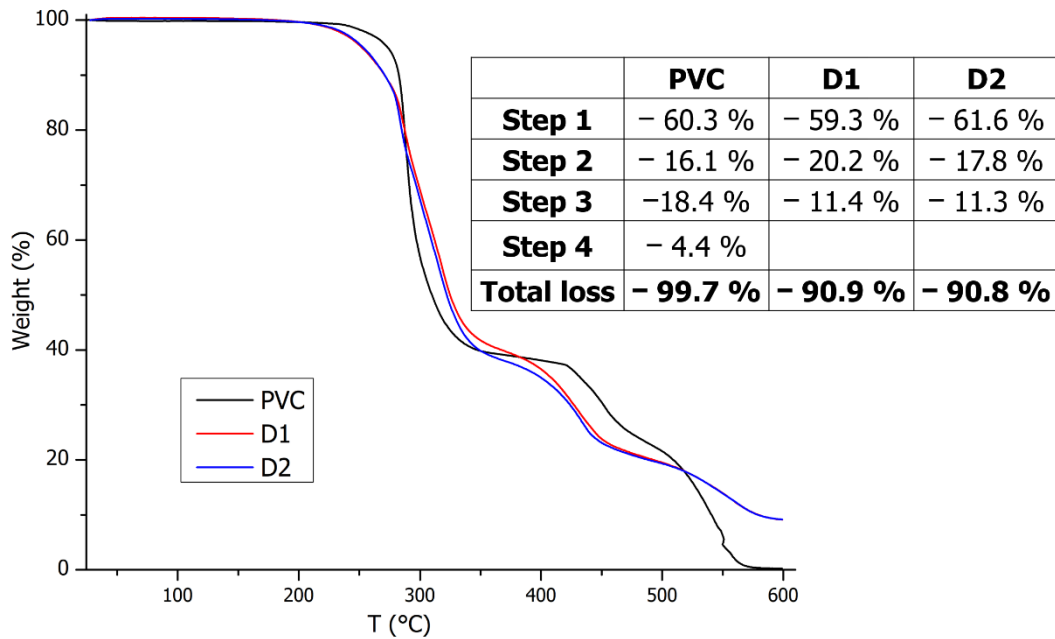|	**PVC**	**D1**	**D2**
Step 1	− 60.3 %	− 59.3 %	− 61.6 %
Step 2	− 16.1 %	− 20.2 %	− 17.8 %
Step 3	−18.4 %	− 11.4 %	− 11.3 %
Step 4	− 4.4 %		
Total loss	**− 99.7 %**	**− 90.9 %**	**− 90.8 %**

Figure 9.1 Thermal analysis of PVC, D1 and D2 substrate.

Rheological measurements of Ti0Zr and Ti10Zr sol
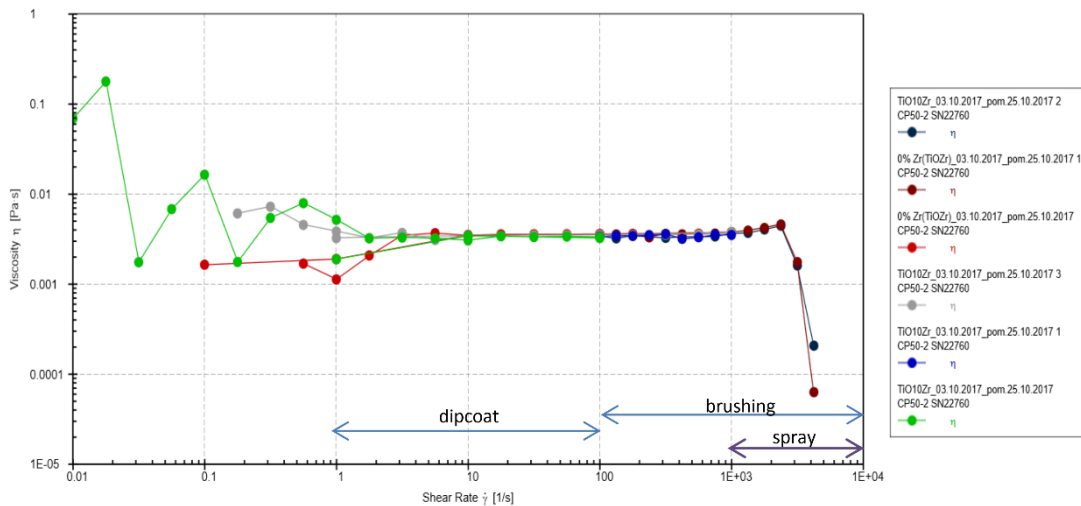

Figure 9.2 Dynamic rheological measurements of Ti0Zr and Ti10Zr deposition sol. These two solutions are not appropriate for spray deposition, but their viscosity is appropriate for dip-coating (measured at National Institute of Chemistry by Matic Šobak).

Field test of Ti10Zr thin films on float glass with a demonstration of their anti-fogging effect [125]

The change in transparency of the long-term exposed objects is important characteristic for transparent materials. It can be measured through the ratio in the intensity of light transmitted by the glazing and intensity of the light falling on a surface. Transparency is easily definable with a lux meter by measuring material total transmittance and depends on the absorption and reflection factors.

Transmittance was measured by using a handheld lux meter (LED light meter) (Extech Instruments, Nashua, NH, USA). Two lux meters were positioned on a levelled surface, one lying outside/beside and one under (through) the window. The difference between the two lux meters positioned beside each other (outside the window) did not exceed 0.5%. The results were calculated as

$$R = \Theta_V/\Theta_{Vglass}$$

where Θ_V and Θ_{Vglass} are the fluxes outside/beside and under the window, respectively. For easier interpretation, a deviation from an ideal transmittance is given in the plots as 1-R. In this case, values are increasing with time, as the windows get less transparent due to dirt deposits. A lux meter measures luminous flux, which is scaled to reflect «visible flux» by using the luminosity function. The results were averaged from three different measurement positions below the tested sample (left, middle, right position on the opened edge of the window sample).
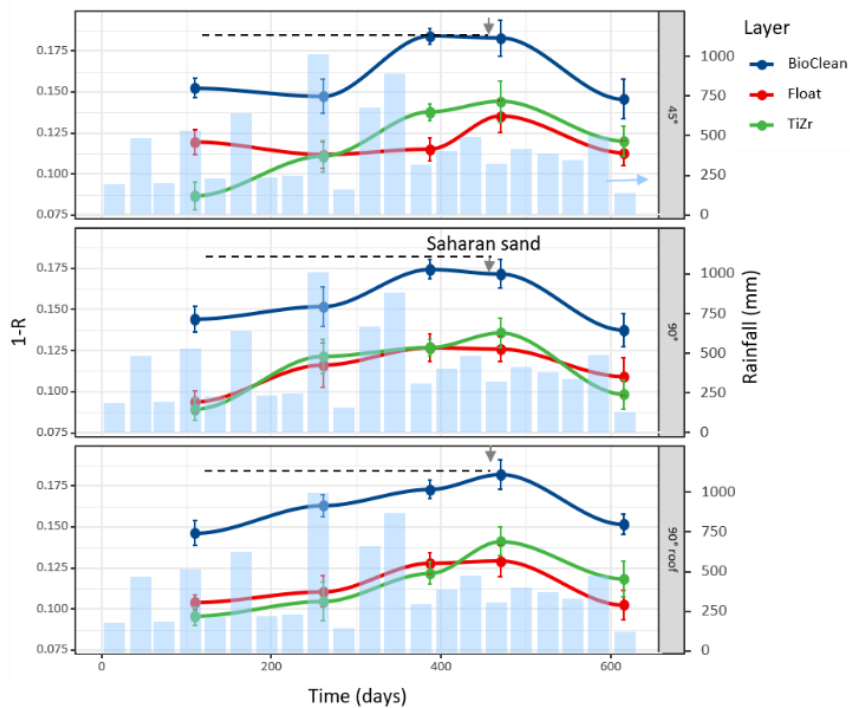

Figure 9.3 The averaged results from the three locations of field testing change in light transmittance expressed as 1-R according to Lux Meter

Haze values give the scattering of light by a plane-parallel surface. The method is recommended in the documentary standard ASTM D1003. The scattered light is responsible for the reduction in the contrast of the objects that are viewed through the investigated glazings.

The laboratory measurement of the haze was performed on small samples (4×9 cm^2) after in-field/laboratory transfer for each measurement. Haze value is according to ASTM D1003 defined as the ratio of diffuse to total luminous transmittance (DT/TT %). Luminous transmittance is weighted with regard to the relative sensitivity of the human eye in the photopic state. DT and TT were measured on a Perkin Elmer Lambda 900 UV-VIS spectrometer (Waltham, MA, USA) that is equipped with an integrating sphere. Both transmittances were measured in the 380–780 nm range using 10° CIE standard observer and CIE standard illuminant A.
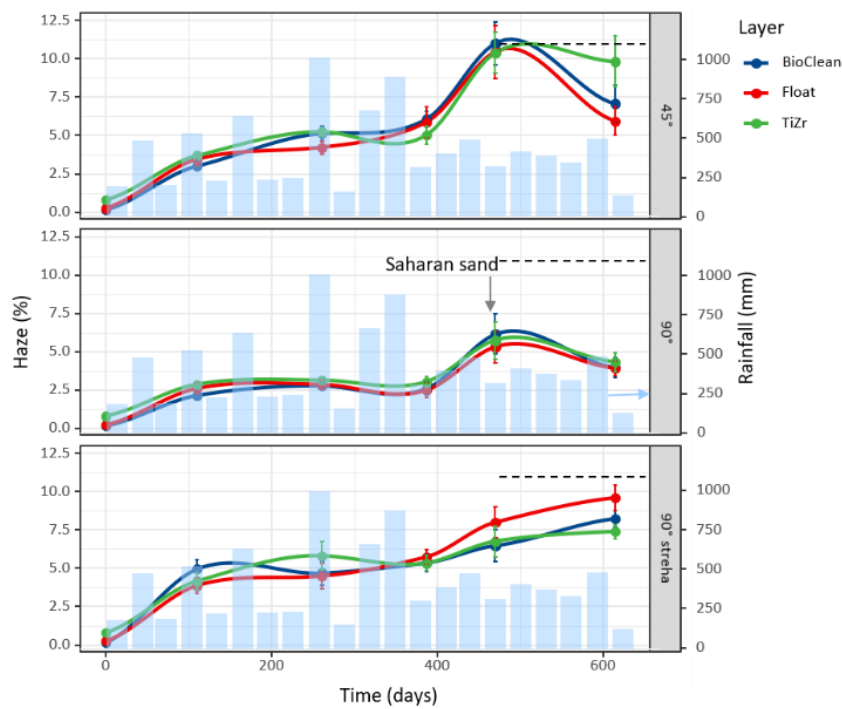

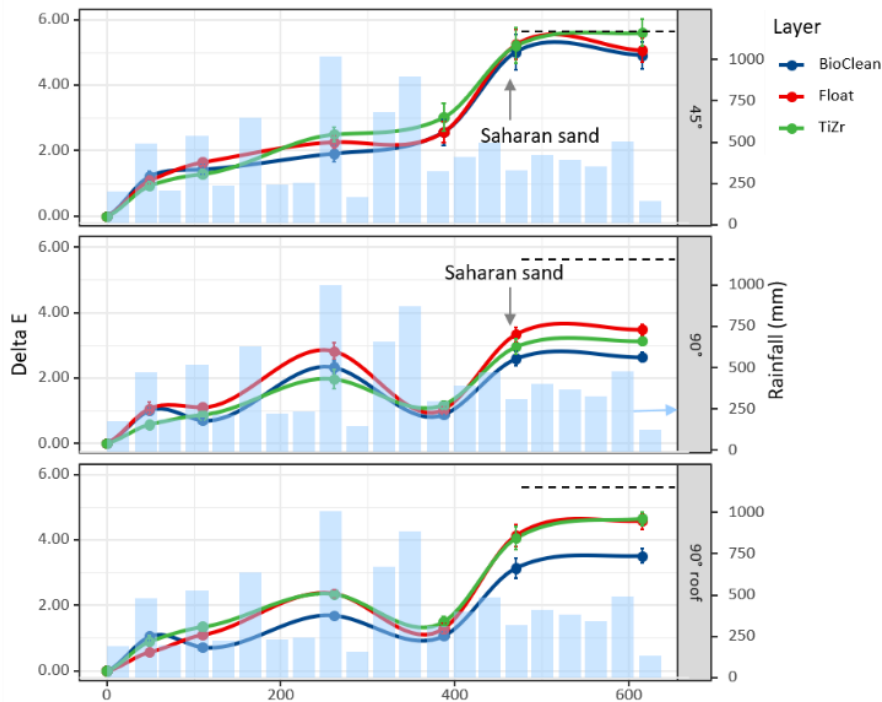*Figure 9.4 The averaged results from the three locations of field testing changes in haze.*

Figure 9.5 The averaged results from the three locations of field testing changes in ΔE values.

Another important characteristic of the functional coatings is color. Color differences can be described as the relative distance between two mathematically specified colors, according to the International Commission on Illumination (CIE). The difference is usually shown as ΔE and is calculated by comparing reference and sample L*a*b* values. The drawback of ΔE data is that calculations quantify the magnitude of a color difference but do not necessarily indicate the direction of the difference. However, portable instruments are available, which enables in-field measurements.

CIE L*a*b* characterization was used as a way of assessing the change of color (ΔE) by using a handheld meter (EasyCo, Erichsen, Germany). The apparatus was measuring the L*, a*, and b* coordinates of the glass with a whiteboard positioned under it. The whiteboard was taken as a background and, since the technique enables differentiation between the contributions from the light scattering expressed by ΔL* and the color changes described by Δa* and Δb* values, the global change of color (ΔE*) values were obtained from the equation

$$\Delta E_{ab}^* = (\Delta L^{*2} \times \Delta a^{*2} \times \Delta b^{*2})^{1/2}$$

The difference (Δ) was measured as the difference of the parameters (L*, a*, b*) measured with glass underneath from those of the whiteboard. Each measurement was averaged over five data points at different positions (four in the corners of the window and one in the center).

The biggest factor influencing the behavior of surfaces was the position of the windows. The biggest changes were detected in windows with 45 ° installation, while the smallest in 90 ° inclination; the 90 ° installation with a roof performed a little worse in all cases. This can be explained with the washing effect, where the water from rain cleans 90 ° surface more efficiently than 45 ° due to greater gravitational power, while the 90 ° surface under the roof receives less rain in general. All three measurement

techniques confirmed the trend after pollution with inorganic sand (day 480), that is, they all show general improvement of the surfaces with the period of steady rain which followed this event, showing the importance of exposure of surfaces to rainwater. the differences between the three surface materials (BioClean, float, TiZr) were not as pronounced. They all showed the same trend and none of the surfaces showed a significant deviation of the temporal evolution from the other two. In addition to the position of the surfaces, the location of exposure also had a large influence on the visual appearance of the surfaces.
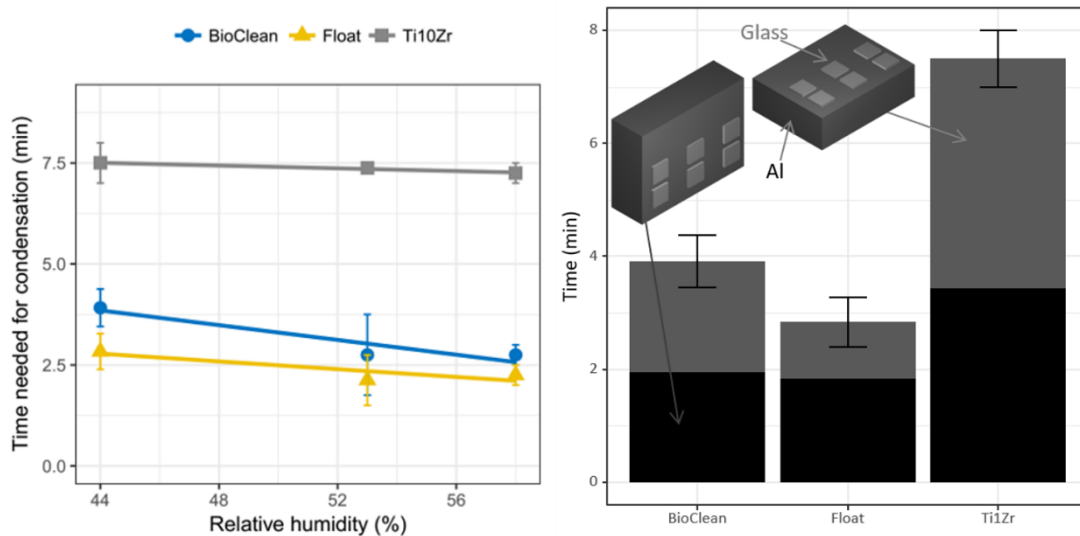

Figure 9.6 Dependence of time of formation of water droplets (condensation) on the surface on the relative humidity across samples (left) and dependence on the orientation of the sample (right). Interestingly, the time was also shorter if the samples were exposed in a vertical configuration as compared to the horizontal one. This difference may seem unimportant, but in a practical view, it means that windows that are installed in more horizontal configuration will benefit more of the anti-fogging coating. (measured at University of Ljubljana, Faculty of Chemistry and Chemical Technology by Andraž Šuligoj)

The anti-fogging ability of the TiZr surface was evaluated through the determination of the droplet formation time in the laboratory, as well as on the outside surface of a real built-in window.

The condensation experiment was conducted in a laboratory environment at 22 ∘C at three different relative humidities (44%, 52%, and 58%). An aluminum block ($20 \times 20 \times 8$ cm^3) was put in the freezer (-12 °C) to cool. The block was put out and three samples of glass/coatings were placed on its surface in a horizontal and vertical position. The time of the visual appearance of condensate water droplets was measured.

The TiZr surface layer showed the longest time needed for large-enough droplets to form to scatter light and, hence, reduce the transparency of glass/coating. Not surprisingly, float glass formed visible water droplets first, followed by BioClean glass. The antifogging effect of the TiZr coating, on the other hand, can be explained with the presence of titania phase, by the occurrence of oxygen defects upon UV-irradiation with the additional help of numerous Si–OH and Ti–OH surface groups already present on the particles of silica and titania, respectively.

103